IMPACT OF EXTREME PRECIPITATION EVENTS ON THE WATER TABLE AND GROUNDWATER RECHARGE

by

CLAUDIA REBECCA CORONA

B.A., Williams College, 2013

M.S., San Francisco State University, 2016

A dissertation submitted to the

Faculty of the Graduate School of the

University of Colorado in partial fulfillment

of the requirement for the degree of

Doctor of Philosophy

Department of Geological Sciences

2023

Committee Members:

Shemin Ge

Suzanne P. Anderson

Jesse E. Dickinson

Michelle A. Walvoord

Ben Livneh

Robert S. Anderson

Corona, Claudia Rebecca (Ph.D., Geological Sciences)

Impact of Extreme Precipitation Events on the Water Table and Groundwater Recharge

Dissertation directed by Professors Shemin Ge and Suzanne P. Anderson

ABSTRACT

Extreme precipitation events (EPEs) play a crucial role in influencing soil water storage and groundwater recharge worldwide. With climate change, extreme precipitation events are expected to increase in intensity, creating an urgent need to examine their effects on water resources. On the land surface, the wide-ranging impacts of EPEs are visible. These impacts can be described as destructive, causing mass flooding, property damage and putting lives at risk. Below the surface however, the impacts of EPEs on subsurface processes are less clear and warrant urgent study. In this dissertation, I examine the impacts of extreme precipitation events on water table mechanics and groundwater recharge.

I begin my study locally, by investigating the role of an extreme precipitation event that occurred along the Colorado Front Range in September 2013. The event quickly caused widespread flooding, but flood waters diminished just as quickly. For many years, it remained unclear whether that EPE-water had infiltrated the soil and if so, for how long the EPE-water may have impacted local soil water storage and water tables. My first goal was thus to examine the subsurface hydrologic response to the 2013 Colorado EPE using an unsaturated-flow model and field data from a site that had experienced the event. I find that after the EPE, the water table at a field site remained elevated relative to average water levels, for at least 18 months after the

event, while the soil water storage was higher than average for two water years after the event. Thus, infiltration from EPEs is present for much longer than flood waters, and may aid recharge.

Having investigated the subsurface response to an EPE at a site, the next step was to expand the study to examine whether similar responses occurred across varying soil texture classes and EPEs for other sites in the United States. I find that greater EPE amounts generally lead to higher water-table displacements, but that soil properties are also a strong control of displacement and determine the length of time needed for the water-table to recede after an EPE.

Finally, I conduct a comprehensive, model-based study in which I investigate the response of twelve different soil texture classes to EPEs of varying amounts and durations. Water-table response times are shorter with increasing EPE amount, and that water-table response occurs much faster in coarser-grained soils (i.e., sand), while taking upwards of hundreds of days to respond in finer-grained soils. Water-table displacement is positively correlated with increasing EPE amount and poorly correlated with longer EPE duration. Soil properties appear to be the greater control in water-table recession time, despite EPE amounts. Finally, I calculated first-order recharge rates and found average recharge equaled 70% of the total, with the amount of total recharge primarily controlled by the amount of the EPE and the soil properties.

In summary, EPEs replenish subsurface water storage, but water-table displacement and prolonged recession could be detrimental for ground stability.

ACKNOWLEDGEMENTS

I am here because of the people around me – family, friends, and strangers who believed in this spunky little Latina from urban Los Angeles. First, *doy gracias* to my parents, Rebeca and Leonardo, my siblings, Jennie and Leonard, and my partner, Laura, who are my #1 supporters. Second, I am grateful for: Mr. Tony Alvarado who taught me to love reading as a kid, Ms. Celia Gonzalez, my 8th grade math & science teacher and life-long mentor, who taught me to think critically and be brave, and Mr. Andrew Stephens, my high school science teacher, who introduced me to environmental science and the great outdoors. I also want to thank Santiago Escruceria, Geoff McQuilkin, Peter Vorster, Herley Jim and the Mono Lake Committee, all of whom have been like a second family in the Eastern Sierras of CA.

I want to thank Shemin Ge for accepting me as her Ph.D. student many years ago and showing me how to improve as a researcher, writer, and thinker. It is my hope that I can be as impactful in a student's academic career as she has been on mine. I want to thank Suzanne Anderson for her mentorship these last two years, for her light-heartedness, and for her guidance in helping me improve my research and writing skills. To my committee: Jesse, Ben, Michelle, and Bob, thank you for teaching me how to be a better researcher, meeting with me and believing in me along the way. I also thank Dan Mitchell, the "jack of all trades", Kara Bajdas, the "super woman", and everyone in the front office for their kindness over the years.

Finally, I acknowledge the institutions that funded my work: the National Science Foundation Award #EAR-1834290 to Principal Investigator, Shemin Ge, the Department of Geological Sciences, and the North Central Climate Adaptation Science Center at the University of Colorado, Boulder. Thank you. I am forever grateful for this experience.

TABLE OF CONTENTS

LIST OF TABLES

LIST OF FIGURES

CHAPTER 1: INTRODUCTION

1.1 Background

Extreme precipitation events (EPEs) are a globally-occurring climate phenomena in which precipitation falls at higher amounts than average in a timespan that can last as little as a few minutes or as much as 60 days (Perica et al., 2013; Pendergrass, 2018; Du et al., 2022). Once considered rare, EPEs are occurring at higher frequencies than predicted, with studies suggesting that climate change will result in more precipitation falling as part of larger, intense events and less as part of average occurrences (Trenberth, 2011; Westra et al., 2013; Li et al., 2019; Myhre et al., 2019).

The impacts of EPEs on water resources are of great concern for communities worldwide (Tashie et al., 2016; Wasko et al., 2021). On the surface, EPEs can be disastrous for people and property, leaving a trail of destruction and death in their wake. Below the surface, the impact of EPEs is less clear, specifically in terms of the physical mechanisms. Traditional infiltration theory suggests that such events immediately result in runoff and little if any of the precipitation will infiltrate the soil surface (Horton, 1941). More recent studies have used field data and model results to discover that a higher percentage of EPE-water than previously thought is infiltrating the soil surface, flowing downward through the subsurface, and reaching the water table in varying lengths of time depending on the subsurface conditions (Jasechko and Taylor, 2015; Golian et al., 2021; Boas and Mallants, 2022).

The unsaturated zone connects EPEs to groundwater, where soil hydraulic properties influence infiltration and manage recharge to the water table. Unfortunately, as it remains difficult to study what we cannot readily see or access, the subsurface response to EPEs is poorly understood. As surface water resources become more scarce with increasing temperatures

affecting snowpack and widespread droughts affecting water reservoirs, EPEs are likely to play a key role in influencing subsurface water storage, ultimately affecting water supplies and water resource planning worldwide (Taylor et al., 2013; Shao et al., 2018; Boas and Mallants, 2022).

1.2 Summary of work

Understanding how subsurface water storage and flow can vary in response to extreme precipitation events is becoming increasingly important for community planners, water resource managers and researchers. This dissertation focuses on examining the impacts of EPEs on the water table and recharge to better understand the physical mechanisms that connect EPEs and water resources. Such understanding is key for water resource availability and natural hazard planning efforts.

In **Chapter 2**, I investigate the effects of an extreme precipitation event on the physical processes in the vadose zone that control infiltration and soil water storage. The week-long extreme precipitation event occurred in Boulder, CO, in September 2013 and surpassed all previous records for daily and monthly rainfall in Boulder. The event resulted in catastrophic above-surface flooding yet the response of the subsurface to the event and the effects on soil water storage remained poorly understood. This case study uses a one-dimensional variably saturated flow model, HYDRUS-1D, to model subsurface response to the EPE. The upper boundary condition is set by precipitation and the bottom boundary is denoted by a deep drainage boundary condition. Data from a field site in the Boulder Creek Watershed in the Front Range was used to assemble model input parameters.

Model results show that the subsurface responds to the 2013 EPE in a temporally analogous manner to well field measurements. A rapid increase in the water table is observed and subsurface soil water storage remains above pre-EPE levels for 18 months after the EPE. A

sensitivity analysis is also conducted to identify the hydrologic parameters and soil properties that most significantly affect subsurface response to the EPE. The sensitivity analysis finds that adjusting the water content values, both residual and saturated, as well as varying air-entry pressure values have strong influences on water-table fluctuations. Adjusting water content values and air-entry pressure values also affect the recovery time for soil water storage to return to a pre-EPE state. The broader implication of this work is that analyzing subsurface response to EPEs can help illuminate how local and regional watersheds with varying soil texture classes worldwide respond to EPE-induced water-table fluctuations and subsurface water storage change.

In **Chapter 3**, I expand the scope of the study to consider varying climates and soils across the United States. Local precipitation data for each case is used to characterize an EPE, defined as a 1-day precipitation event with an annual exceedance probability of 0.1%. The purpose of considering 17 cases is to expand the understanding of the role of subsurface processes in controlling EPE-driven infiltration through the vadose zone and to the water table. I use pressure head - water content data from the Unsaturated Soil Hydraulic Database (UNSODA) and precipitation data from site-specific locations throughout the U.S. to construct HYDRUS-1D subsurface flow models. The inverse estimation function of HYDRUS-1D is used along with the UNSODA soils and precipitation data to infer unsaturated zone soil hydraulic parameters. The respective inverse solutions, case-specific EPEs and UNSODA soils are then used to model local water-table response to EPEs. Normal and EPE cases are run and compared to examine water-table displacement (Δ_{WTD}) and recession time (t_{rec}). The Δ_{WTD} range from 0.5 - 2.4 m across sites and are not directly controlled by EPE amount; instead, Δ_{WTD} is inversely related to available porosity. Soils with low available porosity undergo large Δ_{WTD} compared to

soils with higher available porosity. Despite larger EPEs, modeled water tables that experience greater EPEs recede faster than those that experience smaller EPEs. Furthermore, water-table recession times, t_{rec}, are inversely related to hydraulic diffusivity. For all cases, t_{rec} ranges from months to years suggesting an increased role by the subsurface in buffering EPEs. A hydrologic buffer could have important benefits for water-limited regions in times of drought.

In **Chapter 4**, I conduct a comprehensive soil-water modeling effort, where I use soil hydraulic property data for twelve soil textures identified by the United States Department of Agriculture (USDA), to define twelve 1D models. For the simulations, different EPE durations and amounts are applied: 1-day (0.20 m, 0.40 m), 7-day and 20-day (0.20 m, 0.40 m , 0.60 m). Four aspects of water-table dynamics are considered: response time, displacement, recession time and first-order recharge estimates. In total, 96 simulations are run and compared to form a more comprehensive understanding of water-table response across soil textures to varying EPE amounts. Results show that water-table response varies with soil texture class across EPEs of various durations and amounts, however, the variations cannot be explained solely by saturated hydraulic conductivity, available porosity, or climate (i.e., precipitation amount or duration).

While an increase in EPE amount and duration generally leads to increases in recharge, an increase in EPE durations is not positively correlated with greater recharge. Water-table response to EPEs is faster in coarser-grained soils than finer-grained soils. Water-table recession times vary between 2.4 and 8.0 years. Overall, average recharge totals from the EPEs considered range from 31% to 96% of the EPE amount, with the average at ~70%, indicating an opportunity for greater aquifer recharge for communities in need of restoring subsurface water resources. This modeling effort provides a broader understanding of how EPE impacts on subsurface response affect water-table fluctuations and groundwater recharge.

CHAPTER 2: EXAMINING SUBSURFACE RESPONSE TO AN EXTREME PRECIPITATION EVENT USING HYDRUS 1-D

Abstract

North-central Colorado experienced an extreme precipitation event (EPE) in September 2013, during which the equivalent of 80% of the region's annual average precipitation fell in a few days. Widespread flooding occurred above-ground but the short- and long-term subsurface response remains unclear. The objective of the study is to better understand the dynamic subsurface response, namely how the water table and soil water storage responded to a large amount of infiltration in a brief period of time and how the hydrologic properties of the subsurface influence the response. Better understanding of subsurface response to EPEs is expected to increase with the advent of more intense and frequent EPEs in the coming decades. A one-dimensional subsurface flow model, HYDRUS-1D, is employed to simulate and examine infiltration of an EPE at a site in the Boulder Creek watershed, Colorado. The model is calibrated using local field data over a six-year period. Rapid water table response is observed in the field. The modeled subsurface stores water for 18 months, acting as a hydro-buffer during recovery. To examine influence on model results, a sensitivity study of soil hydraulic parameters is conducted. The sensitivity study finds that changes in n, an empirical parameter related to pore-size distribution, most significantly affects water table depth. The implications are that 1D models may provide useful estimates of water table fluctuations and subsurface hydro-buffer capacities in response to EPEs, which could be of use to regions preparing for EPE impacts on water resources.

This chapter has been previously published:

Corona, C.R. and Ge, S., 2022. Examining Subsurface Response to an Extreme Precipitation Event Using HYDRUS-1D. Vadose Zone Journal, 21(3), p.e20189. https://doi.org/10.1002/vzj2.20189

2.1 Introduction

At the extremes of precipitation occurrence are the events that result in floods or droughts, known as extreme precipitation events (EPEs). On the wetter side, EPEs are defined by greater than average precipitation that can span minutes to days (Trenberth et al., 2003; Westra et al., 2013; Lehmann et al., 2015). An EPE occurred in September 2013 along the Colorado (CO) Front Range, United States (U.S.), that unleashed 430 mm of rain – 84% of the 510 mm annual average for the region –in a few days (Uccellini, 2014). A 100 km corridor between Fort Collins, CO and Aurora, CO experienced the most intense precipitation, which led to a disaster zone declaration by the Federal Emergency Management Agency (FEMA) for a ~65,000 km^2 area, about a quarter of the state (Uccellini, 2014). The resulting floods ravaged foothill and valley communities, causing billions of dollars of property and infrastructure damage and the tragic loss of eight lives (Coffman, 2013). The above-surface flooding response to similar extreme events, has been documented and photographed in CO for over 125 years (BASIN, 2005). The subsurface physical response to EPEs however, is not as easily observed or measured in real-time, making it one of the more poorly understood hydrogeologic topics of the 21st century (Vereecken et al., 2015).

Subsurface response to EPEs may involve rapid fluctuations of soil water storage and abrupt water table depth changes (Freeze and Witherspoon, 1967; Jasechko and Taylor, 2015; Tashie et al., 2016). French et al. (1996) examined subsurface response to regular and intense

precipitation at a high elevation study site in the southwest region of the U.S. The shallow soils at this high elevation site extended a meter below ground-level to fractured bedrock. The hypothesis stated that if infiltrating water could penetrate this one-meter physical transition, then it could likely result in groundwater recharge (French et al., 1996). Examination of soil water data found that fall and winter events (October – April) more often infiltrated below a one-meter depth. It was suggested that this was due to: 1) the longer duration of the precipitation events and/or snowmelt, and 2) lower evapotranspiration rates. In contrast, summer events (May – August) were observed to be short–duration and affected by high evapotranspiration, diminishing infiltration past the one-meter depth. The study concluded that it was unclear how soil profiles deeper than a meter may respond to varying precipitation events - either normal or intense, and more research was suggested.

Ng et al. (2010) studied the effects of different climate predictions on diffuse episodic recharge for a study site in the southern High Plains of the U.S. They found that high-rainfall periods, equivalent to EPEs, were more likely to result in recharge during the winter months (December – March), when evapotranspiration is lower and plant roots are dormant. At the same time, the study acknowledged that EPEs and interannual variability were not represented, which may have underestimated a significant fraction of the total recharge predicted. They called for future studies to use field measurements of interannual variability including EPEs where possible, especially for predicting recharge in arid environments, as is the case for the southwestern U.S., the Middle East, most of Australia, and northern African.

Shao et al. (2018) found that consecutive wet years promoted groundwater recharge more significantly than years with average precipitation. This is an important finding because the number of wetter years and drier years are expected to increase in the future whilst years of

average precipitation are expected to decrease (Lehmann et al., 2015; Trenberth, 2011; Wasko et al., 2016). In particular, precipitation events are expected to shorten in duration and increase in intensity (Pendergrass and Knutti, 2018; Pfahl et al., 2017; Prein et al., 2017). This highlights an urgent need to move beyond annual precipitation and use comprehensive interannual variability including EPEs in modeling efforts to better understand subsurface response.

A better understanding of subsurface response to extreme precipitation events can improve future planning of groundwater resource allocations (Gurdak et al., 2009; Kløve et al., 2013). Using the HYDRUS-1D subsurface flow model with average soil hydraulic parameters estimated by Schaap et al. (2001), Corona et al. (2018) found that the prescribed flux (precipitation) and period (30 days, 180 days, 365 days, 730 days) were the most statistically significant predictors of whether an infiltration flux became steady or transient recharge. The study examined the combinations of daily precipitation rates and soil texture classes that could lead to recharge, finding that daily precipitation of lower intensity and finer-grained soils resulted in little to no recharge, while daily precipitation of greater intensity and coarser-grained soils, like sand, resulted in greater recharge. A sensitivity study of parameter influence on infiltration fluxes in the vadose zone was also conducted, but did not consider precipitation variability within a period and the subsequent soil response. Where available, field observations of water table depths and soil water content changes are a useful guide to better understand the EPE-subsurface connection (Jasechko and Taylor, 2015; Thomas et al., 2016). Where data is limited, numerical models coupled with available field data can provide some understanding of the EPE-subsurface connection (Mo'allim et al., 2018; Dadgar et al., 2020).

The objective of this study was to build a HYDRUS-1D model with local field data and examine how the subsurface responded to the EPE that impacted north-central CO in September

2013. The first research question is: (1) How does the water table fluctuate in response to the EPE? And what can a sensitivity study show about parameter uncertainty? The second research question is: (2) How does soil water storage respond to an EPE? Exploring these questions can shed new light on infiltration flux through the subsurface, dynamic changes in subsurface water storage, and the temporal duration of subsurface system response to EPEs.

2.2 Materials and methods

2.2.1 Study area and field data

The Gordon Gulch drainage basin is located 30 km west of Boulder, CO, at an elevation of 2400 to 2800 meters above sea level (Figure 1). The basin has a total area of ~3.6 km^2; the upper basin has an area of ~1.0 km^2, and the lower basin has an area of ~2.6 km^2. Gordon Gulch lies in a montane climate zone, with an average annual precipitation of 520 mm/year (BcCZO, 2020). The basin, hereinafter "Gordon Gulch", was chosen due to the extensive data available. In 2011, the Boulder Creek Critical Zone Observatory (BcCZO) installed six wells in the upper basin of Gordon Gulch. The wells have been monitored and maintained by the BcCZO since December 2011.

Wells #1, #2, and #6 have working pressure transducers which record water table depth variations at 10-min intervals. Well #1 was chosen because it has the largest vadose zone extent (~10 m) of the three wells measuring water table depth, making it the ideal candidate for examining pressure head and soil moisture response to EPEs above the water table. Well #1 is 150 meters away from the small ephemeral stream and 12 meters above the streambed.

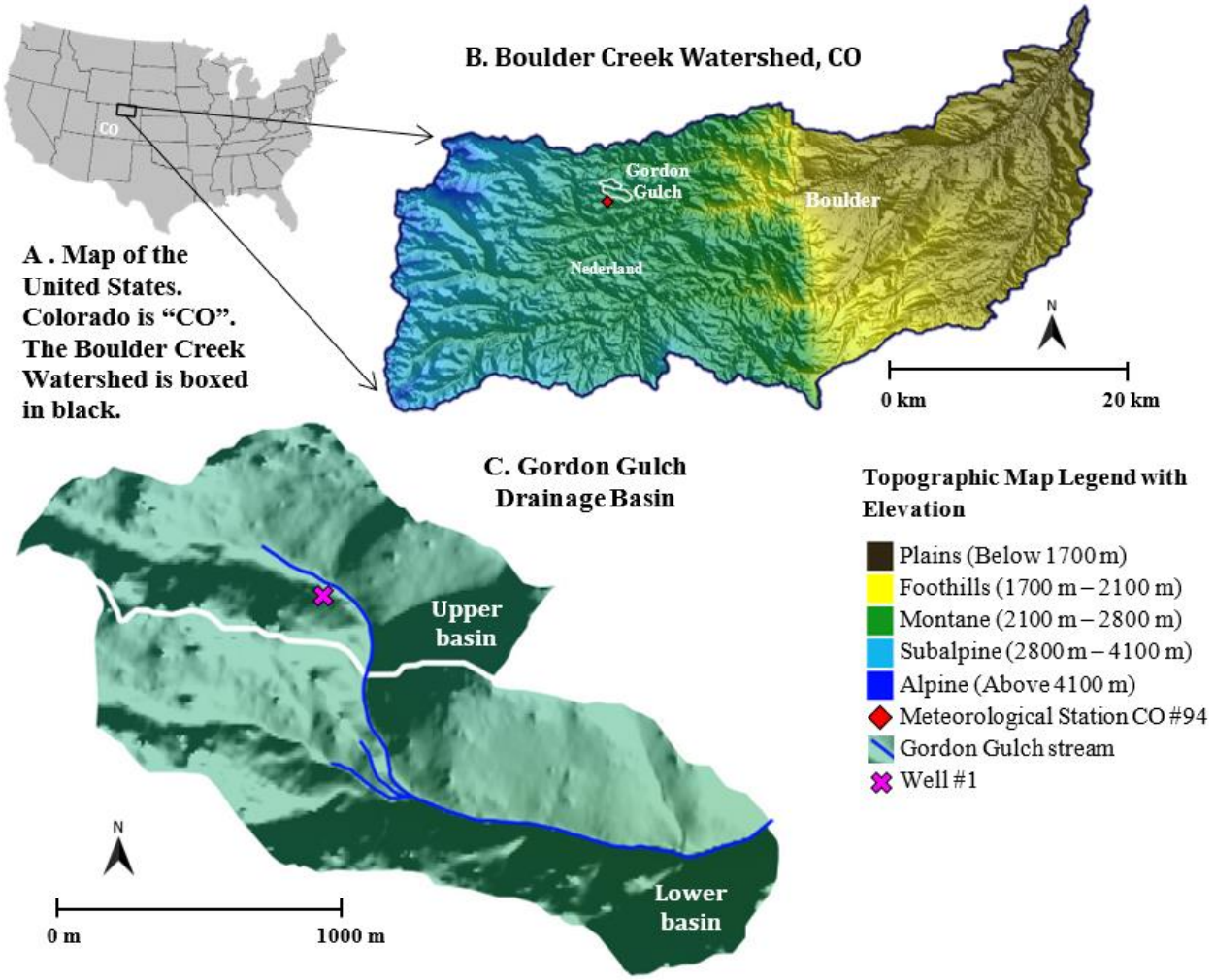

Figure 2.1. A. Map of the United States with the Boulder Creek Watershed, CO, boxed in black. B. Topographic map with elevation of the Boulder Creek Watershed. The Gordon Gulch drainage basin is outlined in white. C. Topographic map of the Gordon Gulch drainage basin, which is in the Montane zone of ~2400 - 2800 m. The blue line indicates a stream. The pink "X" marks the location of well #1, a well in the upper basin that has recorded water table depth at the since December 2011.

The flow record of the nearest stream gauge has not shown evidence of stream influence on well #1 (Henning, 2016; Anderson and Ragar, 2021a; Salberg, 2021). In contrast to well #1, well #2 is influenced by nearby streamflow, while well #6 is affected by lateral flow and upslope infiltration (Henning, 2016; Anderson and Ragar, 2021b; Salberg, 2021). Wells #2 and #6 are henceforth omitted. Well #1 is screened from a depth of 9.4 m to the bottom of the well at 18.55 m, with an average water table depth of ~9.6 m. The soil lithology of well #1 is considered representative of the subsurface of the study site based on the geophysical surveys conducted by

Befus et al. (2011). For this study, the depth of the well penetrating ten meters of the unsaturated zone and ten meters of saturated zone makes it a suitable candidate for studying the dynamics of water table fluctuation.

The daily precipitation data are derived from a meteorological station ~3 km south of the well site, at the Sugarloaf Station #CO94, managed by the National Atmospheric Deposition Program (NADP, 2020). While not co-located, the station experienced the same amount of precipitation as the well site (Uccellini, 2014). It has a record of daily precipitation from 1986 to 2017 (NADP, 2020). To align with the available daily precipitation record, only December 2011 – December 2017 water table depth data is used in this study.

2.2.2 Unsaturated flow in the vadose zone

Subsurface processes are difficult to observe and quantify in real-time. Numerical models, such as the public domain HYDRUS source code (Šimůnek et al., 2008) solve Richards equation to examine one-dimensional water flow in an unsaturated-saturated porous medium and calculate the overall water mass balance. Ignoring the air-phase flow and thermal effects, Richards equation has the following form (Richards, 1931):

$$\frac{\partial \theta}{\partial t} = \frac{\partial}{\partial z}\left[K\left(\frac{\partial \psi}{\partial z} + 1\right)\right] \quad (1)$$

where θ is the water content, t is time (T), ψ is the pressure head (L), $K = K(\psi)$ is the unsaturated hydraulic conductivity dependent on the pressure head (LT^{-1}), and z is the downward distance from the ground surface (L). HYDRUS-1D implements the van Genuchten (1980) equations that use Mualem's (1976) pore-size distribution model. The van Genuchten (1980) equations are a set of closed-form analytical expressions that provide continuous functional relationships for the soil water retention, $\theta(\psi)$ of a soil:

$$\theta(\psi) = \begin{cases} \theta_r + \frac{\theta_s - \theta_r}{[\,1 + |\alpha\psi|^n\,]^m} & \psi < 0 \\ \theta_s & \psi \geq 0 \end{cases} \quad (2)$$

and the unsaturated hydraulic conductivity, $K(\psi)$:

$$K = K(\psi) = K_s S_e^l \left[1 - (1 - S_e^{\frac{1}{m}})^m\right]^2 \quad (3)$$

$$m = 1 - \frac{1}{n}, \qquad n > 1 \quad (4)$$

where S_e is the effective saturation:

$$S_e = \frac{\theta - \theta_r}{\theta_s - \theta_r} \quad (5)$$

where θ_r and θ_s denote the residual and saturated water content; K_s is the saturated hydraulic conductivity, α is a parameter inversely related to the air-entry pressure, n is the pore-size distribution index, and l is a pore-connectivity parameter (Mualem, 1976; van Genuchten, 1980).

Initially, HYDRUS-1D solves equation 1 for ψ (z). The unsaturated hydraulic conductivity as a function of pressure head, $K(\psi)$ in equation 1 is obtained from equations 2 to 5. During each time step, $K(\psi)$ and $\theta(\psi)$ values are obtained iteratively, where ψ (z) values from the prior time step and specified soil parameters ($K_s, \theta_r, \theta_s, \alpha, n, m, l$) in equations 2 - 5 are used to compute $K(\psi)$ at every depth and then used to solve equation 1 for ψ (z). Once the ψ (z) values between iterations converge, HYDRUS-1D proceeds to the next time step.

2.2.3 Model setup

The HYDRUS-1D model can be used to analyze water movement in partially saturated and fully saturated porous media (Šimůnek et al., 2013). The model domain is a 1D vertical column extending downward from the land surface to a depth of 50 m. In the model domain, the pressure heads change from being negative in the unsaturated zone to positive in the saturated

zone. The water table position is found where the pressure head is zero. To reflect the depth of the average water table at the site (Salberg, 2021), the modeled water table was initialized at a 10 m depth.

An initial sensitivity study (not shown) was conducted to identify whether a varying soil column length (z = 20 m, 50 m, 100 m) affected water table fluctuations. Model runs showed that the water table fluctuations were similar when comparing the 50 m and 100 m lengths; as a result, a 50 m length was chosen. The soil column is discretized into 241 nodes. A sensitivity study of refining soil profile discretization (101, 201, 241, 301, 501 nodes) found no significant differences in model results with profile discretization of finer than 241 nodes. The area of interest in this study is the unsaturated zone (z = 0 to 10 m), with denser node spacing in the first 10 meters of the profile (z = 0 to 10 m), with a spacing of 0.072 m between nodes. From z = 10 m to 50 m, node spacing is less dense and increases linearly from 0.072 m to 0.72 m.

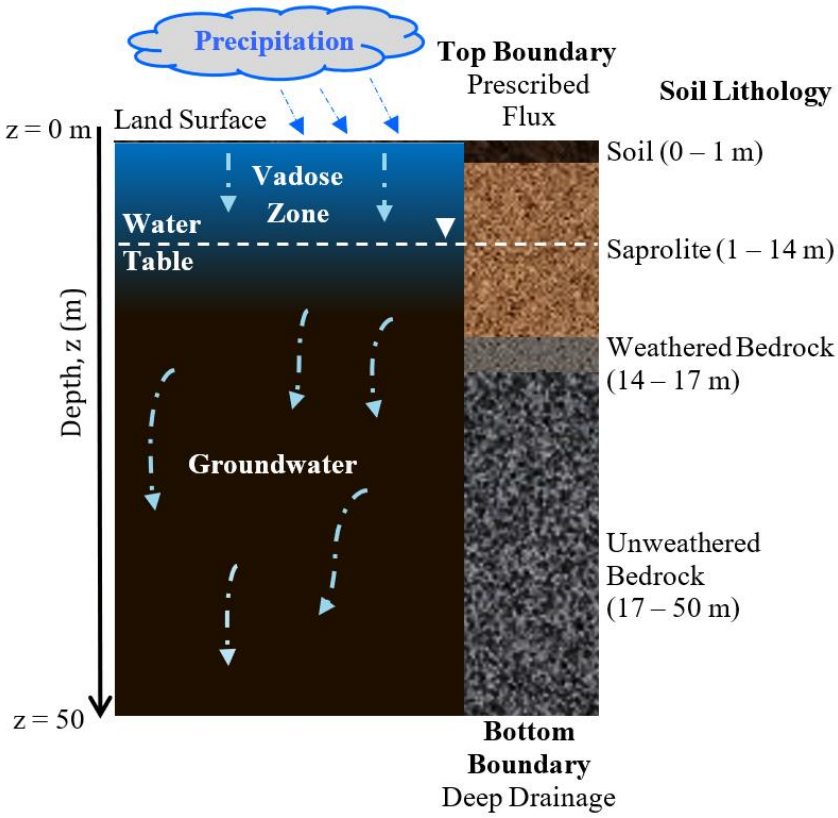

Figure 2.2 One-dimensional model setup. The top boundary is defined by a prescribed flux condition. The bottom boundary is defined by a deep drainage condition. The soil lithology is characterized by the following thickness: 1 m soil, 13 m saprolite, 3 m weathered bedrock and 33 m unweathered bedrock.

A prescribed flux is applied as the top boundary condition (Figure 2.2). A deep drainage flux is applied at the bottom of the soil column. The drainage flux out of the column, $q(\psi)$ is approximated by the following expression (Hopmans and Stricker, 1989):

$$q(\psi) = -Ae^{(B\,|\,\psi_{bottom} - GWL\,|\,)} \quad (6)$$

The variable $q(\psi)$ (LT^{-1}) is the flux across the bottom boundary. The A (LT^{-1}) and B (L^{-1}) are adjustable empirical parameters. The ψ_{bottom} (L) is the pressure head at the bottom boundary and GWL (L) is a long-term equilibrium water table position relative to the bottom boundary, where GWL = 50 m for this study. We calibrated the A and B parameters iteratively to fit the available water table data, following the methodology of Neto et al. (2016). In this study, the unit of length *(L)* is meters (m), and the unit of time (T) is days (d). Model setup allows for a conceptualization of the system such that model results can explain the field observations. Lithology is characterized by four soil texture classes: soil, saprolite, weathered bedrock, and unweathered bedrock (Figure 2.2). This composition has been identified by geophysical surveys, soil pit hand-dug records and well lithology records (Befus et al., 2011; Anderson et al., 2013a; Shea, 2013). The initial parameters $K_s, \theta_r, \theta_s, \alpha,$ and n (Table 2.1), are obtained from a previous, calibrated model and field study of the upper Gordon Gulch drainage basin (Henning, 2016).

Table 2.1. Van Genuchten parameters used to define the four soil layers for the base case.

Soil Layer	Residual Water Content θ_r (1)	Saturated Water Content θ_s (1)	Air-Entry Pressure Value α (m^{-1})	Pore-size distribution n (1)	Saturated Hydraulic Conductivity, K_s (m/d)	Tortuosity l (1)
Soil	0.10	0.28	0.18	1.50	3.0	- 2
Saprolite	0.10	0.20			2.0	
Weathered Bedrock	0.05	0.15			1.5	
Unweathered Bedrock	0.05	0.10			1.0	

Figure 2.2 shows the soil stratigraphy of the well, where a portion of the saprolite layer (10 – 14 m), the entire weathered bedrock layer (14 – 17 m) and the entire unweathered bedrock layer (17 – 50 m) are below the 10 m water table, and considered fully saturated. Since there is no pore space for air to enter in the saturated zone, changes to the α value for the unweathered and weathered bedrock layers have little influence on model results. Similarly, adjusting the n value for the fully saturated layers would not influence model results.

During initial calibration, the tortuosity parameter l was calibrated in conjunction with the other parameters. A literature review found that a tortuosity value of $l = 0.5$ led to poor predictions of unsaturated hydraulic conductivity in 235 soil samples of varying textures (Schaap and Leij, 2000). Schaap and Leij (2000) suggested that the tortuosity be optimized at values of -1 or lower. Yates et al. (1992) suggested that optimal values for l can range from -3 to over 100. Thus, simulations were run with the initial value of 0.5 and in increments/decrements of 0.5 from -10 to 10. A tortuosity of $l = -2$ was determined to be the optimal value for this study.

The model is initialized with a prescribed pressure head distribution that linearly decreases from $\psi = -10$ m at the surface (z = 0 m) to $\psi = 40$ m at the bottom of column (z = 50 m). For model spin-up we use the daily average precipitation minus evapotranspiration, as the recharge boundary condition on the model top. To account for evapotranspiration, we examined previous studies that estimated potential evapotranspiration for the Gordon Gulch basin and found that potential ET values may range from 31% to over 100% of the annual average precipitation (Langston et al., 2015; Hale, 2018; Salberg, 2021). Most recently, Salberg, (2021) calculated monthly total evapotranspiration loss for a catchment-scale water budget of Gordon Gulch. They suggested that ~435 mm of the average 580 mm annual precipitation of the Gordon Gulch drainage basin was lost to ET, a ~75% average. Thus, an evapotranspiration rate of 75% is

used, which is also backed by regional climate model estimates of evapotranspiration (55% – 85%) for the region (Sanford and Selnick, 2013; Reitz et al., 2017). Given the 75% loss to evapotranspiration, the model recharge is 25% of the precipitation amount.

The model was spun-up for 400 days to allow the model to equilibrate to a steady state, considered the initial condition. The initial condition is the state from which the model's transient simulations can initiate. For the transient simulations, we apply the 2011-2017 precipitation record minus evapotranspiration. The transient model is run and calibrated by iteratively adjusting the soil hydraulic parameters: K_s, θ_r, θ_s, α, n. Calibration results in a parameter scenario that allows the modeled water table to best match the field observations. We note that these parameters may not be the only ground truth parameter scenario in the field, they represent the best scenario based on available data and provide model output that can most closely match the field observations.

2.2.4 Statistical indicators

The coefficient of determination (R^2) and the root mean square error (*RMSE*) are used in this study to provide a first order assessment comparing the modeled and observed water table fluctuations. The R^2 describes the proportion of the variance of the field observation data that can be explained by the model. The R^2 can range from 0 to 1, with higher values indicating less probability of error variance. R^2 values greater than 0.50 are acceptable (Moriasi et al., 2007).

The *RMSE* index quantifies the error of a model in predicting observations by measuring the residual spread from the observations. In the equation, P_i denotes the model predicted values and O_i denotes the field observations for a sample n.

$$RMSE = \sqrt{\frac{\sum_{i=1}^{n}(P_i - O_i)^2}{n}} \quad (7)$$

The *RMSE* is the square root of the average of the squared errors. Thus, a lower *RMSE* typically suggests a lower chance of error, with an *RMSE* of zero suggesting a perfect fit between the predicted and observed. The *RMSE* is commonly used because it calculates the error of a comparison in the units of the constituent of interest (Moriasi et al., 2007; Reusser et al., 2009). It has been proposed that *RMSE* values less than half of the standard deviation of the observations may indicate a low probability of error (Moriasi et al., 2007; Singh et al., 2004).

2.2.5 Sensitivity analysis

Once the base case is constructed, we conduct: (1) a sensitivity study of parameters to understand parameter influence on results, and (2) post-processing analysis of simulated soil water storage. The sensitivity study focuses on the local unsaturated zone, where we consider only the soil (0 - 1 m) and the saprolite (1 - 14 m) layers. Six sensitivity simulations are conducted for three parameters (two per parameter): the residual water content (θ_r), the empirical parameter inversely related to the air-entry pressure (α), and the pore-size distribution (n). For each sensitivity simulation, the respective parameter is increased or decreased for the soil and saprolite layers of the base case model (Table 2.2).

Table 2.2 Sensitivity Analysis Changes to van Genuchten parameters: θ_r, α, and n.

Soil Layer	Residual Water Content, θ_r (1)	Parameter Inversely related to the Air-Entry Pressure, α (m^{-1})	Pore-size distribution n (1)
Base Case	0.10 0.10	0.18	1.50
Increase (↑) from the Base Case			
Soil	0.15	2.00	5.50
Saprolite	0.15	2.00	5.50
Decrease (↓) from the Base Case			
Soil	0.01	0.10	1.25
Saprolite	0.01	0.10	1.25

The chosen range of values reflects low and high averages across the 12 soil textural classes as described by Carsel and Parrish (1988). For θ_r, a decrease from the base case (θ_r =

0.01) suggests less water remaining in a soil pore at high tension. An increase (θ_r = 0.15) suggests more water remaining in a soil pore at high tension, which may be indicative of a clay-rich soil (van Genuchten, 1980). For α, a decrease (α = 0.10) suggests a higher minimum matric suction required for air to enter pore spaces, while an increase (α = 2.00) suggests a lower minimum matric suction required. For n, a decrease (n = 1.25) represents a wider pore-size distribution (larger variation in pore sizes in the soil), while an increase (n = 5.50) represents a narrower pore-size distribution.

A preliminary sensitivity analysis of changes in the saturated water content (θ_s) showed similar trends in water table fluctuations to changes in residual water content (θ_r). The residual water content is often overlooked and difficult to assess, in contrast to θ_s, which is often easier to characterize (van Genuchten, 1980; Vanapalli et al., 1998). In a landmark paper, van Genuchten (1980) suggested that the poor matching between the predictive soil water retention curve and the observed curve could be attributed to the θ_r value, which was estimated to be zero. van Genuchten (1980) suggested that future studies consider the importance of having an independent procedure for estimating θ_r. Despite decades of progress, correctly assessing the θ_r for a soil remains a challenge (Vanapalli et al., 1998; Vogel et al., 2001). Including it in the sensitivity analysis as present could help us better understand the consequences of changing the residual water content in subsurface flow modeling. Changes to the saturated hydraulic conductivity, K_s, and tortuosity, l, had negligible effect on model results and henceforth omitted.

2.3 Results

2.3.1 Base case

Water table depths of the field observations and the base case model are compared in Figure 2.3A. Actual model recharge (m/d), described as 25% of the actual precipitation record, is

plotted on the second y-axis. Throughout the six-year period, field observations of water table depth range from ~8.0 m to ~9.7 m. Similarly, base case water table depths range from ~7.6 m to ~9.8 m. Visually, the base case matches the field observations well.

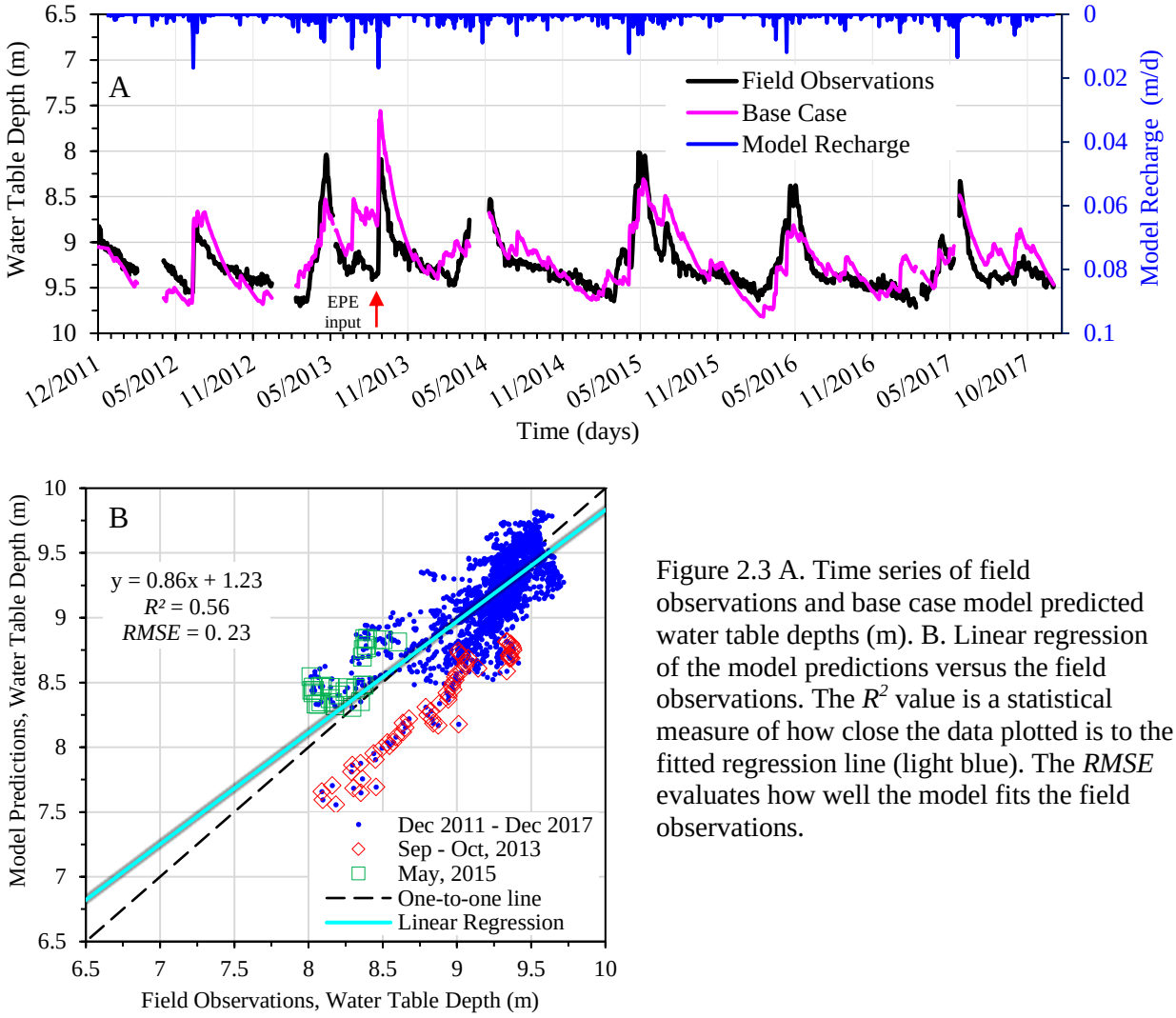

Figure 2.3 A. Time series of field observations and base case model predicted water table depths (m). B. Linear regression of the model predictions versus the field observations. The R^2 value is a statistical measure of how close the data plotted is to the fitted regression line (light blue). The *RMSE* evaluates how well the model fits the field observations.

The September 2013 EPE (red arrow) is an exception, where the base case model predicts a shallower water table depth than the field observations. A linear regression between (Figure 2.3B) the model predictions and the field observations suggest that the model predicts shallower water table depths relative to the field observations. For example, during the EPE, an ~8.1 m

field measurement was predicted to be ~7.6 m by the base case. While the model overestimates water table depths at certain times during the EPE, the changes remain within ~6% of the field observations, suggesting an overall good fit.

The green squares indicate a rainy May in 2015, and the base case model predicts deeper water table depths compared to the field observations. Around 05/2015 (Figure 2.3A), the base case predicts a water table depth of ~8.3 m, compared to the shallower depth of ~8.0 m, of the field observations. This underestimation is within 4% of the field observation. The linear regression gives a R^2 value of 0.56 for the six-year time series.

Singh et al. (2004) published guidelines stating that *RMSE* values less than half the standard deviation (SD) of the field observation data could be interpreted as indicating a good fit of the model to the field observations. The SD of the field observations for the six-year period is 0.40 m. Following the guidelines of Singh et al. (2004), an *RMSE* value equal to or less than 0.20 m, is considered a good model fit. For this study, *RMSE* values between 0.20 m and 0.30 m, and indicate an acceptable model fit. Models with an *RMSE* value higher than 0.30 m indicate a poor fit. The base case *RMSE* (=0.23 m) indicates an acceptable model fit.

2.3.2 Sensitivity analysis of hydraulic parameters

With the base case established, we examine parameter uncertainty in model results by conducting a first-order sensitivity analysis of van Genuchten parameters: θ_r, α, n for the soil and saprolite layers (Table 2.2).

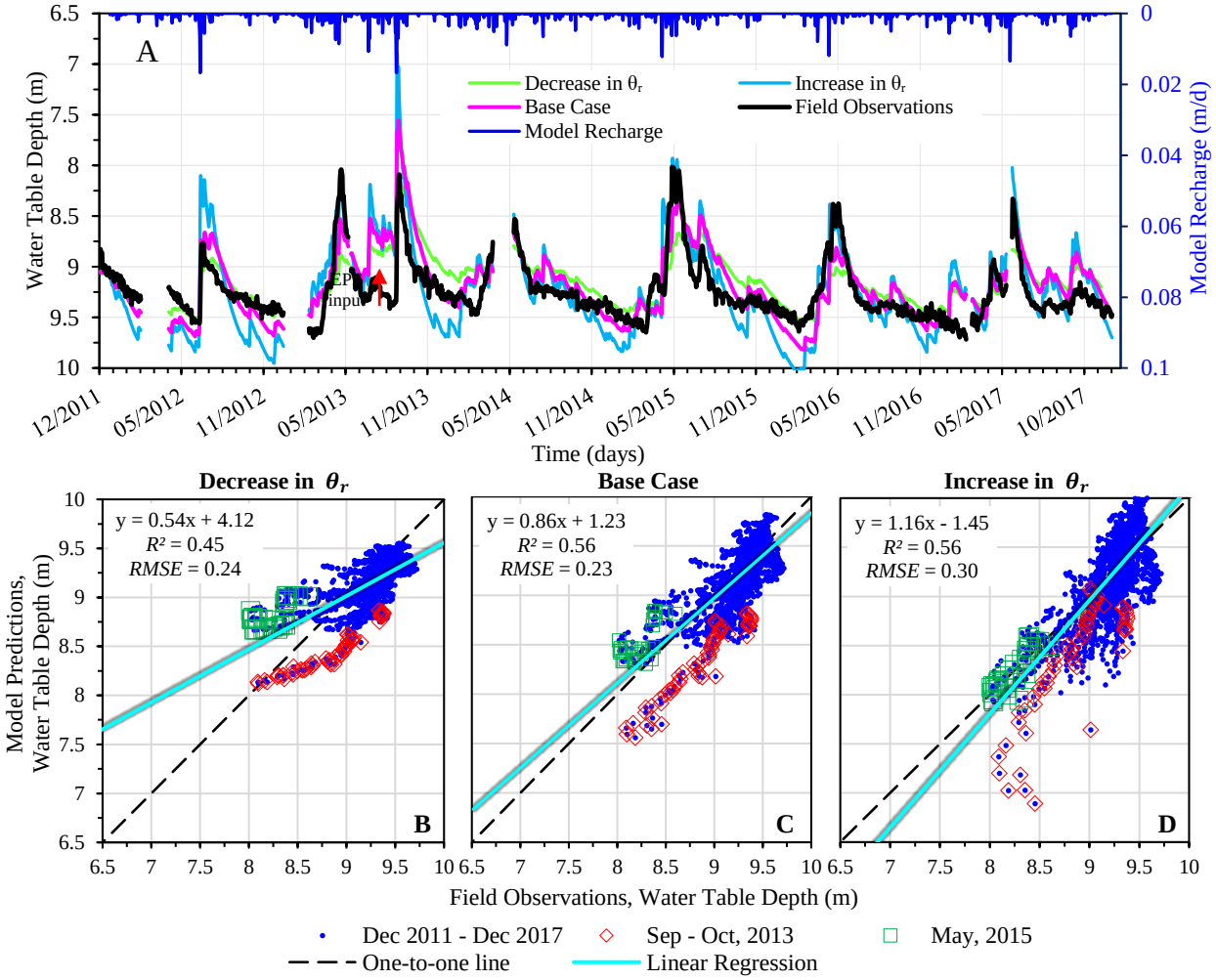

Figure 2.4 A. Time series of field observations and model predictions of water table depths (m) for varying residual water content, θ_r. The "decrease in θ_r" represents a 0.09 decrease from the base case to 0.01 for both layers 1 and 2. The "increase in θ_r" represents a 0.05 increase to 0.15 for both layers 1 and 2. B – D: Linear regression of the model predictions versus the field observations for the decrease (B) and increase (D) in θ_r.

Figure 2.4A shows model sensitivity to changes in residual water content, θ_r. When θ_r is decreased for both layers one and two, the model consistently predicts higher water table depths

(overestimates). The decrease in θ_r affects the correlation between the observations and base case, with R^2 = 0.45. The *RMSE* (= 0.24 m) indicates an acceptable model fit. Increasing θ_r causes an exaggerated response with water table fluctuations over- or under- estimating the field observations (Figure 2.4A, 2.4D). An increase in θ_r results in a dramatic. The R^2 remains at 0.56, and the *RMSE* (= 0.30 m) indicates an acceptable model fit at the cusp of being a poor model fit.

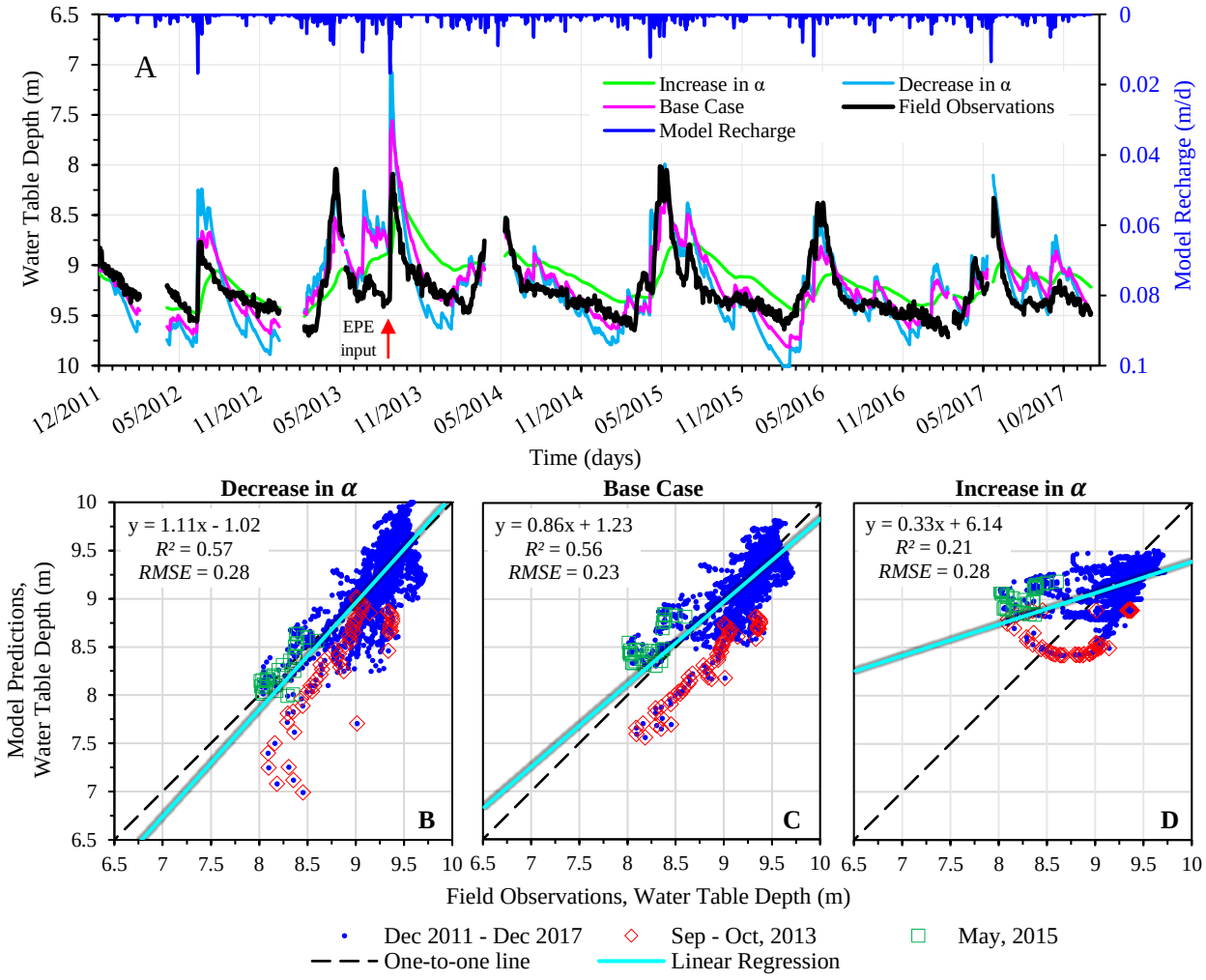

Figure 2.5 A. Time series of water table depths (m) from field observations and model predictions (increase, base case, decrease) for alpha, α. The "decrease in alpha, α" represents a 0.08 decrease from the base case to 0.10, for both layers. The "increase in alpha, α" represents a 1.82 increase to 2.00. B – D: Linear regression of the model predictions versus the field observations for the decrease (B) and increase (D) in α.

Figure 2.5A shows model sensitivity to changes in α (m^{-1}), a parameter inversely related to the air-entry pressure. The base case $\alpha = 0.18$ (m^{-1}). For the sensitivity study, α is decreased for the soil and saprolite layers (layers one, two) to 0.10 (m^{-1}). A decrease in α allows the model to conform to field observations, but consistently predicts slightly deeper water table depths (Figure 2.5A). Figure 2.5B shows that a decrease in α slightly improves the R^2 (= 0.57). The *RMSE* (= 0.28 m) indicates an acceptable model fit. When α values are increased to 2.0, water table fluctuations are subdued (Figure 2.5A). The R^2 value decreases (= 0.21 m) with an increase in α, suggesting a poor correlation (Figure 2.5D) between model results and field observations. The respective *RMSE* (= 0.28 m) indicates an acceptable model fit.

Figure 2.6A shows model sensitivity to changes in n (1), an empirical parameter that characterizes pore-size distribution index, where $n > 1$ (eq. 4). HYDRUS-1D sets the default values for n, by soil texture class. For the sensitivity study, n is decreased to 1.25 from the base case. A decrease in n allows the model to better conform to field observations, but predicts slightly deeper water table depths (Figure 2.6A). The decrease in n marginally improves (Figure 6B) the R^2 (= 0.58), and the *RMSE* (= 0.28 m) indicates an acceptable model fit. In contrast, an increase in n to 5.50 causes a dampened response and water table fluctuations are subdued. An increase in n lowers R^2 to 0.38 (Figure 2.6D), highlighting a poor correlation between field observations and model results. The *RMSE* (= 0.25 m) indicates an acceptable model fit.

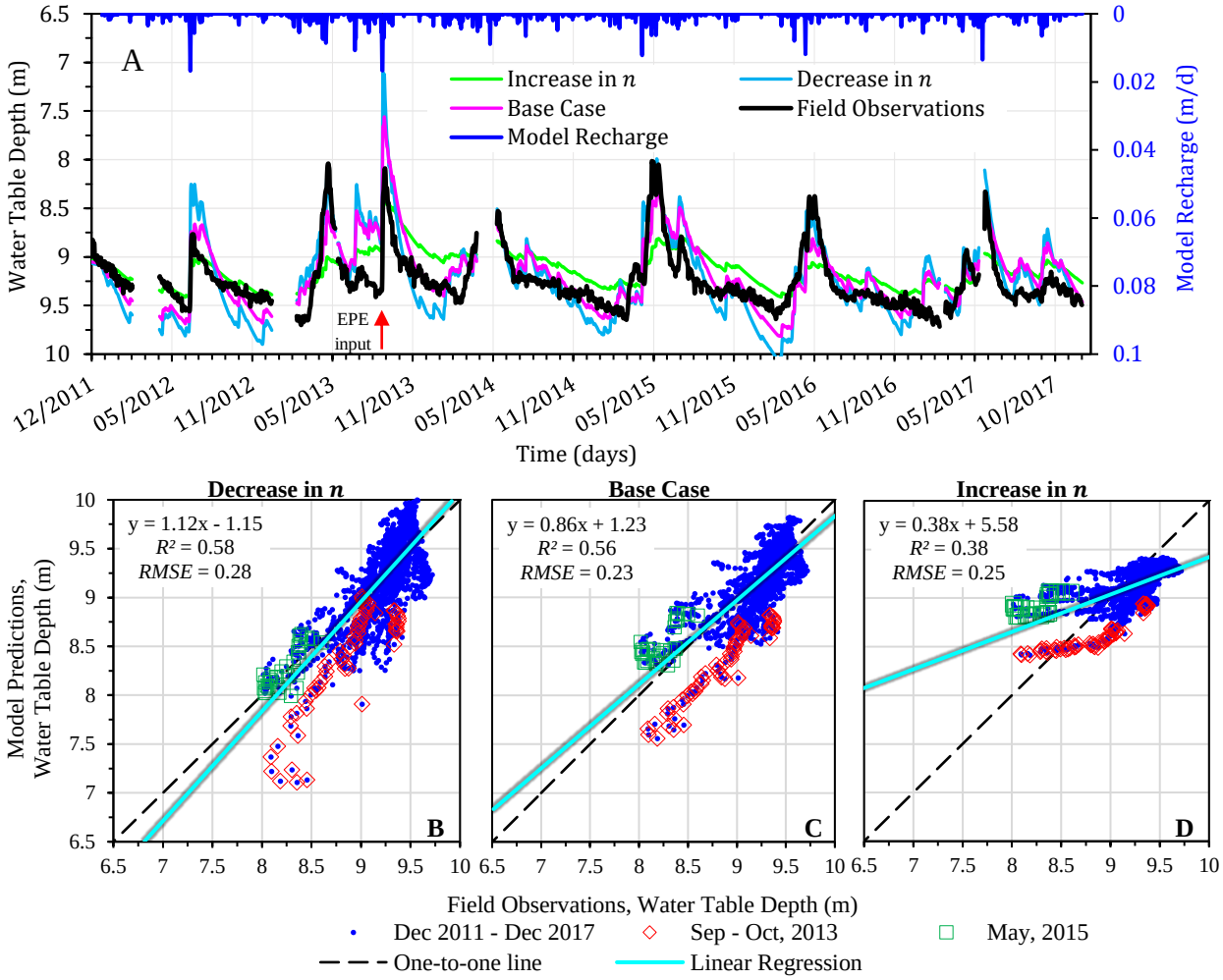

Figure 2.6 A. Time series of water table depths (m) from field observations and model predictions (increase, base case, decrease) for the pore-size distribution, n. The "decrease in n" represents a 0.25 decrease from the base case to 1.25, for both layers. The "increase in n" represents a 4.00 increase to 5.50, for both layers. B – D: Linear regression of the model predictions versus the field observations for the decrease (B) and increase (D) in n.

2.3.3 Soil water storage of the base case

In HYDRUS-1D, the soil water storage, V (m) is defined as the volume of water per unit area at a point in time. The V (m) is calculated as:

$$V = \sum_e \Delta z_i \frac{\theta_i + \theta_{i+1}}{2} \quad (8)$$

where θ_i and θ_{i+1} are water contents evaluated at elements i and i+1, and Δz_i is the size of the element (Šimůnek et al., 2008, 2013). The summation in equation 6 is taken over the 241

elements in the flow domain. Figure 2.7 shows the base case variability in soil water storage, V (m) from December 2011 to December 2017 by water year, denoted by 'WY'. For example, WY2013 denotes the water year from October 1st, 2012, to September 30th, 2013. The dashed lines represent the average soil water storage for the respective water year.

The soil water storage V (m) for the profile ranges from 6.50 m to 6.62 m (Figure 2.7). Soil water storage (m) values (i.e., 6.50 m) are the product of the average water content across the entire domain, (i.e., 0.13) and the total column length, 50 m (i.e., 0.13 x 50 m = 6.50 m). As such, a higher V suggests that a greater portion of the available pore space is saturated, indicating that the subsurface is wetter than average (Figure 2.7). A lower V suggests that less of the available pore space is saturated, indicating that the subsurface is of average wet conditions or drier. A wetter subsurface may result in recharge, while a drier subsurface may result in little or no recharge. For example, soil water storage from 01/2013 and 03/2013 shows lower soil water storage, indicating little or no recharge. In contrast, after the September 2013 EPE, at the end of WY2013, the soil water storage is at its highest point in the six-year record. The following WY2014 and WY2015 (dotted lines) exhibit the highest average V per WY, indicating that the EPE influenced subsurface processes for two water years after its occurrence.

2.4 Discussion

2.4.1 Water-table response to the 2013 EPE

The September 2013 EPE had a long-term consequence in the subsurface, as shown by the Gordon Gulch field observations of water table fluctuations. The one-dimensional, four-layered, homogeneous base case model represented the best scenario based on available data and provided model output that could most closely match the field observations. Visually, a comparison of the field observations and base case model showed good compatibility.

Figure 2.3A shows a consistent downward trend in the water table depth that reaches its deepest point (~9.6 m), every March of every year except 2014. In March 2014 (after the EPE), the deepest point is ~9.25 m, a shallower depth than any other year. It is not until March 2015 that the water table deepens to ~9.6 m again. We speculate that the contrast between the consistent water table depths of ~9.6 m, and the shallower water table depth of March 2014 (~9.2 m) is evidence that the water table remained shallower in large part due to the EPE footprint, which remained until at least March 2015. The field observations and model results agree that the subsurface continued to respond to the EPE infiltration flux for at least 18 months after the event, longer than previously suggested (Henning, 2016).

For further comparison between the field observations and model results, we calculated the R^2 coefficient to measure the goodness of fit between the field observations and base case model. In addition, the *RMSE* was used to calculate the square root of the variance of the residuals to indicate how close the observed data are to the model results. The base case model is considered an acceptable model fit as indicated by the R^2 (= 0.56) coefficient, and *RMSE* (= 0.23 m) value (Table 2.3). The results present opportunities for improvements while highlighting the limitations of the 1D modeling approach. For example, the 1D modelling approach does not simulate lateral flow process at the hillslope scale or regional scale which could affect the goodness of fit. The greatest deviation in correlation occurred during the EPE, where the base case predicted a higher water table (~7.5 m) than the field observations (~8.2 m), though still within a 10% margin of the field data. While out of the scope of this study, a 2D or 3D model accounting for lateral flow may improve the goodness of fit between the field observations and modeled results.

Table 2.3 Model response to increases and decreases of the van Genuchten parameters: θ_s, α, and n.

	Residual Water Content, θ_r (1)	Air-Entry Pressure, α (m^{-1})	Pore-size distribution, n (1)	Base Case
Parameter Change	Increase ↑	Increase ↑	Increase ↑	R^2 = 0.56 *RMSE* = 0.23
Water Table Response	exaggerated	dampened	dampened	
R^2 value	0.56	0.21	0.38	
RMSE	0.30	0.28	0.25	
Parameter Change	Decrease ↓	Decrease ↓	Decrease ↓	
Water Table Response	dampened	exaggerated	exaggerated	
R^2 value	0.45	0.57	0.58	
RMSE	0.24	0.28	0.28	

2.4.2 Sensitivity analysis of hydraulic parameters: θ_r, α, n

A sensitivity analysis examined how model response may be affected by parameter change. The R^2 value calculated for each sensitivity analysis ranged from 0.21 (poor correlation) to 0.58 (acceptable correlation). The *RMSE* value calculated for each sensitivity analysis ranged from 0.24 m to 0.30 m (Table 2.3). All *RMSE* values were indicative of acceptable model fit, with one model (increase in θ_r) at the cusp between acceptable and poor, despite an acceptable R^2 value. The lack of *RMSE* values indicating a good fit model could be attributable to the high sensitivity that the *RMSE* has to outliers, i.e., the largest differences between field observations and model results. Two EPEs of different temporal extents, the September 2013 EPE, and the May 2015 month-long rain event, resulted in significant differences between the field observations of water table depths and the model results. These EPE-derived outliers skewed the RMSE away from indicating a good model fit. Future studies examining EPEs may benefit from statistical methods that are not strongly biased towards outliers.

The visual outcome of the sensitivity runs can be described by two general responses: dampened or exaggerated (Table 2.3). An exaggerated response indicates shallower and deeper

water table depths relative to the base case. A dampened response would indicate the opposite of exaggeration – more smoothed, tempered variation.

2.4.3 Residual water content, θ_r

From the sensitivity analysis, decreasing the residual water content, θ_r (Figure 2.4D), yields a dampened water table response. Increasing the θ_r (Figure 2.4B), yields an exaggerated water table response. These responses are likely due to the local effective porosity of the material (Horton et al., 1988). The effective porosity, also thought of as the "drainable porosity", is defined as the percentage of interconnected void space with respect to the bulk volume (Brooks and Corey, 1964):

$$\phi = \frac{V_p}{V_b} \tag{9}$$

Where ϕ is the effective porosity (1), V_p is the total volume of interconnected voids (m^3), and V_b is the bulk volume (m^3). A soil with a higher effective porosity, ϕ has a larger (>) total volume of interconnected voids, V_p, relative to the bulk volume, V_b. Decreasing θ_r (with θ_s held constant) increases the total volume of interconnected voids, V_p, relative to the bulk volume, V_b, indicating a higher ϕ. Decreasing θ_r can result in water being more readily held in pore spaces (higher ϕ), slowing the rate of flow. Water held in pore spaces may result in a slower drainage out of the pore spaces, which can dampen fluctuations of the water table. In contrast, increasing θ_r (with θ_s held constant), decreases the total volume of interconnected voids, V_p, relative to the bulk volume, V_b, indicating a lower ϕ. A lower ϕ can be indicative of a faster draining soil with minimal available pore space for water to fill. A low ϕ may allow faster flow through the subsurface, thus resulting in more rapid water table response (Figure 2.4B).

2.4.4 Air-entry pressure, α

The alpha parameter, α (m^{-1}) is inversely related to the air-entry pressure, the matric suction value required to fill (empty) pore spaces (Nimmo, 2006). Its purpose is to serve as an approximation of the steepest section of the soil water retention curve (van Genuchten, 1980). Where the soil water retention curve is steepest, the water content (typically plotted on the y-axis) is most sensitive to changes in the pressure head (typically plotted on the x-axis). This is also mathematically evident in the van Genuchten equations (eq. 2), where α as part of the denominator influences the fraction from which the quotient determines water content as a function of pressure head, $\theta(\psi)$ given $\psi < 0$ (Brooks and Corey, 1964; Mualem, 1976; van Genuchten, 1980). The base case $\alpha = 0.18$ m^{-1} is considered the best fit for the field data.

Results from the sensitivity study show that decreasing α (relative to the base case) causes the water table to fluctuate more rapidly (Figure 2.5A). Conceptually, a decrease in α translates to an increase (due to the inverse-relation) in the minimum matric suction value that air must attain to enter a pore space. Whilst pressure builds so that air can attain the higher matric suction to enter a pore space, water can enter (drain) these same pores with greater ease. The ease at which water can fill (drain) pores in the unsaturated zone is known as the unsaturated hydraulic conductivity, K (m/d). A decrease in α can allow water to fill (empty) pores with greater ease, resulting in a larger K value which consequently results in more rapid downward flow, and thus more dramatic water table fluctuations, as seen on Figure 2.5A.

An increase in α translates to a decrease (due to the inverse-relation) in the minimum matric suction value that air must attain to enter a pore space. A lower minimum matric suction value means that air can more easily enter (exit) pores. Water has difficulty entering pore spaces now relative to air, and as a result, the unsaturated hydraulic conductivity, K of the soil,

decreases. A smaller K value implies slower and delayed downward flow to the water table. The downward flow is dampened with time as it slowly moves downward, resulting in smoother water table fluctuations (Figure 2.5A).

2.4.5 Pore-size distribution index, *n*

Changes to the pore-size distribution parameter, *n*, result in higher correlation between the field observations and model results. In the van Genuchten soil hydraulic functions used to determine θ (eq. 2), both α and ψ are raised to the power of the pore-size distribution parameter, *n*. The *n* parameter is further used to determine the empirical parameter, *m* (1) (eq. 4), where *m* is an exponent used to solve for the unsaturated hydraulic conductivity and the soil water retention (eq. 2 - 3). Figure 2.6 shows that a decrease in *n* causes an exaggerated response, while increasing *n* causes a dampened response. Physically, *n* represents the allowed abundance of varying pore-sizes in a volume of soil (Nimmo, 2006). When water infiltrates a soil with a narrow and uniform distribution of pore sizes, the water flux can more easily fill (or empty) pores at the same matric suction. In the subsurface, matric suction is defined as the difference between pore air pressure and pore water pressure. Conventionally, pore air pressure is equal to atmospheric pressure and is ignored (Chiorean, 2017).

Expanding the allowed distribution of pore-sizes (higher *n*) increases the possible variation of pore sizes. A soil with more highly varying pore sizes requires highly varying matric suction for water to fill (empty) the varying size pores, generally retarding downward flow (Nimmo and Park, 2004; Zhang et al., 2019). In response, the water flux becomes dampened in the subsurface, visually translating to a smoother water table response (Figure 2.6). In contrast, narrowing the allowed distribution of pore-sizes (smaller *n*) reduces the possible variation of pore sizes. Reducing the possible variations in pore sizes allows water to fill (empty) pores more

easily with the same matric suction. Such ease allows water to flow downward at a faster rate, resulting in a more exaggerated water table response (Figure 2.6A).

2.4.6 Soil water storage response to an EPE

The modeled changes in soil water storage suggest new developments that affect our understanding of how the subsurface responded to the 2013 EPE. First, there was a rapid increase in soil water storage in late WY2013. After the EPE, soil water storage remained elevated through WY2014 and into WY2015. The early part of WY2014 had comparatively higher soil water storage during the winter months (12/2013 – 03/2014) relative to all other water years for the same time frame. The heightened soil water storage during this time frame may be a strong indicator that groundwater recharge occurred for several months after the EPE, especially given likely minimal evapotranspiration during the winter months.

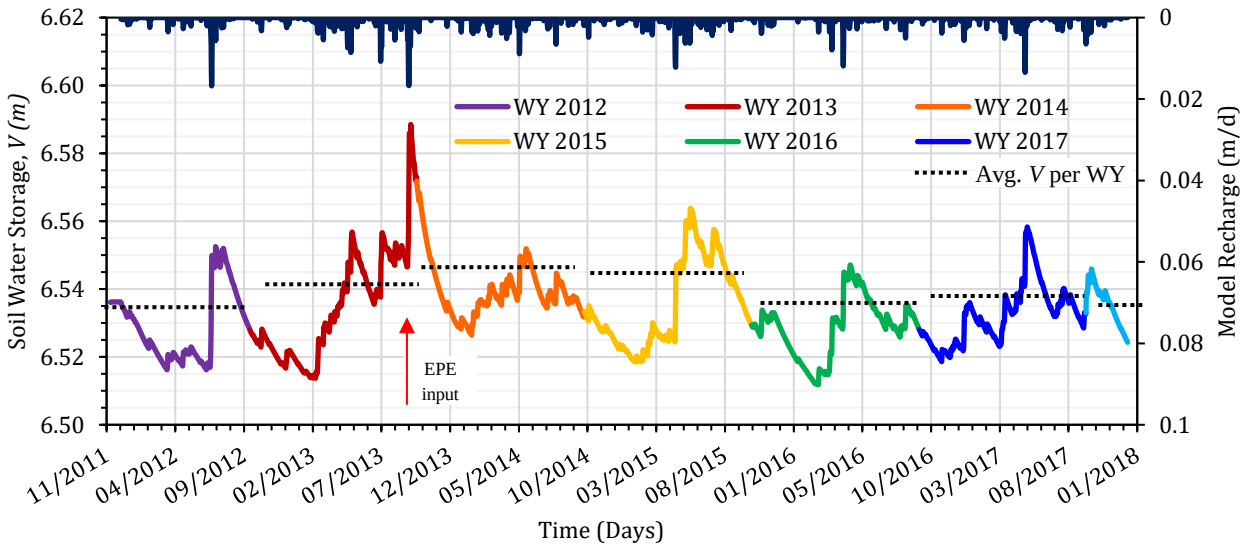

Figure 2.7 December 2011 to December 2017 time series of soil water storage, *V* (m) for the base case. The dotted lines denote the average *V* (m) per water year, WY.

Additionally, the increase in *V* (Figure 2.7) post- EPE is sustained through WY2015. During WY2016 (02/2016), soil water storage reaches a winter low as seen during WY2012

(02/2012) and WY2013 (02/2013), pre-EPE. The modeled changes in soil water storage suggest that a two-year recovery occurred in response to the EPE-induced infiltration flux.

2.5 Conclusions

The 2013 Colorado extreme precipitation event (EPE) not only flooded the surface and rivers downstream but resulted in rapid infiltration and heightened water table response. Here are the conclusions we draw from this study:

- Both the field observations and model results showed a water table rise following the EPE which persisted for ~18 months before the water table recovered to pre-EPE levels.
- Average annual soil water storage post-EPE for water years, WY2014 and WY2015 was higher than all other water years in the record, indicating a wetter subsurface post-EPE.
- The post-EPE could serve as a hydrologic buffer that stores a portion of extreme precipitation for various seasons.
- A sensitivity study of model parameters showed that the modeled water table was most sensitive to changes in the empirical parameter that represents the pore size distribution value, *n*. Since pore-size distribution cannot be measured in the field, it is essential to scrutinize the values to which empirical parameters are set in simulations.

Given the characteristics in geology, hydrology, and geography considered, the model setup and results could be applicable to regions of similar characteristics. By assessing the potential for unsaturated zone profiles to serve as natural storage space for EPE-induced infiltration, this study could provide a scientific basis for water managers to timely utilize the stored water that may be released to streams over time. More research regarding local subsurface response to EPEs is needed, as EPEs are predicted to occur more frequently worldwide (Trenberth, 2011; Lehmann et al., 2015; Wasko et al., 2016). Understanding the effects of individual EPEs on the subsurface

could also provide the basis for predicting aggregated effects over longer time scales. From another viewpoint, in headwater regions, snowmelt is the primary source of groundwater recharge. While the rate of snowmelt is typically not as dramatic as EPEs, snow could occur at an accelerated rate under warming (Pepin et al., 2015). This study could be informative for projecting the potential hydrologic consequences of accelerated snowmelt. More broadly, the results of this study contribute to a better understanding of how the subsurface can function as a long-term hydrologic buffer for infiltration from an extreme precipitation event before recharge occurs.

CHAPTER 3: WATER-TABLE RESPONSE TO EXTREME PRECIPITATION EVENTS

Abstract

Extreme precipitation events (EPEs) will play a significant role in influencing soil–water and groundwater storage worldwide. We examined water-table response to EPEs for 17 cases representative of soils and climate settings across the United States. Precipitation data from NOAA's Precipitation Frequency Data Server were used for each case to characterize 1-day extreme precipitation events (EPEs) with annual exceedance probabilities of 0.1 % over an average baseline date range of 1981–2011. The inverse solution in the HYDRUS-1D modeling software was used to obtain the soil–water retention curve for each case. Non-EPE and EPE scenarios were modeled and compared to examine maximum water-table displacement ($\Delta_{WTD\ max}$) and recession time (t_{rec}). The $\Delta_{WTD\ max}$ ranged from 0.6 to 2.4 m across cases and were not directly controlled by EPE amount; instead, $\Delta_{WTD\ max}$ was inversely related to available porosity. Soils with low available porosity experienced large $\Delta_{WTD\ max}$ compared to soils with higher available porosity. In cases with larger diffusivity values, the modeled water table receded faster than in cases with smaller diffusivity values. This was because water-table recession times, t_{rec}, were inversely related to hydraulic diffusivity. For all cases, recession back to pre-EPE levels ranged from months to years suggesting an increased role by the unsaturated zone in buffering EPEs that should be considered in future EPE-groundwater modeling studies.

This chapter has been previously published:

Corona, C.R., Ge, S., and Anderson, S.P., 2023. Water-Table Response to Extreme Precipitation Events. Journal of Hydrology, p.129140. https://doi.org/10.1016/j.jhydrol.2023.129140

3.1 Introduction

Communities worldwide depend on groundwater for water needs in urban, rural, industrial and agricultural settings (Alley, 2002; Wu et al., 2002; Miguez-Macho et al., 2007). In the United States alone, groundwater use increased by 8% while surface-water use decreased by 14% from 2010 to 2015 (Dieter et al., 2018; Maupin, 2018). In an average precipitation year, groundwater use is offset by the replenishment of groundwater stores due to infiltration from precipitation (Freeze, 1969; Vereecken et al., 2015). The rate of infiltration is controlled by the subsurface soil (rock) physical properties, such as the medium's water content, soil porosity, and soil hydraulic conductivity, all of which influence the timing and distribution of infiltration through the unsaturated zone and to the water table (Freeze and Cherry, 1979).

Traditional theory suggests that low-intensity precipitation events over long periods can lead to a constant rate of infiltration through the subsurface that is ideal for replenishment of groundwater stores (Freeze and Cherry, 1979). However, it remains unclear how the subsurface will respond to climate change, which is expected to cause a decline in low-intensity precipitation events (Lehmann et al., 2015; Li et al., 2019; Myhre et al., 2019) and cause an increase in shorter, more extreme (higher intensity) precipitation events (Westra et al., 2013; Prein et al., 2017; Pendergrass and Knutti, 2018; Sun et al., 2021). A climatic change towards shorter, more extreme precipitation events (EPEs) is likely to affect subsurface response, which, combined with increased economic reliance on groundwater, may exacerbate the strain on groundwater resources (Wilkinson and Cooper, 1993; Green et al., 2011; Dieter et al., 2018).

The potential influence of an EPE on subsurface response can be illustrated by comparing water-table response to two rainfall scenarios, differing only by the addition of an EPE (Figure 3.1). Recall that water table fluctuates over time, generally rising towards the surface with large infiltration events, then decreasing once precipitation stops (Freeze and Cherry, 1979). In the non-EPE scenario (Figure 3.1a), the water table fluctuates in response to average precipitation. Addition of an EPE (Figure 3.1b) may result in a large influx of infiltrating water and rapid water-table displacement towards shallower depths, before receding over time to non-EPE water table levels. Water-table displacement and recession time (Figure 3.1b) after an EPE can provide insightful understanding of subsurface response to EPEs.

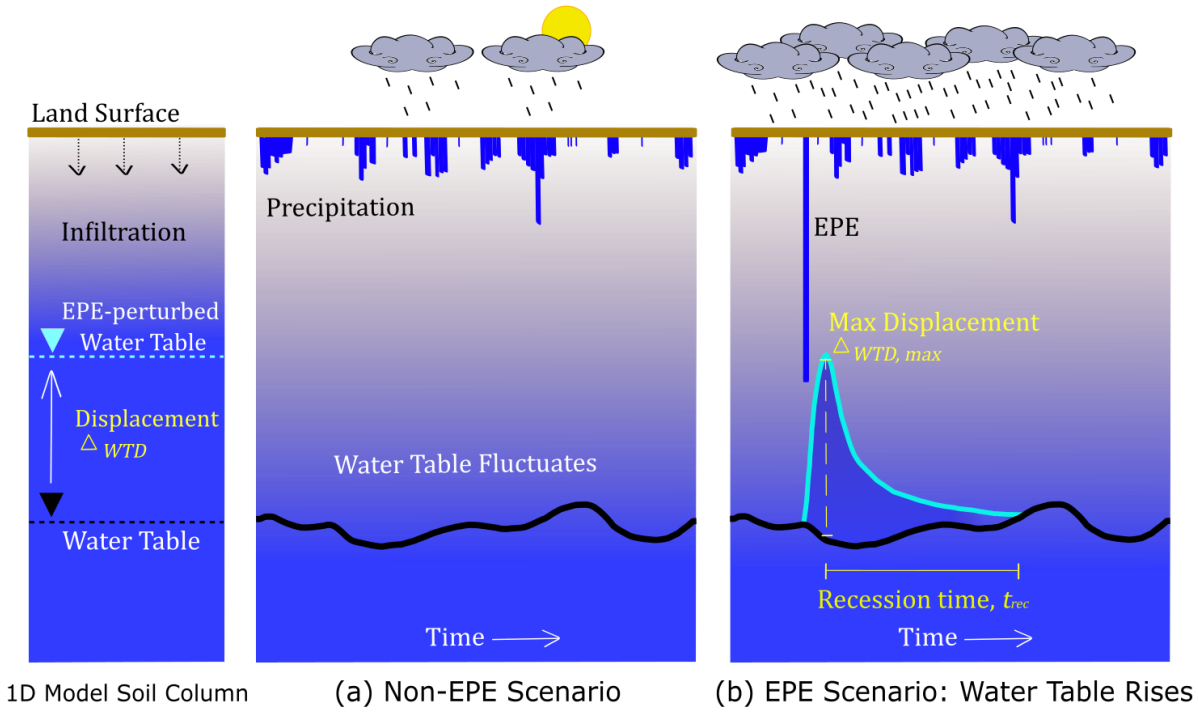

Figure 3.1 Conceptual model showing: the 1D model soil column on the left, (a) The non-EPE scenario portraying the typical water-table fluctuations (black line) expected with normal precipitation patterns over time. (b) EPE scenario, contrasting the water-table response to an EPE (light blue line) with the non-EPE scenario (black line). Following the EPE, the water table was displaced upward, reaching a maximum ($\Delta_{WTD\ max}$) relative to the non-EPE scenario. The recession time (t_{rec}) was defined as the time needed for water-table displacement to recede to within 5% of $\Delta_{WTD\ max}$.

Only recently have the effects of EPEs on groundwater recharge been the subject of field and modeling campaigns (Wang et al., 2015; Thomas et al., 2016; Wittenberg et al., 2019; Golian et al., 2021). For example, rapid transmission of infiltrating water from EPEs to the water table has been detected through stable isotopic composition of precipitation and groundwater in the tropics (Jasechko and Taylor, 2015) and the North China Plain (Zheng et al., 2019). Many studies have focused on determining links between precipitation patterns and recharge during EPEs (Tashie et al., 2016; Golian et al., 2021; Boas and Mallants, 2022). In contrast, fewer studies have considered subsurface conditions, which include soil properties, and their effect on EPE-induced recharge (Crosbie, 2003).

Studies that have addressed subsurface response to EPEs have generated somewhat conflicting results. Examining subsurface response to EPEs in differing semi-arid basin sites, Crosbie (2003) identified a positive correlation between water table depth and recharge, where recharge increased with depth to the water table. They found that recharge amount generally increased with precipitation amount (Crosbie, 2003). For example, at one field site, they found that 200 mm of monthly rainfall resulted in monthly recharge of 100 mm, while 450 mm of monthly rainfall resulted in monthly recharge of 250 mm (Crosbie, 2003). Tashie et al. (2016) identified a positive correlation between recharge and precipitation event duration across a sub-tropical region, and an inverse correlation between recharge and the average rate of precipitation during the event. Where Crosbie (2003) found that recharge increased with depth to the water table, Tashie et al. (2016) found no relation between recharge and depth to water table in the sub-tropical study area. Golian et al. (2021) considered recharge timing and precipitation amount using the groundwater balance equation and water-table fluctuation method (Healy and Cook, 2002), finding that water-table response to EPEs across the semi-arid and arid field sites was

delayed by 6-months. This is in contrast to the faster, days-long response identified in other semi-arid and arid climates (Crosbie, 2003), humid continental climates (Joachim et al., 2011) and sub-tropical climates (Tashie et al., 2016). The differing results of EPE impacts on water tables across varying soils and climate conditions warrants further study. Mathematical models that use existing soil data to examine physical responses to EPEs could help clarify many of these divergent findings (Vereecken et al., 2015).

Mathematical models have been used along with local climate data to explore the effects of EPEs on groundwater recharge. Using the Soil Water Balance (SWB1) model (Westenbroek et al., 2010), Zhang et al. (2016) found that EPEs accounted for a greater fraction of recharge in the Northern High Plains Aquifer (~60%) compared to average precipitation events, despite comprising less than 40% of the total precipitation from 1950 - 2010. While the study did not simulate unsaturated flow, the results showed that more of the infiltration from the EPE became potential recharge compared to average precipitation events, highlighting the importance of EPEs (Zhang et al., 2016). Scanlon et al. (2018) compared regional-scale groundwater level changes between land surface models and remote sensing products, finding that the models underestimated large decadal water storage trends, both increasing and decreasing, relative to the remote sensing product. It was suggested that the discrepancies between the model results and satellite data was due to a lack of representing unsaturated zone processes and soil properties in the land surface models (Scanlon et al., 2018).

To consider the climactic influence on subsurface response, studies have used HYDRUS-1D (Šimůnek et al., 2005), a one-dimensional unsaturated-saturated flow model capable of modeling vadose zone processes (Leterme et al., 2012; Boas and Mallants, 2022; Corona and Ge, 2022). Leterme et al. (2012) used HYDRUS-1D to examine the effects of climate change on

groundwater recharge near a disposal facility for radioactive waste, and found that recharge would decrease in some areas near the disposal site but increase slightly at another nearby site over the next 10,000 years of climatic change. Focusing on an arid basin in central Australia, Boas and Mallants (2022) used HYDRUS-1D to estimate groundwater recharge from EPEs at a bare soil and vegetated site with statistically generated sets of hydraulic properties, finding that more recharge occurred at the bare soil site compared to the vegetated site after every EPE. Corona and Ge (2022) created a HYDRUS-1D model of the subsurface in a semi-arid region to examine water-table response to an EPE, finding that the water table remained elevated for at least 18 months after the event. To our knowledge, no study has yet to consider subsurface response to EPEs across various climates and soils.

As precipitation patterns shift to more extreme events (both droughts and EPEs alike), a knowledge gap remains regarding how unsaturated zone hydrological properties influence water-table response to EPEs. To address this knowledge gap, time series data about EPEs are needed, as well as soil hydrological properties. These data, coupled with a subsurface flow model which considers the physics of the unsaturated zone and water table dynamics provide a mechanism to investigate the subsurface response to EPEs. This study explored water-table response to EPEs in diverse settings, based on water-table response for 17 cases across the United States. First, we used water content as a function of pressure head data from the Unsaturated Soil hydraulic Database (UNSODA) with HYDRUS-1D inverse modeling to obtain the soil-water retention curves for the 17 cases. Second, we create two models for each case: a “non-EPE” scenario and an “EPE” scenario, which are used to explore the differences in water-table response. We address the following questions: (1) How does EPE amount impact water-table response? (2) How do

properties of the unsaturated zone influence water-table response to EPEs? (3) How do properties of the saturated zone influence post-EPE water table recession time?

Table 3.1 Case locations and precipitation stations organized longitudinally from west to east. The precipitation collection agency, station name, ID, and coordinates are provided.

Case Location	Case ID	Soil Data Source	Precipitation Station Name	Precipitation Station ID, Agency	Latitude (°)	Longitude (°)
Mukilteo, Washington	WA	USGS	Mukilteo Lighthouse Park	USGS	47.90	-122.33
Antioch, California	CA	UNSODA	Antioch Pump Plant #3	USC00040232, NOAA	37.99	-121.75
Superior, Arizona	AZ	UNSODA	Queen Valley 0.2 E	US1AZPN0077, NOAA	33.30	-111.29
Las Cruces, New Mexico	NM	UNSODA	Mesilla 2.3 E	US1NMQA0116, NOAA	32.27	-106.77
Betasso, Boulder County, Colorado	CO	BCCZO	Betasso	Boulder Creek CZO (BcCZO)	40.01	-105.33
Fort Collins, Colorado	CO2	UNSODA	Fort Collins	53005, CO State University	40.58	-105.09
Perkins, Oklahoma	OK	UNSODA	Perkins	USC00347003, NOAA	35.97	-97.03
Iowa State University, Iowa	IA	UNSODA	Turkey River, Spillville	431226091570101, USGS	43.21	-91.95
Hancock, Wisconsin	WI	UNSODA	Hancock Experimental Farm	USC00473405, NOAA	44.12	-89.54
Auburn, Alabama	AL	UNSODA	Auburn #2	USC00010425, NOAA	32.60	-85.47
Oak Ridge, Tennessee	TN	UNSODA	Oak Ridge ATDD	USW00003841, NOAA	36.00	-84.24
Watkinsville, Georgia	GA	UNSODA	Athens Ben Epps Airport	USW00013873, NOAA	33.95	-83.33
Laurinburg, North Carolina	NC	UNSODA	Laurinburg	USC00314860, NOAA	34.75	-79.47
Live Oak, Florida	FL	UNSODA	Live Oak 0.4 NE	US1FLSW0001, NOAA	30.30	-82.98
Panola County, Mississippi	MS	UNSODA	Batesville 2.2 SSE	US1MSPN0001, NOAA	34.29	-89.93
Blackstone, Virginia	VA	UNSODA	Fort Pickett	USC00441322, NOAA	37.04	-77.95
Atlantic Highlands, New Jersey	NJ	USGS	Mt. Mitchill Scenic Overlook (MMSO)	MMSO, USGS	40.41	-74.01

3.2 Methods

3.2.1 Data collection

3.2.1.1 Soil hydraulic properties

Study cases are shown on a map of the principal aquifers of the United States (Figure 2a) for reference (U.S. Geological Survey, 2003). We used soil hydraulic data from UNSODA, a database with field and lab measurements of soil properties, such as water content as a function of pressure head, hydraulic conductivity as a function of pressure head, soil bulk density, among other measurements, for sites in the United States (Nemes et al., 2001). Measurements from each UNSODA soil were used to construct case-specific soil characteristic curves (water content as a function of pressure head), and obtain the vertical saturated hydraulic conductivity (K_s) for 14 of the 17 cases (Nemes et al., 2001). U.S. Geological Survey (USGS) data were used for the Mukilteo, WA case (Smith et al., 2017) and the Atlantic Highlands, NJ case (Fiore et al., 2021). Boulder Creek Critical Zone Observatory (BcCZO) data were used for the Betasso site (Anderson and Ragar, 2022).

We also plot the respective soil texture classes onto a modified version of the U.S. Department of Agriculture's (USDA, 1987) soil textural triangle classification system (Figure 3.2b). Soil texture class was reported for each study case, but not detailed textural data. The symbols on the soil texture triangle (Figure 3.2) therefore are only correct to the texture class level. The soil descriptions in the UNSODA database and the USGS reports suggest that twelve of the soils plotted are of a sandy texture, three soils are predominantly silty, and one soil is predominantly clay (Figure 3.2b). The AZ and CO cases are not plotted because the USDA textural triangle does not apply to rock materials (Garcia-Gaines and Frankenstein, 2015).

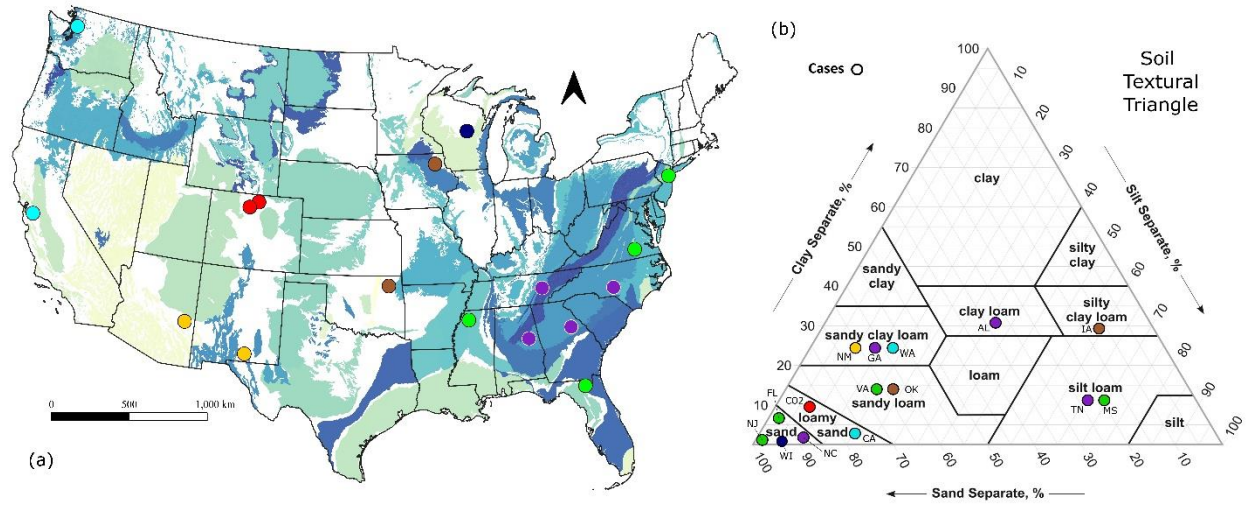

Figure 3.2 (a) Approximate case locations (colored dots) across the United States. Principal aquifer systems are colored on the map for reference (U.S. Geological Survey, 2003). (b) Black triangle delineates the 12 soil textural classes. Dots show soil texture class for soils used in this study, but do not specific clay-silt-sand percentages, which were not reported in site data. Not shown: AZ (tuffaceous rock) and CO (unweathered bedrock).

3.2.1.2 Daily precipitation

Daily precipitation data were sourced from the nearest precipitation station to each case location as shown in Table 3.1. Precipitation stations are managed by the National Oceanographic and Atmospheric Administration (NOAA, 12 stations), the USGS (3 stations), the Colorado State University (1 station), and the BcCZO (1 station). The precipitation datasets used were 95% complete or better for a continuous five-year period between 2000 – 2021.

3.2.1.3 Extreme precipitation events

The precipitation amount that constitutes an EPE can vary with climate (Perica et al., 2013). To maintain a uniform EPE definition across the diverse climates from which cases were derived, we define EPEs using precipitation-depth-frequency curves from the NOAA National Weather Service, Hydrometeorological Design Studies Center's Precipitation Frequency Data Server (NOAA, 2017). NOAA used a regional frequency analysis approach to calculate the annual percent chance of occurrence of precipitation amounts at a station (Perica et al., 2013).

Only precipitation stations with a minimum of 30 data years were considered for calculations of annual exceedance probability, AEP (Perica et al., 2013). For 16 cases, the most recent precipitation date range considered by NOAA was 1981 – 2011. For the WA case, the most recent 20-year precipitation range used was 1940 – 1970 (Miller et al., 1973). To conduct the analysis, first, the maximum precipitation series per year (of a given duration, i.e., 24-hours) from a station was collected and merged with maximum precipitation series data (same duration) from 8 to 16 nearby stations. The collected data (for the station and its surroundings) was then used to calculate a regional average of maximum precipitation measured for the given duration (Perica et al., 2013). This regional average was weighted by the length of the available data record to create a set of data points that represented increasing precipitation amount for various exceedance probabilities. A cumulative distribution function, the Generalized Extreme Value distribution, was then fitted to the data (Perica et al., 2013). The Generalized Extreme Value distribution employs the maximum-likelihood approach for large samples to calculate the probability of exceedingly rare or extreme events (Hosking et al., 1985; Perica et al., 2013).

The National Weather Service conducted the procedure for each precipitation duration (i.e., 1-hour, 3-days, etc.) for all stations (Perica et al., 2013). The end product was a smooth curve relating precipitation depth (m) to annual exceedance probabilities (AEP). The AEP is the probability of a precipitation event exceeding a certain depth once or more in any given year (Hosking and Wallis, 1997; Perica et al., 2013). Figure 3.3 shows AEPs ranging from 1/2 (50% chance of occurrence) to 1/1000 (0.1% chance of occurrence). The WA case AEP was extended to a 1000-year AEP using a line of best fit as described by Miller et al. (1973). To account for the spatial variability of precipitation from case to case, the EPE was defined as a 1-day (or 24-hour) precipitation event with a 0.1% (1-in-1000 year) chance of occurrence (Figure 3.3).

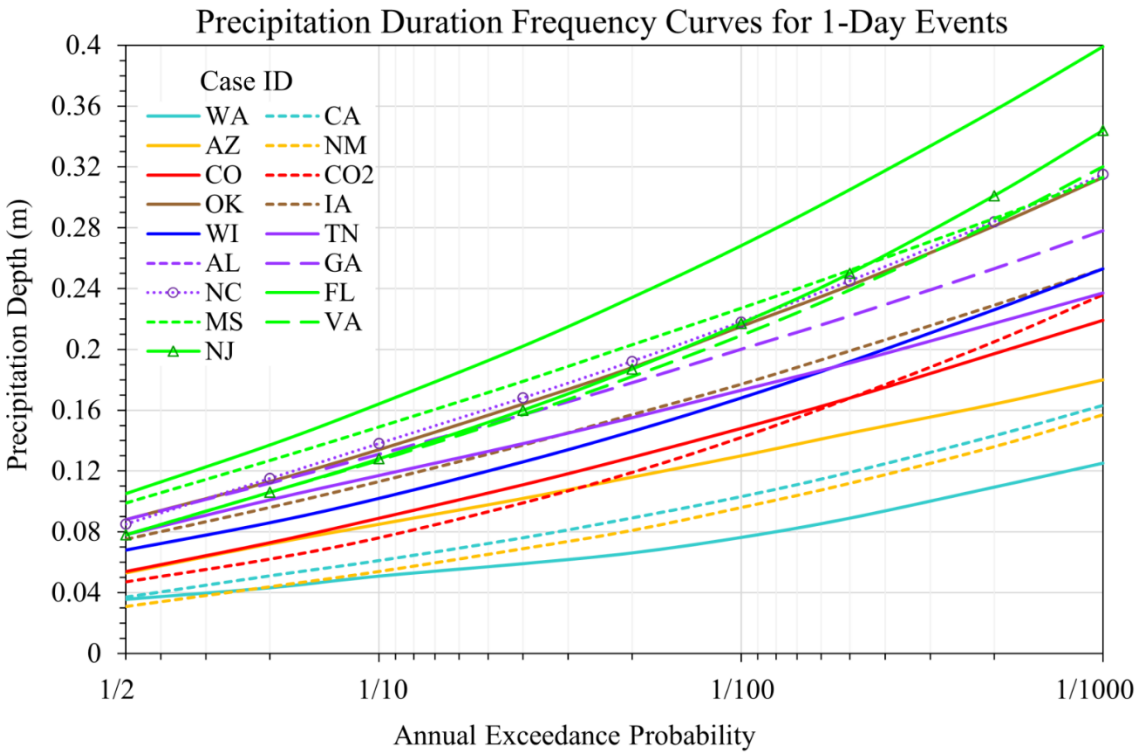

Figure 3.3 Precipitation depth frequency curves for 1-day durations. On the x-axis, the Annual Exceedance Probabilities (AEPs) range from 1/2 (50% chance of occurrence in a year) to 1/1000 (0.1% chance of occurrence in a year) for the 17 cases. We use the 1-day precipitation depth frequency curve at the AEP of 1/1000 to define a case EPE.

3.2.2 Subsurface flow modeling

3.2.2.1 Governing equation

The nonlinear nature of flow in the subsurface was considered by Richards (1931), who hypothesized that the pressure head (ψ) and unsaturated hydraulic conductivity (K) were both functions of the water content (θ) (Richards, 1931; Youngs, 1988). Ignoring thermal effects and air-phase flow, the one-dimensional Richards equation based on water balance takes the form:

$$\frac{\partial \theta}{\partial t} = \frac{\partial}{\partial z}\left[K\left(\frac{\partial \psi}{\partial z} + 1\right)\right] \quad (1)$$

where θ is the water content, t is time (T), ψ is the pressure head (L), K is the unsaturated hydraulic conductivity (L/T), and z is the vertical coordinate representing depth below the surface (L). Numerical models such as HYDRUS-1D (Šimůnek et al., 2008) solve Richards

equation for pressure head distribution in an unsaturated-saturated porous medium. HYDRUS-1D employs the van Genuchten (1980) equations for soil hydraulic properties. Using a pore-size distribution model described by Mualem (1976), the van Genuchten-Mualem equations provide continuous functional relations for soil water retention, and the unsaturated hydraulic conductivity, of a soil (Mualem, 1976; van Genuchten, 1980). The water content and pressure head curve $\theta(\psi)$, is called the soil-water retention curve (SWRC):

$$\theta(\psi) = \begin{cases} \theta_r + \frac{\theta_s - \theta_r}{[\,1 + |\alpha\psi|^{nn}\,]^m} & \psi < 0 \\ \theta_s & \psi \geq 0 \end{cases} \tag{2}$$

where θ_r and θ_s denote the residual and saturated water content, respectively, α is a parameter inversely related to the air-entry pressure, *nn* is a pore-size distribution index, and *m* is a parameter used to relate *nn* to *K* (Mualem, 1976; van Genuchten, 1980). The pore-size distribution index, *nn*, is the relative abundance of each pore size in a representative volume of soil (Nimmo, 2013). The *nn* typically ranges from 1 to 10: smaller *nn* (~ 1.01) represents smaller pores and less variation in pore sizes, while larger *nn* (~ 10) is descriptive of larger pores and greater variation in pore size (Cary and Hayden, 1973; van Genuchten, 1980; Šimůnek et al., 2005). Van Genuchten (1980) showed *nn* to be smaller for clay soil and larger for sandier soils. The hydraulic conductivity-pressure head, *K(ψ)* relation of a soil is given by:

$$K = K(\psi) = K_s S_e^l \left[1 - (1 - S_e^{\frac{1}{m}})^m\right]^2 \tag{3}$$

$$m = 1 - \frac{1}{nn}\,, \qquad nn > 1 \tag{4}$$

where K_s is the saturated hydraulic conductivity (L/T), *l* is a pore-connectivity parameter (dimensionless) and S_e is the effective saturation, also dimensionless (Mualem, 1976; van Genuchten, 1980). The effective saturation (dimensionless), S_e, is calculated as:

$$S_e = \frac{\theta - \theta_r}{\theta_s - \theta_r} \quad (5)$$

For this study, the K_s for each case was obtained from the UNSODA catalog (Nemes et al., 2001). If UNSODA did not specify K_s for a case, the soil series from the UNSODA database was used in a query in USDA's National Resource Conservation Service online browser (NRCS, 2022a) to identify the possible K_s values. This was done for the IA (NRCS, 2022b), NM (NRCS, 2022c) , OK (NRCS, 2022d), TN (NRCS, 2022e), and WI (NRCS, 2022f) cases. Based on the information provided in the soil series report, an average K_s value was assigned to the soil.

3.2.2.2 Model Setup and Assumptions

The model domain was set up as a 1D vertical column extending from the land surface to a depth of z = 50 m. A sensitivity study (not shown) of the effects of soil column length greater than 40 m (i.e., 50 m, 60 m, 75 m, and 100 m) found no significant differences in model results. Thus, 50 m was chosen for the model domain. The model domain consisted of two-layers, with the top layer extending from z = 0 to z = 10 m, and the bottom layer extending from z = 10 m to z = 50 m. The soil column was discretized into 1000 elements of 0.05 m each. Soil hydrologic properties for each case were determined using the inverse estimation in HYDRUS-1D, which minimizes the summation of the squared differences between the observed water content values and the simulated water content values (Šimůnek et al., 2005). The best-fitting soil hydraulic parameters (θ_r, θ_s, α, and nn) were applied uniformly across both layers of the model domain for each case. The K_s value assigned to the bottom layer was smaller than the value assigned to the top layer in order to represent the typical decrease in K_s with depth below the surface.

This 1D approach ignored lateral flow, topographic influence, and multi-layered heterogeneity, factors which influence long-term water-table fluctuations. For this study, 1D infiltration and diffusion were likely dominant processes. The 1D approach used here focused on

the magnitude of the response to EPEs and time of recession with different hydraulic parameters during short-time periods. In contrast to the complications and added assumptions of 3D models, simple 1D models of systems can show generic responses to EPEs and other climate phenomena, allowing for attention to be focused on possible controlling factors that may otherwise be masked (Wilkinson and Cooper, 1993; Corona et al., 2018).

The top boundary condition at the land surface was set as an atmospheric boundary condition (i.e., precipitation over time, units: L/T) with surface runoff possible but without surface ponding. The bottom boundary condition was defined as a deep drainage flux. The downward drainage flux out of the column is generally at a distance away from the water table, where $q(\psi)$ was approximated by (Hopmans and Stricker, 1989):

$$q(\psi) = -Ae^{(B\,|\,\psi_{bottom} - GWL\,|\,)} \tag{6}$$

The $q(\psi)$ (L/T) was a flux crossing the bottom boundary. The A and B were adjustable empirical parameters, where A represents a rate (L/T) and B represents an inverse length (1/L) (Hopmans and Stricker, 1989; Neto et al., 2016). The ψ_{bottom} (L) was the pressure head at the bottom boundary. GWL (L) was a reference pressure head at some distance away (Hopmans and Stricker, 1989); as a first-order approximation, we assumed that GWL = 50 m. The A parameter was related to the saturated hydraulic conductivity, K_s. The B parameter was calibrated iteratively to allow the water table to initialize at the desired water table depth (i.e., 5 m or 27 m) following the methodology of Neto et al. (2016) and Corona and Ge (2022).

We determined the model's initial conditions as follows. First, we assigned an initial pressure head distribution that linearly increased from ψ = - 5 m at the surface (z = 0 m) to ψ = 45 m at the bottom of column (z = 50 m) for 16 of the 17 cases. Of the UNSODA soils, only the AL, WI, and GA cases had water table depth data, which was a limiting factor (Nemes et al.,

2001). To compensate, the modeled water table was initialized at a 5 m depth for the 11 of 14 cases that did not have water table depth data. The steady state water table for each case varied between 3 m and 9 m depth depending on case-specific soil properties and precipitation input. In the model, the unsaturated zone extended from the ground surface to a depth of ~5 - 9 m, where the water table was located. The saturated zone extended from the water table to the bottom of the soil column (z = 50 m). The top layer included unsaturated/saturated conditions, while the bottom layer was fully saturated. To account for the deeper water table at Betasso, the model was initialized with a prescribed ψ distribution that increased linearly from ψ = - 27 m at the surface (z = 0 m) to ψ = 23 m at the bottom (z = 50 m). The water table depth at the Betasso site was initialized at a depth of 27 m to reflect field measurements at the monitoring well (Anderson and Ragar, 2022).

For model spin-up, daily average precipitation minus evapotranspiration was used as the atmospheric boundary condition at the model top. We used existing regional estimates of evapotranspiration to determine a case-specific average (Sanford and Selnick, 2013; Reitz et al., 2017). The model spin-up served two purposes: 1) to allow the model to equilibrate to a steady state from which transient runs were executed, and 2) to iteratively calibrate the B parameter.

The resulting steady state model was the starting condition from which transient conditions commence (i.e., variable precipitation is applied). The transient model used case-specific daily precipitation minus case-specific evapotranspiration. For cases with UNSODA and BcCZO soil data, the transient models employed a 5-year precipitation dataset. For cases with USGS soil data, the available precipitation dataset record (~2-5 years) was used. The transient model had two scenarios: a “non-EPE” scenario where only the non-EPE precipitation record was applied (Figure 3.1a) and an “EPE” scenario that included a 1-day EPE near the beginning

of the precipitation record (Figure 3.1b). The results from the two scenarios were compared for each case to examine the differences in water-table response.

3.2.3 Water-table response: displacement and recession

Two aspects of water-table response were considered: water-table displacement, Δ_{WTD}, and the recession time, t_{rec}. Once the non-EPE scenarios and EPE scenarios were run, the respective water table depths from the model output were calculated. The water-table displacement, Δ_{WTD}, was calculated as the difference between the EPE and non-EPE modeled water table levels (m) computed at each time step. The maximum difference in water-table response between the EPE and non-EPE scenario was designated the $\Delta_{WTD\ max}$. After max displacement, the water table remained elevated above non-EPE levels for varying amounts of time (months to years), eventually receding to non-EPE scenario simulation levels. The water table recession time, t_{rec}, was defined as the time needed for water table-displacement, Δ_{WTD} to recede to within the 5% of $\Delta_{WTD\ max}$ (Figure 3.1b). From a temporal perspective, this approach only focused on the period of response to EPEs and the subsequent recovery, which occurred within a few years and is not representative of long-term water-table fluctuations.

3.3 Results and discussion

To show an example of how the water table may respond to an EPE, we introduce data from the Betasso site in the Front Range of Colorado, part of the Boulder Creek Critical Zone Observatory (BcCZO). In 2013, a monitoring well at Betasso captured groundwater response to an EPE (Anderson et al., 2013b; Langston et al., 2015), which we modeled using a 1D approach. Following the case study, subsequent sections discuss water-table displacement, Δ_{WTD}, and water table recession time, t_{rec}, as a function of soil properties for all 17 cases. We note that while the soil texture classes and EPE amounts presented were related to soil measurements and

precipitation station data from various sites, these cases may apply to other sites provided similar conditions, such as: water table depths, EPE amounts, and geological materials.

3.3.1 Case study: Betasso, Boulder Creek Critical Zone Observatory

The Colorado Front Range experienced a catastrophic precipitation event that lasted a week in September 2013. The heaviest rain fell over a ~24-hour period several days into the storm, with local sustained rainfall rates of 25-50 mm/hour and 24-hour rainfall annual exceedance probabilities < 1/1000 years (Gochis et al., 2015). The presence of co-located precipitation gages and monitoring wells for months before the storm afforded a rare opportunity to examine an extreme event in detail. Corona and Ge (2022) had previously modeled the Δ_{WTD} in response to this EPE at Gordon Gulch, a site ~10 km to the west of Betasso. At Gordon Gulch, the EPE resulted in water-table displacement of 1.50 m and recession time of ~18 months in a well with a water table at ~9 m depth (Corona and Ge, 2022). At the Betasso site, more rain was received during the 2013 EPE than the Gordon Gulch site. The groundwater level at Betasso rose ~2.4 m as the water table rose from ~27.5 m to 25.1 m (depth below land surface) over a period of about fourteen days. We acknowledge that this was a rare case where the 1-Day EPE was preceded by two days of precipitation and followed by three more days of precipitation (Anderson et al., 2022). The purpose of this case study was to show how numerical models can adequately simulate field measurements that captured the water-table response to an EPE.

Figure 3.4 compares water table depths modeled for an EPE and a non-EPE scenario with the measured water table depths at Betasso. The EPE scenario used the measured precipitation record, while the non-EPE scenario was created by setting the precipitation to 0 for the heaviest rain day (September 12, 2013). Other parameters and input data are identical in both scenarios (Figure 3.4). The modeled water-table displacement from the EPE scenario and the measured

water-table displacement generally agree, with the modeled water table peak at ~25.0 m and the measured peak at ~25.2 m.

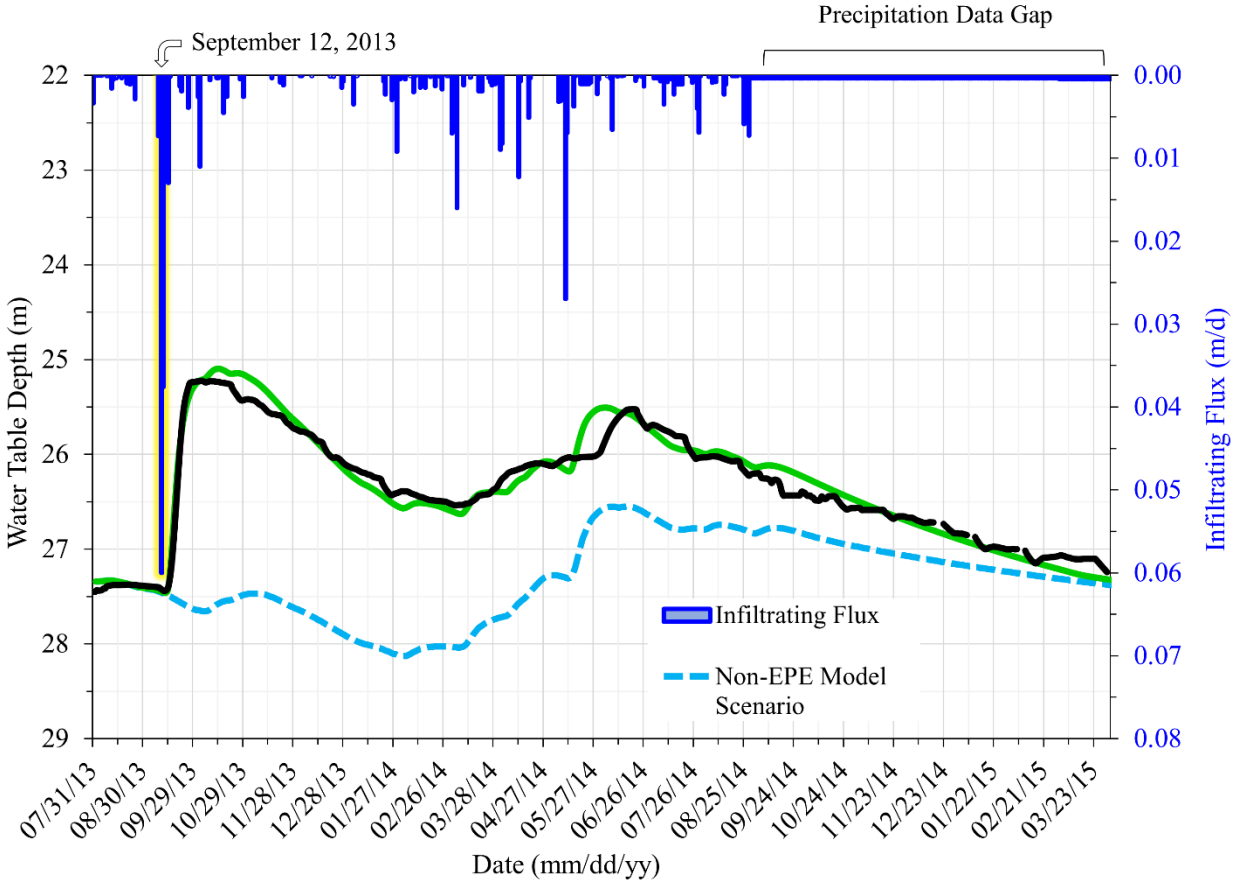

Figure 3.4 Measured water-table history at Betasso (black line) from August 2013 to April 2015, showing response to the September 2013 EPE. Modeled water table with EPE (green line) and the non-EPE (dashed blue line) scenarios shown. The infiltration flux (m/d) (dark blue line) was derived from a meteorological station at Betasso. The one-day September 12, 2013 EPE is highlighted in yellow. From September 2014 through early 2015, the Betasso meteorological station went offline for repairs. To compensate, the annual average precipitation amount was used to estimate daily precipitation minus evapotranspiration (0.00045 m/d) for the data gap.

The model, however, simulates the peak occurrence about 25 days after the EPE, whereas the field observations measured peak occurrence 14 days post-EPE. The two quantitative differences are likely due to the model assumptions of using a simple 1D model with two layers of similar hydraulic parameters. Nevertheless, the 1D model is a good assumption for the Betasso monitoring well as the well is located at a local drainage divide. The 1D results

accomplish general agreement with field observations. Both the measured and the EPE modeled water table remained elevated for at least 1.6 years after the EPE, receding back to match the non-EPE model scenario water table in the spring of 2015.

3.3.2 Water-table displacement

3.3.2.1 Water-table displacement in response to EPE amount

For the 17 cases, modeled water tables were displaced by at least 0.65 m (WA) and at most by 2.40 m (CO). The average Δ_{WTD} was 1.20 m. The case with the smallest EPE of 0.16 m (NM) produced a Δ_{WTD} of 2.14 m. The case with the largest EPE of 0.40 m (FL) produced a Δ_{WTD} of 1.50 m (Table 3.2). Three cases (AZ, NM, CO) show greater water-table displacements (Δ_{WTD} > 1.80 m) for a given 1-day EPE amount, with an EPE of 0.16 m/d for the NM case, 0.18 m for the AZ case and 0.22 m for the CO case. To better understand why Δ_{WTD} may be higher for the AZ, NM, CO cases, the unsaturated zone properties are considered.

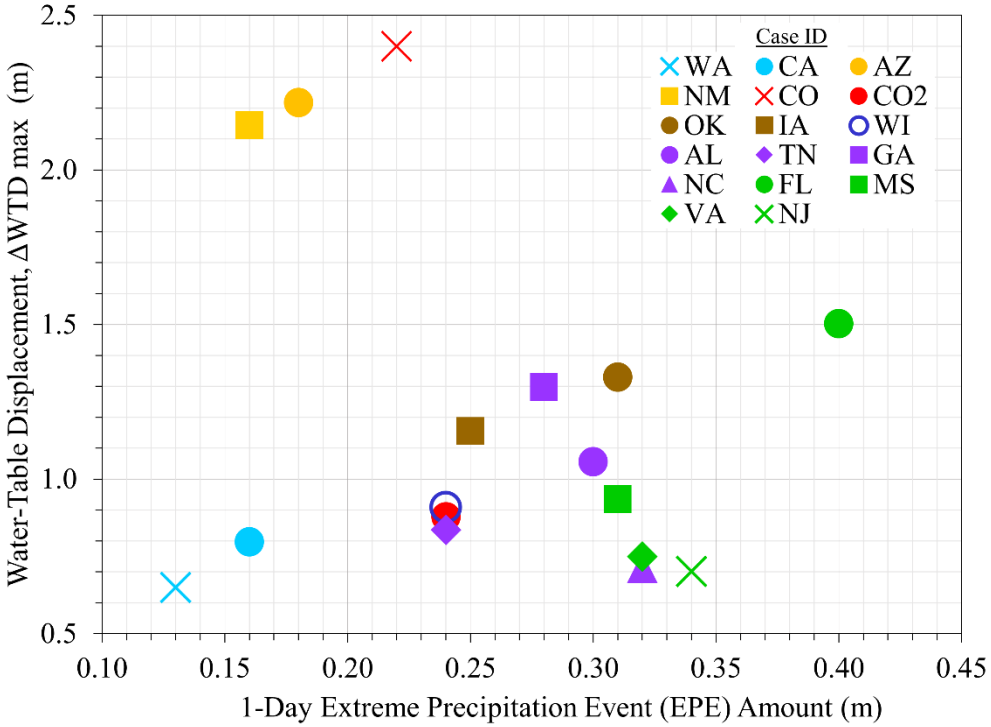

Figure 3.5 Scatter plot showing modeled water-table displacement, $\Delta_{WTD\ max}$ at 17 cases in response to 1-day EPE amounts.

Table 3.2 Precipitation station date range, EPE input amount, steady-state water table depth (m), modeled water table depth range (m), and $\Delta_{WTD\ max}$ (m) for each model case.

Case ID	Precipitation Data, Date Range	EPE Amount (m)	Steady state Water Table Depth (m)	Modeled Range of Water Table Depth (m)	$\Delta_{WTD\ max}$ (m)
WA	06/21/2015 – 07/05/2017	0.13	5.0	4.0 – 5.5	0.65
CA	10/01/2002 – 06/30/2021	0.16	5.9	4.8 – 6.5	0.80
AZ	05/01/2017 – 05/01/2022	0.18	7.0	4.5 – 8.0	2.22
NM	03/01/2010 – 03/01/2022	0.16	7.0	4.5 – 7.5	2.14
CO	06/01/2013 – 06/01/2019	0.22	27.4	25.0 – 28.0	2.40
CO2	09/01/2008 – 09/01/2021	0.24	5.0	4.0 – 5.3	0.88
OK	01/01/2013 – 07/31/2021	0.31	6.7	5.5 – 7.1	1.33
IA	12/01/2011 – 12/20/2020	0.25	5.2	4.2 – 5.6	1.16
WI	01/01/2010 – 02/04/2022	0.24	4.1	3.2 – 4.5	0.91
AL	01/01/2010 – 02/28/2022	0.30	4.9	3.5 – 5.2	1.06
TN	01/01/2000 – 08/31/2021	0.24	5.1	4.4 – 5.6	0.84
GA	05/01/2008 – 11/21/2021	0.28	8.8	8.0 – 9.4	1.21
NC	01/01/2000 – 10/30/2021	0.28	5.0	4.4 – 5.3	0.71
FL	10/10/2007 – 10/25/2021	0.40	4.0	3.0 – 4.4	1.50
MS	01/01/2010 – 01/05/2022	0.31	4.8	3.8 – 5.2	0.94
VA	01/01/2010 – 12/31/2021	0.32	4.4	3.5 – 4.8	0.75
NJ	07/27/2016 – 11/24/2021	0.34	3.8	2.8 – 4.1	0.70

3.3.2.2 Available porosity a control of water-table displacement

In the subsurface, water content, θ, is defined as $\theta = V_w / V_t$, where V_t is the total volume of the medium (i.e., soil or rock) and V_w is the volume of water (Freeze and Cherry, 1979). When all the pores in the medium are filled with water, the local water content equals porosity, $\theta = n$. In the unsaturated zone, θ is less than porosity, $\theta < n$ (Freeze and Cherry, 1979). For the cases considered, θ_r ranges from 0.03 (CO) to 0.26 (AL) and θ_s ranges from 0.25 (AZ) to 0.50 (AL).

The difference, $(\theta_s - \theta_r)$, can be considered the available porosity of the unsaturated medium. Available porosity plays a role in the van Genuchten equations (equation 2), where the available porosity controls the soil-water retention curve. These open voids are the fraction of the soil volume that is available to accept water (Nimmo, 2013).

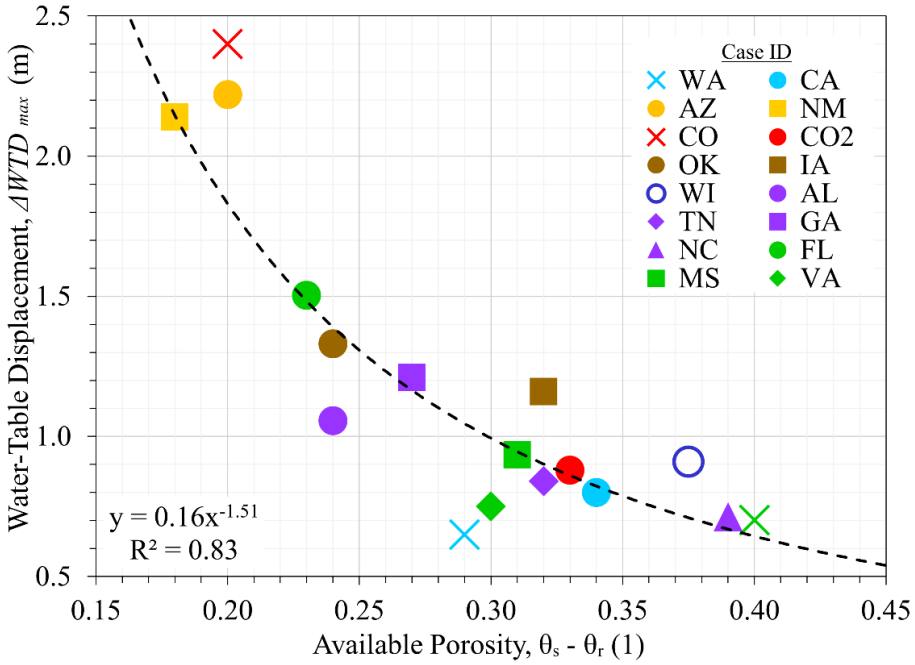

Figure 3.6 Modeled maximum water-table displacement, $\Delta_{WTD\ max}$ for each case as a function of available porosity.

Figure 3.6 shows modeled $\Delta_{WTD\ max}$ in response to EPE as a function of available porosity. Higher $\Delta_{WTD\ max}$ occurs at the cases with lower available porosity. The three cases with the highest $\Delta_{WTD\ max}$ (> 1.8 m) had the smallest available porosity values, ranging from 0.18 (NM) to 0.20 (AZ, CO). The remaining 14 cases have available porosities between 0.23 and 0.40 and Δ_{WTD} values from 0.65 m (WA) to 1.50 m (FL). Of particular note are the CO and CO2 cases, with available porosities of 0.20 (CO) and 0.33 (CO2), and $\Delta_{WTD\ max}$ of 2.40 (CO) and 0.88 (CO2) respectively. The CO case exhibits comparatively less available porosity and a high $\Delta_{WTD\ max}$ (as verified by field measurements) while the CO2 case exhibits more available porosity and a smaller simulated $\Delta_{WTD\ max}$. Our model results suggest that in the unsaturated zone, available porosity exerts a strong control on water-table response to EPEs. The plotted trendline shows that

a power function can explain 83% of the variability, where less available porosity leads to higher water-table displacement and vice versa. Physically, the available porosity controls the amount of water required per unit volume of soil material to transition from partially-saturated to fully-saturated. For a soil with a small available porosity, a small amount of water can quickly fill partially-saturated pores leading to large rise in $\Delta_{WTD\ max}$. For a soil with a large available porosity, the same amount of water results in a smaller rise in $\Delta_{WTD\ max}$. Thus, less available porosity (AZ, NM, CO) is correlated with larger $\Delta_{WTD\ max}$, and greater available porosity is correlated with smaller $\Delta_{WTD\ max}$.

3.3.2.3 Soil-water retention curves (SWRC) and water-table displacement

To further understand how Δ_{WTD} is affected by soil properties we consider the soil-water retention curve (SWRC) for each case. The SWRC relates the energy state of the pressure head, ψ to the local volumetric water content, θ, at equilibrium above the water table in a soil (van Genuchten, 1980). From the SWRCs of the soils (Figure 3.7), it can be understood how the available porosity is a controlling factor of Δ_{WTD}, but also how the absolute porosity, (n), plays a role in influencing water-table displacement. The porosity ($\theta_s \sim n$) of the cases range from 0.25 (AZ) to 0.50 (AL). A lower n (Figure 3.7) indicates that a smaller volume of pore space available to accommodate infiltrating water. The respective lower n of 0.25 (AZ) and 0.30 (CO) allows for larger Δ_{WTD} (Figure 3.6). However, the next lowest n = 0.32 of the OK soil, does not exhibit the 3rd largest Δ_{WTD}, instead the NM soil (greater n = 0.38) does. This can be understood by examining the SWRCs (Figure 3.7). The OK soil has a low n = 0.32 , and a higher available porosity than the NM soil. Therefore, the OK soil has more pore space available for water to fill, inhibiting a larger $\Delta_{WTD\ max}$. Thus, the porosity and available porosity, can serve as a first-order indicator of how large $\Delta_{WTD\ max}$ may be.

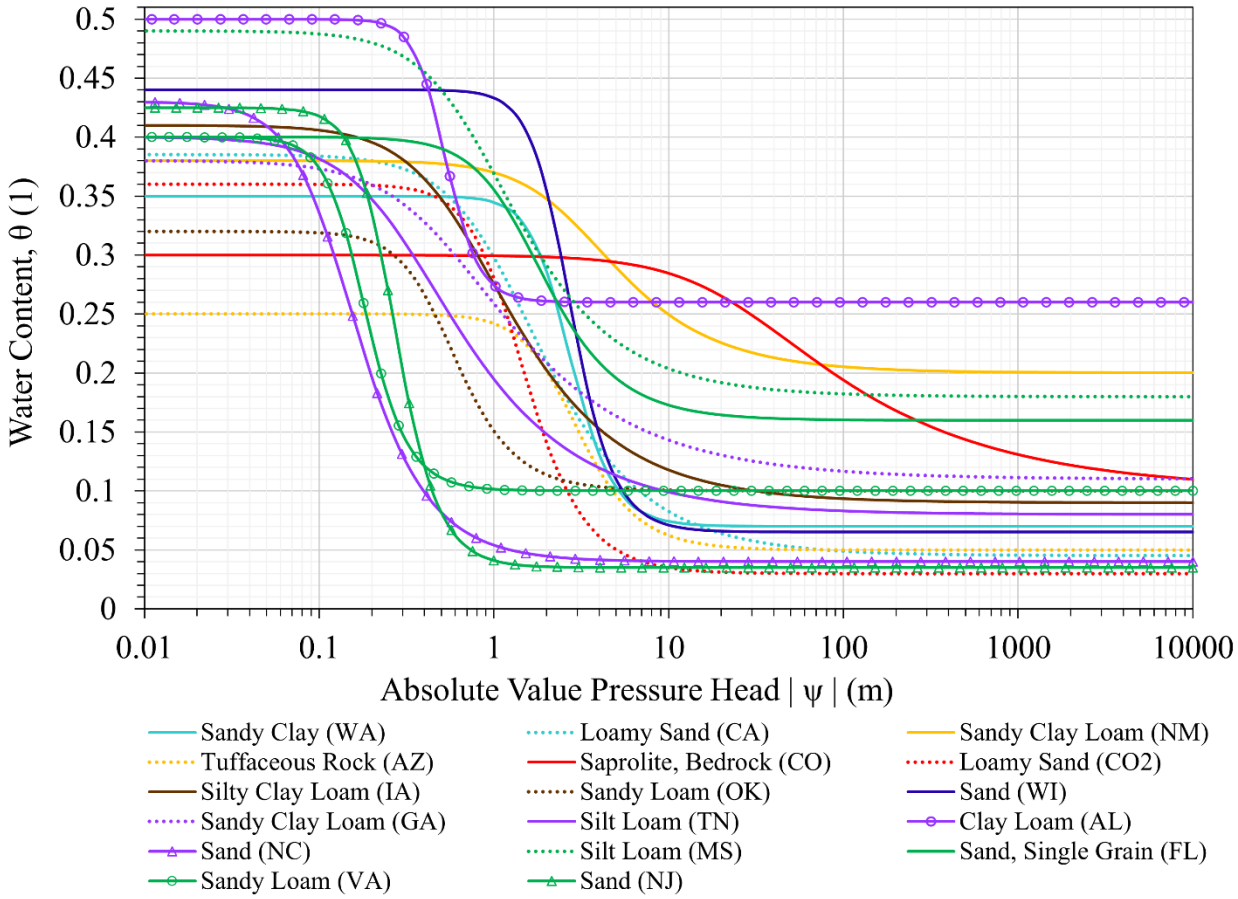

Figure 3.7 Soil Water Retention Curves (SWRCs) from inverse modeling for the seventeen study cases.

Once the water table has reached its peak displacement, the wetting process transitions into a drying process. The water table begins to recede, and the once saturated soil begins to lose water. For the purpose of this study, an increase in negative pressure head will be discussed as an increase in absolute value pressure head. This allows ψ to be plotted on a logarithmic scale (Figure 3.7). An increase in absolute value pressure head results in a decrease in water content from θ_s. The α (m^{-1}) is inversely related to the air-entry pressure, denoting the physical setting at which there is enough pressure to empty the largest pore of the soil (Kosugi et al., 2002; Nimmo, 2013). Water in the pore space is subsequently replaced by air. As the soil dries and the $|\psi|$ becomes larger than the air-entry pressure, the water content decreases, depicted in a SWRC as a sloped line that could be gentle or steep depending on the $\theta - \psi$ relation. As the soil continues to

dry and the pressure head becomes even larger, the water content decreases asymptotically towards the residual water content. The SWRC generally follows a smooth Z-shaped curve (Figure 3.7) between the bounds at θ_s and at θ_r, and the available porosity can be seen as the difference between these limits.

The soil-water retention curves of the 17 cases are spread across a wide range of available porosities (Figure 3.7). Most of the soils exhibit a moderate to steep $\theta - \psi$ slope. The SWRC for the AZ, NM, and CO materials exhibit comparatively gentler slopes. Gentler SWRC slopes are indicative of saturation retention over greater changes in absolute value pressure head (Figure 3.7). Most cases maintain full saturation up to a pressure head of $|\psi|$ ~0.1 m. Two of the cases with larger Δ_{WTD}, AZ and NM, maintain saturation until $|\psi|$ ~ 1.0 m. In particular, the CO material remains saturated at $|\psi|$ > 10 m.

The SWRC also helps illustrate the relatively lower porosity ($n \sim \theta_s$) of the materials with higher water-table displacements. For example, the porosity of the CO material is low ($n \sim$ 0.30) and the available porosity is even lower (0.20). The combination of low n and low available porosity suggests that a smaller volume of water is needed to raise the water table. Thus, the information provided by the SWRC for a soil, specifically the θ_s, θ_r, and $\theta - \psi$ relations can prove useful as first-order indicator when examining the potential water-table displacement of a soil responding to an EPE.

3.3.3 Water-table recession time

3.3.3.1 Saturated hydraulic diffusivity

Water table recession is governed by drainage over time in the saturated zone (Freeze and Cherry, 1979). After peak water-table displacement occurs, the water table recedes. We defined water table recession time, t_{rec}, as the time it took for 95% of the EPE-caused $\Delta_{WTD\,max}$ to recede

to non-EPE scenario levels. Depending on the $\Delta_{WTD\ max}$ of the soil, the 5% displacement thresholds varied between 0.04 m and 0.13 m. In the saturated zone, the time it takes for water to flow a certain distance can be examined by considering the hydraulic diffusivity, *D*. The hydraulic diffusivity is a measure of the ability of a material to transfer water relative to its ability to store water. The *D* (L^2/T) is a function of the fluid and medium properties of a saturated aquifer and can be calculated given the saturated hydraulic conductivity, K_S (L/T), specific yield, S_y (dimensionless) and aquifer thickness, A_t (L). For this study, A_t was the distance from the water table to the bottom of the soil column. Thus, the estimated saturated aquifer thickness was, $A_t \sim 41 - 46$ m for 16 cases and $A_t \sim 23$ m for the Betasso case. The specific yield, S_y, is a storage term for unconfined aquifers, defined as the volume of water released from storage per unit surface area of aquifer per unit decline in the water table (Freeze and Cherry, 1979). S_y is approximately equal to the porosity, *n*, which can be equated to the saturated water content, θ_s. Therefore, *D* for the saturated aquifer was defined as:

$$D = \frac{K_S}{\theta_S / A_t} \tag{7}$$

The hydraulic diffusivity, *D* (m^2/d) describes how fast a pressure pulse propagates through a saturated medium (Wang, 2020). We examined the water table recession time (t_{rec}) as a function of *D* and found that t_{rec} varied from 0.40 years to 2.10 years for *D* values ranging from 37 m^2/d to 129 m^2/d (Figure 3.8). For cases with smaller *D* values (< 80 m^2/d), the water table took longer to recede to non-EPE scenario levels (Figure 3.8), with t_{rec} ranging between 1.49 years (IA) to 2.10 years (NM). Where *D* was larger (> 80 m^2/d), recession times were shorter, ranging from 0.45 years (WA) to 1.25 years (NC). Given that *D* represents a characteristic length squared over a characteristic time (Bruce and Klute, 1956), the following equation was fit to the data:

$$t_{rec} = \frac{L^2}{D} \quad (8)$$

Where t_{rec} is recession time (years), L is a fitting parameter representing a characteristic length (m), and D is the saturated hydraulic diffusivity (m^2/d). The best-fitting parameter for the data was L = 9.30 m, representing the characteristic distance that the EPE signal may have diffused through in the subsurface. The fitted line highlights a negative trend: longer recession times are correlated with smaller D values, while shorter recession times are correlated with larger D values.

Figure 3.8 shows that the slope of dt_{rec}/dD steepens as D become smaller, which could be important for cases with smaller K_s values than those considered here. In contrast, the slope is gentler for larger D values, indicating that t_{rec} may reach a limiting value as D increases. Based on the results, we hypothesize that a recession time minimum may exist, which we define as the minimum amount of time it may take for the water table affected by an EPE to recede back to pre-EPE levels. This minimum may be ~0.4 years. More research is needed to explore this idea. The plot of D versus t_{rec} (Figure 3.8) shows a strong correlation for larger D, but the correlation is scattered for smaller D. Recession times longer than 1.3 years with diffusivities less than ~ 80 m^2/d are not well explained by the line fit equation. Recession times longer than ~1.45 years are attributed to smaller D, 37 ~ 80 m^2/d, and lower porosity (θ_s ~ 0.33) on average (Table 3.3, Figure 3.8). Recession times shorter than ~1.3 years are attributed to larger diffusivities (65 ~ 130 m^2/d) and higher porosity (θ_s ~ 0.42) on average (Table 3.3, Figure 3.8). To further explore the relation between D and soil/rock properties, we plotted the respective soil texture classes onto a modified version of the U.S. Department of Agriculture's (USDA, 1987) soil textural triangle classification system (Figure 3.9).

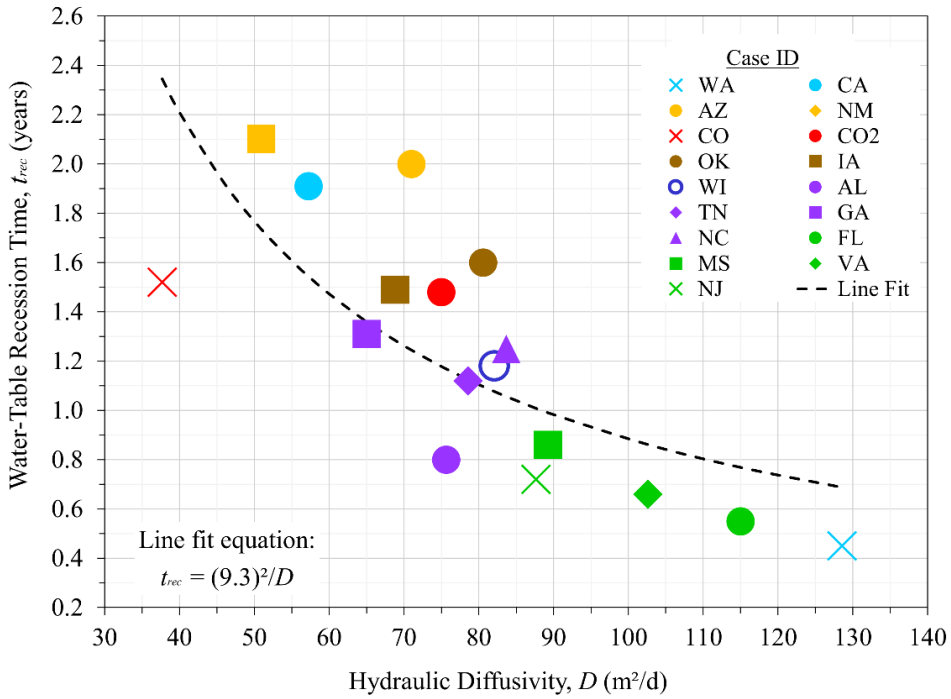

Figure 3.8 Modeled recession time, t_{rec} versus saturated hydraulic diffusivity, D (m^2/d) for each case.

Table 3.3 Average saturated hydraulic conductivity, K_s, porosity, n, hydraulic diffusivity, D, and recession time, t_{rec} for each model case.

Case ID	Averaged Saturated Hydraulic Conductivity, K_s (m/d)	Porosity (dimensionless) n	Diffusivity D (m^2/d)	Recession Time t_{rec} (yrs)
WA	1.00	0.35	128.57	0.45
CA	0.50	0.39	57.27	1.91
AZ	0.40	0.25	71.00	2.00
NM	0.45	0.38	50.92	2.10
CO	0.50	0.30	37.67	1.52
CO2	0.60	0.36	75.00	1.48
OK	0.60	0.34	80.60	1.60
IA	0.65	0.41	68.80	1.49
WI	0.80	0.44	82.10	1.18
AL	0.85	0.50	76.65	0.80
TN	0.70	0.40	78.58	1.12
GA	0.60	0.38	65.05	1.31
NC	0.80	0.43	83.68	1.25
FL	1.00	0.39	115.00	0.55
MS	0.95	0.49	89.25	0.86
VA	0.90	0.40	102.60	0.66
NJ	0.85	0.44	87.63	0.72

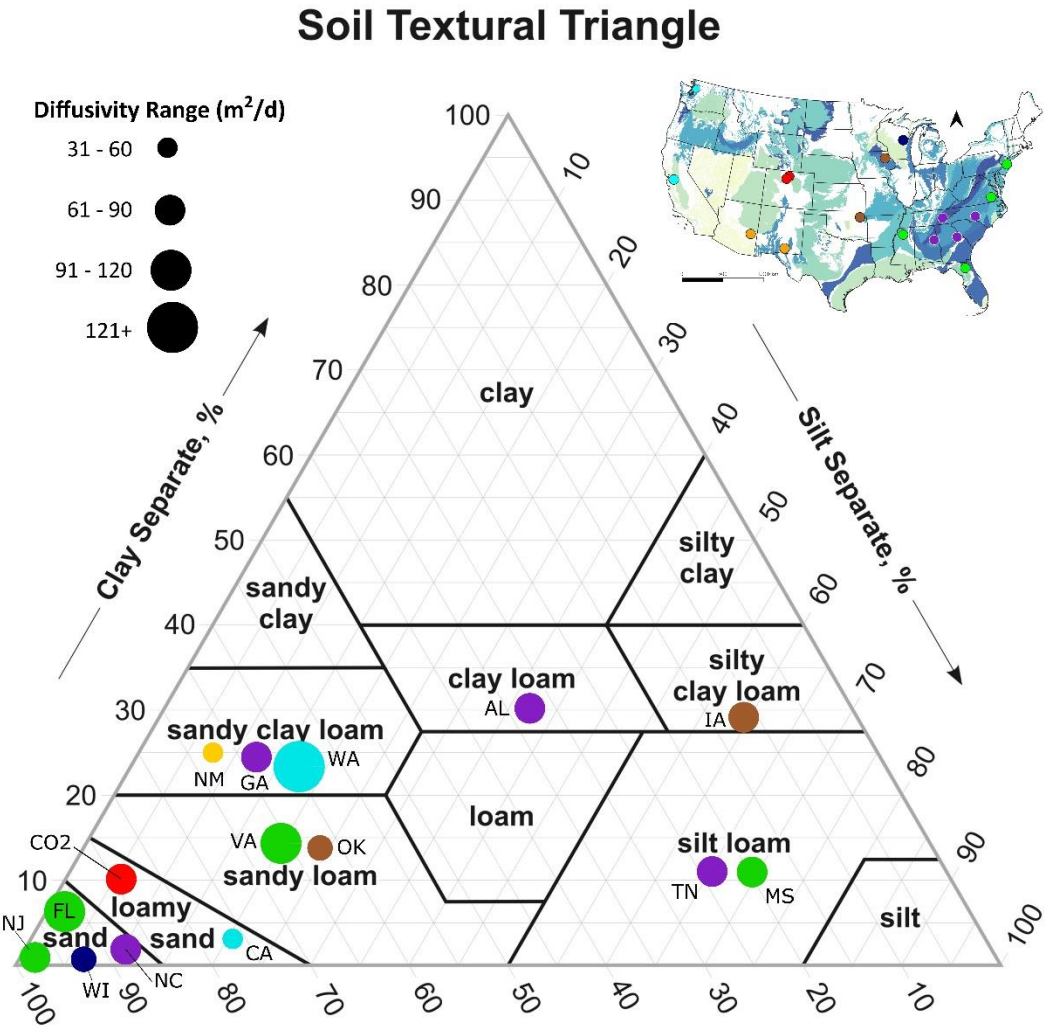

Figure 3.9 Dots show soil texture class for soils used in this study, but do not specific clay-silt-sand percentages, which were not reported in site data. Circle size denotes range of diffusivity values for the soils considered. Not shown: AZ (tuffaceous rock) and CO (unweathered bedrock). Inset: Figure 2 for reference.

The hydraulic diffusivities of the seventeen cases cover a wide range of soil textures (Figure 3.9). Sandier soils tend to be moderately to well-drained, which is reflected by larger *D* values (Figure 3.9). Soils with mixed amounts of clay, silt, and sand, drain at variable rates, which is reflected by the range of recession times for similar *D* values (Figure 3.9). We acknowledge that more data could be helpful in understanding the connections between soil materials and diffusivity, and urge future studies to consider clay-rich soils, which are not well-represented in this study.

3.3.3.2 Saturated hydraulic conductivity

The difference between high and low diffusivities is implicitly related to the soil hydraulic properties (K_s, θ_s) that construct the D (equation 7). The K_s and t_{rec} are inversely correlated (Figure 3.10), with circle size defined by the value of θ_s. Cases with smaller K_s and θ_s values (i.e., tuffaceous rock, unweathered bedrock, sandy clay loam) have smaller diffusivities. Physically, this suggests that when infiltration from an EPE reaches the saturated zone, the pressure pulse takes more time to propagate through the medium, thus resulting in longer recession times. In contrast, cases with larger K_s and θ_s values (i.e., sandy soils) allow for water to be transmitted relatively faster through the medium, indicating a larger diffusivities and shorter recession times.

From a climate perspective, cases with smaller K_s and longer recession times are also those with lower 1-day EPE amounts, which may reflect drier soils (low- to mid- K_s) and drier climates (Figure 3.10). Cases with larger K_s and shorter recession times are also those with higher 1-day EPE amounts, which may reflect more conductive soils and wetter climates (Figure 3.10). Provided that recession times for water tables remain elevated for 0.4 years to 2.1 years after an EPE, the elevated water tables could be a welcome opportunity for communities-in-need to extract water resources. In terms of direct extraction, communities in mountainous regions and near ephemeral streams are most likely to benefit. Done efficiently, this recession time window could be exploited during summer months when little to no rain is expected in generally drier regions (i.e., southwest U.S, drier parts of Australia, Africa). For example, if soils with lower diffusivities, in dry regions, experience EPEs, then water could be pumped out for storage to be used at a later time. Indirectly, elevated water tables could also provide more baseflow to streams, rivers, and lakes, which would subsequently benefit more communities.

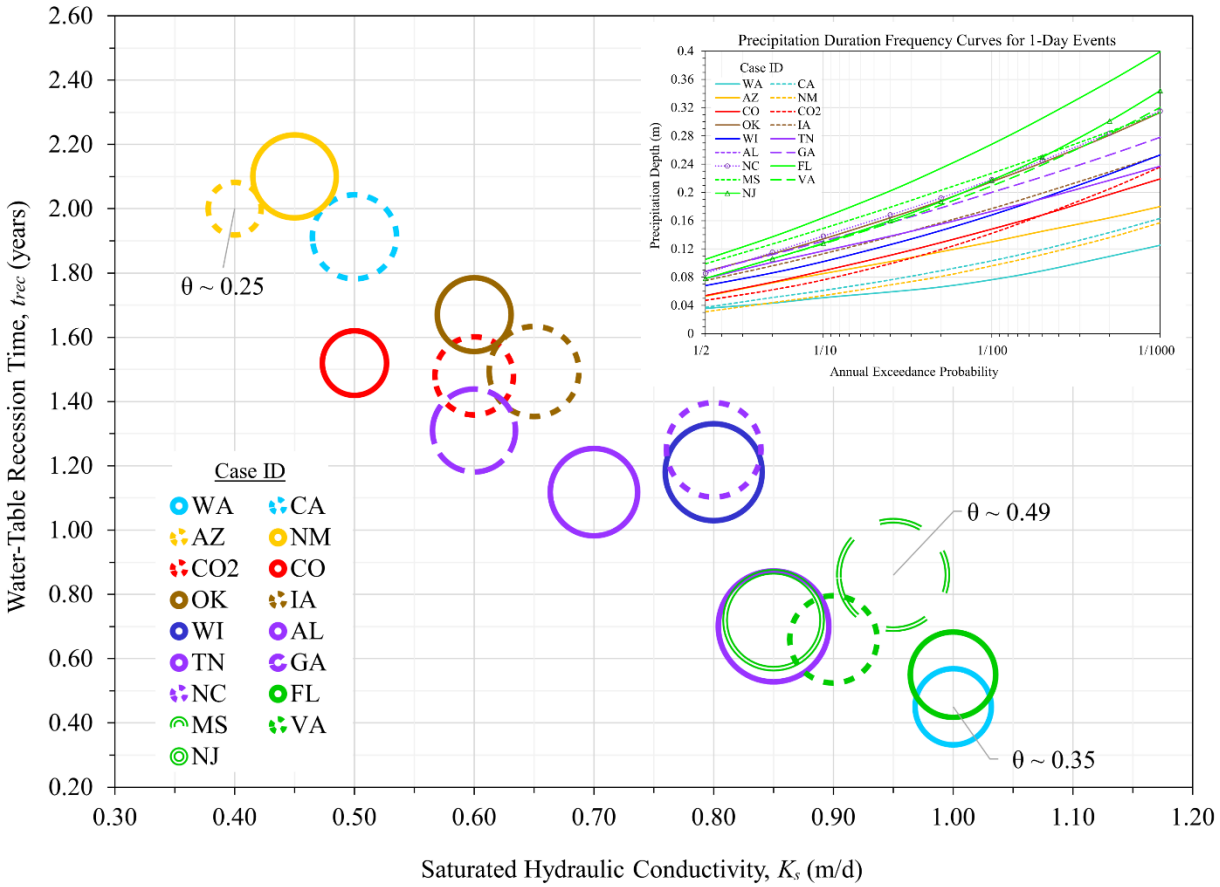

Figure 3.10 Modeled values of recession time, t_{rec} versus saturated hydraulic conductivity, K_s (m/d) values of each case. Symbol sized according to θ_s of each case. Inset: Figure 2 for reference.

With climate change affecting annual snow-to-rainfall precipitation ratios (Trenberth, 2011), elevated water tables could be tapped by wetter regions when less precipitation occurs (Wilkinson and Cooper, 1993). This could be of great benefit for areas expected to suffer from elevation-dependent warming (Pepin et al., 2015). Overall, the ability to pump water resources after EPEs could help modulate water resource extraction based on community need.

3.3.4 Future considerations and implications

A future in which EPEs become more frequent could lead to an increased likelihood of larger flooding events (Wasko et al., 2021; Geris et al., 2022) and water quality issues (Nguyen et al., 2021; Geris et al., 2022). For example, Geris et al. (2022) found that an EPE in a semi-arid

region was simultaneously responsible for 1) widespread flooding, 2) high groundwater recharge, and 3) subsurface contaminant mobilization due to elevated water tables promoting local landfill drainage. Subsurface response to EPEs has also resulted in increased likelihood of slope failures (Smith et al., 2017; Hou et al., 2021), and building foundation issues (Garcia-Gaines and Frankenstein, 2015).

In recognition of the predicted increase and frequency of EPEs (Du et al., 2022), it is important to identify the controls that cause water-table displacement variations from one soil texture class to another. Our approach highlights the importance of organized soil sample datasets like UNSODA (Nemes et al., 2001). In the absence of more intensive field studies, $\theta(\psi)$ and K_s from soil sample catalogs may serve as empirical controls on water-table response to EPEs in future modeling efforts. In addition to the data discussed in this study, UNSODA contains soil data for more than 100 sites in over 20 countries across the European, African, Asian and Australian continents (Nemes et al., 2001). Regions at risk of EPEs (Sun et al., 2021) could undergo this analysis and examine whether: (1) the available porosity of a soil controls water table displacement and (2) how the K_s and D controls water table recession time. Such tests could indicate if the relations highlighted here could be more generally applicable globally.

3.4 Conclusion

As the link between climate and groundwater, soil hydraulic properties that control subsurface response warrant greater attention in the face of increasingly likely EPEs. In the unsaturated zone, our results show that across varying soil-types and precipitation cases, EPEs cause significant variations in water-table displacement and recession times. Future studies can be broadened to explore water-table response and recession time in soil properties and precipitation space.

3.4.1 Summary

We examined water-table response, namely water-table displacement, and recession time to EPE-induced infiltration. We used water content and pressure head data from 17 cases along with inverse modeling to determine soil-water retention curves. We used a 1d modeling approach to show that water-table response to EPEs can be significant and to explore how varied materials (hydraulic properties) affect the response. For each case, the transient modeling included the "non-EPE" scenario where no EPE was applied and the "EPE" scenario where the 1-day EPE was added to the non-EPE scenario. The modeling results of the non-EPE and EPE scenarios were compared to determine the Δ_{WTD} and t_{rec}. The following conclusions are drawn from the results of this study:

- Subsurface response to EPEs led to water-table displacements ranging from 0.6 to 2.4 m across the 17 study cases.
- Available porosity in the unsaturated zone exerts a strong control on water-table displacement. Low available porosity leads to larger water-table displacement and vice versa.
- Saturated hydraulic diffusivity is a major control of water-table recession time, t_{rec}. A factor of three variation in D caused about a factor of four variation in recession times.
- Results hint at a limiting value for the recession time, set by the hydraulic diffusivity, D.

We further urge field collection, lab analysis, and consideration of soil hydraulic property data to validate future modeling studies related to water table fluctuations and groundwater recharge.

CHAPTER 4: EXTREME PRECIPITATION VARIABILITY AND SOIL TEXTURE CONTROLS OF WATER TABLE RESPONSE

Abstract

Observed increases in the frequency, intensity, and duration of extreme precipitation events (EPEs) across the United States (U.S.), are projected to continue with climate change. EPEs are expected to influence water-table mechanics, but the extent of the influence and how the influence is controlled by soil texture, remains a knowledge gap. We conduct a modeling effort to examine the water-table response: response time, displacement, recession time, and recharge totals of twelve soil textures to 1-day, 7-day, and 20-day EPEs. We find that water-table response times are shorter with increasing precipitation amount and vary from ~8 days to ~279 days. Water-table response is faster in coarser-grained soils and can take upwards of two-hundred days in finer-grained soils. Water-table displacement is positively correlated with increasing EPE amount, and weakly correlated with longer duration. Water-table displacements range from 0.5 - 1.7 meters, and can be higher in mixed-grained size soils than in coarser soils. Recession times range from 2.4 years to > 6 years for all soils, indicating that soil properties are the greater control of recession time compared to EPE amounts and durations. We also calculate first-order recharge rates from EPEs and find that average recharge totals range from 31% (clay) to 96% (sand), with the overall average equaling ~70% recharge. Total recharge is primarily a function of total EPE amount and soil properties. Broadly, this modeling effort provides a more comprehensive view of the influence of soil texture on groundwater response to EPEs.

4.1 Introduction

In July 2022, six precipitation events in the states of Missouri, Kentucky, Illinois, California, Texas, and Mississippi surpassed the local threshold for classification as "1-in-1000-year" rainfall events (Sistek, 2022) as defined by the National Oceanic and Atmospheric Administration (NOAA). Over a 7 - 21 day period between December 26, 2022 and January 17, 2023, large areas of central and northern California experienced record-breaking extreme precipitation events associated with atmospheric rivers (NOAA, 2023a). Measured precipitation totals for the EPEs ranged from 0.39 m at the San Francisco International Airport to 0.92 m at Santa Cruz, CA (Gaines, 2023). Precipitation frequency estimates for Santa Cruz, CA showed that the 0.92 m precipitation amount exceeded the local threshold for a 20-day, 1000 year event for the area (NOAA, 2023b). Extreme precipitation events (EPEs) are expected to become more frequent with climate change (Li et al., 2019; Myhre et al., 2019; Sun et al., 2021). The occurrence of EPEs comes with elevated risks of channel or river overflow, road flooding due to over-saturated drains, property destruction and lost economic output that can total billions of dollars (NOAA, 2023c). Despite the hazards, drought-stricken regions across states like California and Texas can benefit from extreme precipitation events, especially if the water infiltrates and the subsurface properties allow for groundwater recharge. Unfortunately, subsurface response to EPEs and groundwater recharge estimates from EPE-induced infiltration remains poorly understood.

The unsaturated zone is the variably saturated region of soil and aquifer that vertically extends downward from the ground surface to the water table (Freeze and Cherry, 1979). During infiltration, some amount of water may be lost through evapotranspiration, while some water may be stored in the soil, and the remaining amount will flow downward until reaching the water

table, where it is considered recharge (Freeze and Cherry, 1979). The unsaturated zone is thus the conduit between the atmosphere and groundwater.

Case studies using field techniques and modeling approaches have shown that high infiltration rates and groundwater recharge can occur during and after EPEs, through both highly-porous material like alluvium, limestone, and volcanics (Jasechko and Taylor, 2015), desert sand soils (Zhang et al., 2016; Zhou and Zhao, 2021; Boas and Mallants, 2022), and semi-arid silt loam soils (Shao et al., 2018). However, there is a much less robust understanding of how EPEs of different intensities will be transmitted by comparison of different soil textures, especially soils that are of moderate- or low-porosity. In contrast to the studies regarding highly porous materials, Corona and Ge (2022) and Corona et al. (2023) examined the water-table response to the same EPE in two drainage basins within the Boulder Creek Watershed along the Front Range of Colorado. These studies used field data and modeled the response of less-porous material, finding that water from the EPE infiltrated the surface and was transmitted through the unsaturated zone and to the water table within weeks (Corona and Ge, 2022; Corona et al., 2023). This was a surprising finding given the low porosity and low-to-mid-level hydraulic conductivity of the subsurface materials at both sites. Corona et al. (2023) then expanded the study to site-specific soils across the United States, but did not consider soils with higher clay and silt percentages, an area of research that warrants examination. As climate change influences precipitation patterns(Trenberth, 2011), there is increased interest in studies that examine post-EPE recharge for soils of lower porosity.

While studies considering the impacts of single EPEs on water table response and groundwater recharge exist, there is not a study that has undertaken a comprehensive examination of 1) EPE amounts of 1-day, 7-day, and 20-day durations influence water-table

response in varying soil textures, and 2) how total recharge differs across soil texture classes for varying EPEs. As the link between the precipitation and groundwater, subsurface response warrants greater attention in the face of increasingly likely EPEs. Though not examined here, infiltration from EPEs has also been shown to increase contaminant transport and sewage-mixing with groundwater (Geris et al., 2022), which has short- and long-term implications for the protection of subsurface water resources. A comprehensive modeling effort that includes a wide range of soil texture classes and EPEs of varying durations and intensities could help better understand potential subsurface response to infiltration from extreme precipitation events.

4.1.1. Objective

This study used the model HYDRUS-1D (Šimůnek et al., 2005) to simulate water-table response of varying soil textures to rain events of different durations and amounts. The objectives of this study are to address (1) How does the water-table response time differ? (2) How does the water-table displacement differ? (3) How does the water-table recession time differ? And (4) What is the estimated recharge from each storm scenario for each soil across duration?

4.2 Methods

4.2.1 Data

4.2.1.1. Soil hydraulic properties

Soils belonging to the same textural class share similar hydraulic properties (Garcia-Gaines and Frankenstein, 2015). We selected an example soil texture from each of the 12 soil texture classes defined by the U.S. Department of Agriculture (USDA) (Carsel and Parrish, 1988). USDA soil texture classes, are defined based on particle size (sand, silt and clay) distributions of the less than 2 mm sized material (Soil Science Division Staff, 2017). We

acknowledge that a range of hydraulic parameters are possible for each soil texture class, but for the purposes of this study, use representative soil hydraulic properties for each soil textural class (Table 4.1) as reported by Carsel and Parrish (1988).

Table 4.1. Soil hydraulic properties of the 12 soil texture classes, in order of increasing K_s.

Soil texture class	Residual Water Content θ_r (1)	Saturated Water Content θ_s (1)	Air-entry Pressure α (1/m)	Pore-size Distribution Index n (1)	Saturated Hydraulic Conductivity K_s (m/d)
Clay	0.125	0.490	2.000	1.60	0.05
Silty Clay Loam	0.100	0.440	1.500	1.70	0.06
Clay Loam	0.110	0.420	4.000	3.00	0.07
Silty Clay	0.070	0.360	4.000	2.00	0.08
Sandy Clay	0.110	0.400	4.000	3.00	0.10
Silt Loam	0.050	0.470	2.200	1.41	0.11
Sandy Clay Loam	0.050	0.390	4.000	1.50	0.12
Silt	0.050	0.460	2.500	1.40	0.20
Loam	0.080	0.430	3.600	1.60	0.70
Sandy Loam	0.075	0.420	4.000	1.90	1.10
Loamy Sand	0.050	0.400	6.000	2.10	2.50
Sand	0.045	0.385	6.000	2.20	5.00

4.2.1.2 Extreme precipitation events

We considered EPEs of 1-day, 7-day and 20-day durations to explore how EPE variations affect water table response. For the durations, we consider EPE amounts (m) of 0.20 and 0.40. For the 7-day and 20-day durations, we include an EPE amount of 0.60 m (Table 4.2). For each duration, an EPE amount is applied at a steady rate.

Table 4.2. EPE durations and amounts applied to the 12 soil textures.

	EPE Duration (days)								
	1-day			7-day			20-day		
EPE Amount (m)	0.2	0.4		0.2	0.4	0.6	0.2	0.4	0.6

4.2.2 Subsurface flow modeling

We note that the simulations considered here are all one-dimensional treatments. Furthermore, the models have homogeneous soils with functional relationships between water content, hydraulic conductivity, and pressure head change. We describe the model methodology in the subsequent sections.

4.2.2.1 Governing equation

Transient, vertical flow in the vadose zone can be described by a simplified, one-dimensional form of Richards equation (Richards, 1931):

$$\frac{\partial \theta}{\partial t} = \frac{\partial}{\partial z}\left[K\left(\frac{\partial \psi}{\partial z} + 1\right)\right] \tag{1}$$

where θ (dimensionless) is the water content, t [Time] is time, ψ [Length] is the pressure head, K [L/T] is the hydraulic conductivity, and z [L] is the vertical coordinate downward. In this simplified form, thermal effects and air-phase flow are ignored. Here, time is in days, d, or years, yrs. Length is in meters, m.

The numerical model HYDRUS-1D (Šimůnek et al., 2005) solves Richards equation for pressure-head distribution in a variably-saturated porous medium. HYDRUS-1D utilizes the van Genuchten-Mualem equations (Mualem, 1976; van Genuchten, 1980) to allow for continuous functional relations for soil-water retention and the hydraulic conductivity, K of a soil. The van Genuchten-Mualem equations state:

$$\theta(\psi) = \begin{cases} \theta_r + \dfrac{\theta_s - \theta_r}{[\,1 + |\alpha\psi|^{n}\,]^{m}} & \psi < 0 \\ \theta_s & \psi \geq 0 \end{cases} \tag{2}$$

where the unsaturated hydraulic conductivity curve, $K(\psi)$ of a soil:

$$K = K(\psi) = K_s S_e^l \left[1 - (1 - S_e^{\frac{1}{m}})^m \right]^2 \quad (3)$$

$$m = 1 - \frac{1}{n}, \qquad n > 1 \quad (4)$$

where S_e is the effective saturation:

$$S_e = \frac{\theta - \theta_r}{\theta_s - \theta_r} \quad (5)$$

where θ_r and θ_s represent the residual and saturated water content, K_s is the saturated hydraulic conductivity (m/d), α is a parameter inversely-related to the air-entry pressure, n is the pore-size distribution index, and l is a pore-connectivity parameter (Mualem, 1976; van Genuchten, 1980).

4.2.2.2 Model setup and assumptions

Although real-world subsurface soils are likely heterogeneous, the simulations of water flow in homogeneous profiles allow for a simplified evaluation of the soil-averaged controls on water-table response and groundwater recharge. In HYDRUS-1D, the model domain was set up as a one-dimensional vertical column extending downward from the land surface to a depth of 50 m. The column was discretized into 1000 elements. The hydraulic properties of the 12 soil textures (Table 4.1) were used to create 12 homogeneous profiles.

A prescribed flux with surface ponding at the land surface was used as the top boundary condition (Šimůnek et al., 2005):

$$-K\left(\frac{\partial \psi}{\partial z} + 1\right) = q_0(t) - \frac{d\psi}{dt} \quad at\ z = 0 \quad (6)$$

The flux q_0 is the net infiltration rate at time t, the difference between precipitation and evapotranspiration that may occur. Surface ponding was allowed up to a positive pressure head of, ψ = 0.15 m. A deep drainage flux is applied as the boundary at the bottom of the soil column.

The downward drainage flux out of the column, $q(\psi)$, was approximated by the following expression (Hopmans and Stricker, 1989):

$$q(\psi) = -Ae^{(B\,|\,\psi_{bottom} - GWL\,|)} \text{ at z = 50 m} \quad (7)$$

The variable $q(\psi)$ (meters/day, or m/d) is the flux crossing the bottom boundary. Here, *A* and *B* are adjustable empirical parameters. *A* (m/d) is related to the flux at saturation, K_s(m/d). *B* has dimensions of inverse length (1/m) and is calibrated to initialize the water table depth at a depth of 6 m. The ψ_{bottom} (m) is the pressure head at the bottom boundary. *GWL* (m) is a reference pressure head at some distance away (Hopmans and Stricker, 1989); as a first-order approximation, we assumed that *GWL* = 50 m.

Each simulation was initialized with a prescribed pressure head distribution decreasing linearly from ψ = -5 m at the surface (z = 0 m) to ψ = 45 m at the bottom of column (z = 50 m). For model spin-up, an average infiltration flux of 0.0005 m/d was used. Time discretization ranged from a minimum time step of 10^{-9} days to a maximum time step of 5 days. The model was spun-up to allow the water table to equilibrate to a steady-state. After steady-state was reached, the EPE was applied. The EPE amount was applied at a steady rate for the specified duration of the event (Table 4.3). The three event totals and three event durations resulted in eight different EPE scenarios (a 1-day duration event was not run for the highest rainfall total, 0.6 m) for each of the 12 soils, totaling 96 simulations.

4.2.3 Examining model results

Four aspects of water-table response were considered: 1) water-table response time to the infiltration from the EPE, t_{rep}, 2) water-table displacement, Δ_{WTD}, 3) water-table recession time, $t_{rec,}$ and 4) recharge. Once EPE simulations were run, water table depths over time were calculated from model output. The water-table response time, t_{rep}, was calculated as the time

needed for the water table to rise from the pre-event steady-state level to its max displacement, $\Delta_{WTD\,max}$. The water-table displacement, Δ_{WTD}, was calculated as the difference between the EPE water table and steady-state water table levels at the daily time step. After water-table displacement, the water table remained elevated for varying amounts of time, eventually receding to non-EPE water table levels. Following EPE input, the precipitation input is set at 98% of the pre-EPE rate (0.00048 m/d) for the remainder of the simulation. Water-table recession occurs after peak water-table displacement, when the water table physically lowers (i.e., recedes) back to a pre-EPE level. The water table recession time, t_{rec}, was defined as the time it took for the water table to recede to 5% of $\Delta_{WTD\,max}$. From a temporal perspective, this approach only focused on the period of response to EPEs and the subsequent recovery. We only consider the EPE impact on the subsurface and exclusively examine the interaction between EPE-induced infiltration and subsurface properties, transient precipitation is not considered. Given the modeling approach, the simulations do not represent long-term water-table fluctuations.

4.3 Results and Discussion

4.3.1 Water-table response time

For all simulations, water-table response time, t_{rep}, is faster with increasing precipitation amount (Table 4.3). The fastest response times occurred in the coarsest-textured (sand) soils. The slowest response times occurred in the finest textured soil (clay), taking as much as 279 days. Response times of intermediate textured soils fell in between these extremes, with faster responses for coarser-grained size classes like sandy loam and loamy sand, and slower responses for finer-grained size classes like silty clay (not shown). Precipitation duration has a minor influence on response time.

Table 4.3. Average, fastest, and slowest response time (days) across EPEs for all soils.

	EPE Duration							
	1 - day		**7 - day**			**20 - day**		
EPE Amount (m) →	0.20	0.40	0.20	0.40	0.60	0.20	0.40	0.60
t_{rep} (days) average for 12 soils	121	92	121	72	44	135	82	53
Fastest t_{rep} (days) and soil texture class	14 Sand	7 Sand	20 Sand	10 Sand	8 Sand	27 Sand	22 Sand	20 Sand
Slowest t_{rep} (days) and soil texture class	235 Clay	214 Clay	235 Clay	127 Clay	77 Clay	279 Clay	155 Clay	100 Clay

4.3.2 Water-table displacement

4.3.2.1 Maximum water-table displacement

Figure 4.1 shows the $\Delta_{WTD\ max}$ for each soil texture class in response to varying EPE amount and duration. The colored bars highlight the three end-members of the USDA soil textural triangle: red is clay, blue is silt, and yellow is sand (Figure 4.1). Across durations, displacements range from 0.45 m (clay) to 1.66 m (silt loam).

Figure 4.1 shows considerable difference in maximum water-table displacement between the 1-day and 7-day durations for soils finer than silt. This is attributed to the saturated hydraulic conductivity of the finer-grained soils, where K_s < 0.20 m for soils finer than silt (Table 4.1). For the 1-day duration, the precipitation rate is high, which could become a high infiltration rate depending on the hydraulic conductivity of the soil permits. Here, the lower K_s of the finer-grained soils limits the infiltration rate, and as a result, surface ponding and runoff occurs. For the 1-day duration, soils with K_s values < 0.20 m/d do not allow for infiltration rates that match the precipitation rate, thereby losing water to surface runoff (not shown), subsequently impacting the $\Delta_{WTD\ max}$. In contrast, and for the same precipitation amount (i.e., 0.40 m), the 7-day duration allows for a lower precipitation rate that does not exceed the saturated hydraulic conductivity of the soil. Traditional theory suggests that lower precipitation amounts over several days lead to

higher total infiltration and higher water tables (Philip, 1956; Gray and Norum, 1967; Diamond and Shanley, 1998).

A comparison of the 7-day bar plot and the 20-day bar plot (Figure 4.1) shows similar $\Delta_{WTD\,max}$ for most soils. This can be attributed to the soil's saturated hydraulic conductivity, where even the finest-grained soil, clay, has a K_s ~0.05 m/d, which is similar to the highest steady daily precipitation rate of the 7-day and 20-day durations. This rate, for the 7-day, 0.60 m EPE amount is ~ 0.057 m/d. Overall, $\Delta_{WTD\,max}$ increases with increasing precipitation amount. From Figure 4.1, it thus appears that the maximum water-table displacement is more strongly controlled by 1) soil texture and 2) total EPE amount.

4.3.2.2 Influence of precipitation amount on water-table displacement

Figure 4.2 shows Δ_{WTD} for the first 100 days after the EPE for all precipitation amounts and durations. Given the steady application of each EPE, the precipitation rate increases as the precipitation total increases for the same duration, or conversely, as the duration decreases for the same precipitation total. For the 0.20 EPE amount, all durations (left-most column in Figure 4.2) show similar Δ_{WTD} despite the fact that the precipitation intensity of the 1-day events was greater than that of the 7-day or 20-day events.

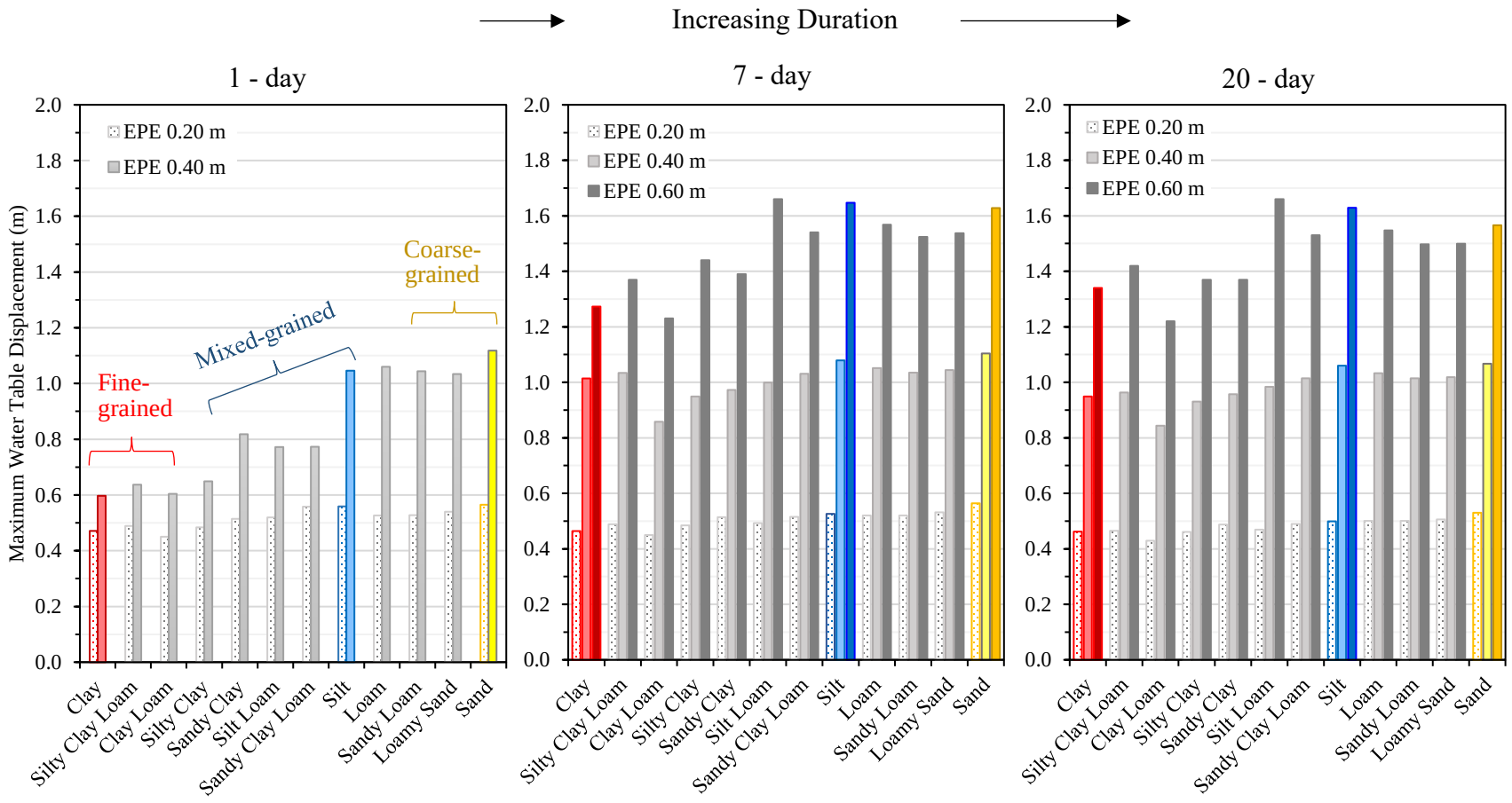

Figure 4.1. Max water table displacement $\Delta_{WTD\ max}$ (m) for each of the 12 soils for 1-day, 7-day, and 20-day EPEs of varying amounts. The colored bars highlight the three end-members of the USDA soil textural triangle: red is clay, blue is silt, and yellow is sand. Results show that water-table displacement is a result of total amount, not duration.

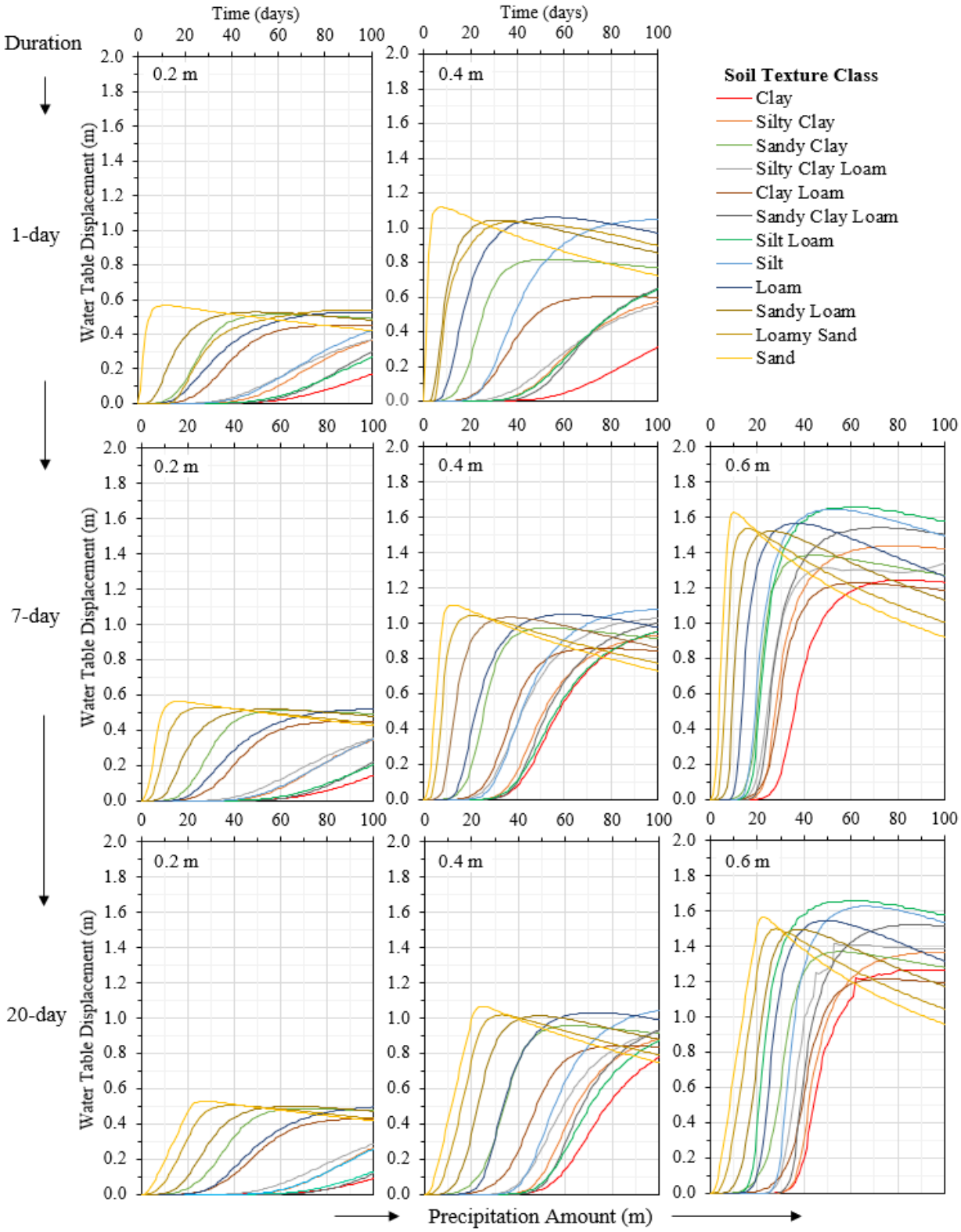

Figure 4.2. Water-table displacement (m) over the fist 100 days, for each soil. Event duration increases from top to bottom (1-, 7-, 20-day) for EPE durations and precipitation amount (0.2, 0.4, 0.6) increases from left to right.

Water table displacements are of similar heights across the same EPE amount (Figure 4.2). Comparing the 0.40 m EPE (center-column), $\Delta_{WTD\ max}$ is ~0.05 m higher, for the 7-day event than the 1-day or 20-day events. The right-column, middle-panel shows that $\Delta_{WTD\ max}$ is slightly higher during the 7-day, 0.40 m EPE compared to the 20-day duration of the same amount. In addition, mixed-grain size soils (silt loam, loam) reach slightly higher displacement than sandier soils for the 20-day, 0.60 m EPE amounts. The higher $\Delta_{WTD\ max}$ of the mixed-grained soils could be a result of lower available porosity and low K_s (Corona et al., 2023). In general, it is expected that longer duration and lower precipitation amounts lead to higher water tables and greater recharge due to a higher likelihood of infiltration not reaching capacity (Horton, 1941).

To examine why the 7-day events may be resulting in higher $\Delta_{WTD\ max}$ than the 20-day events, we consider the modeled pressure head and water content variations over time. Figure 4.3 shows the ψ and θ variations in a sandy soil for the 7-day and 20-day, 0.60 m EPE for various times after the beginning of the EPE. For both durations, the soil is drier (more negative ψ and lower θ) before the EPE ends. At the end of the EPE (red line, both durations), the soil profile is wettest (less negative ψ, higher θ). For the same EPE amount, the sand profile that experiences a 7-day EPE (top row), is under less negative pressure and has higher water content at the end of the EPE, compared with the 20-day (bottom row). The sand profile is temporarily wetter after the 7-day event compared to the 20-day event. A wetter profile indicates a higher hydraulic conductivity and faster downward water flow. Faster downward flow facilitates water table displacement, and could explain why the 7-day events experienced slightly higher $\Delta_{WTD\ max}$ than the 20-day events.

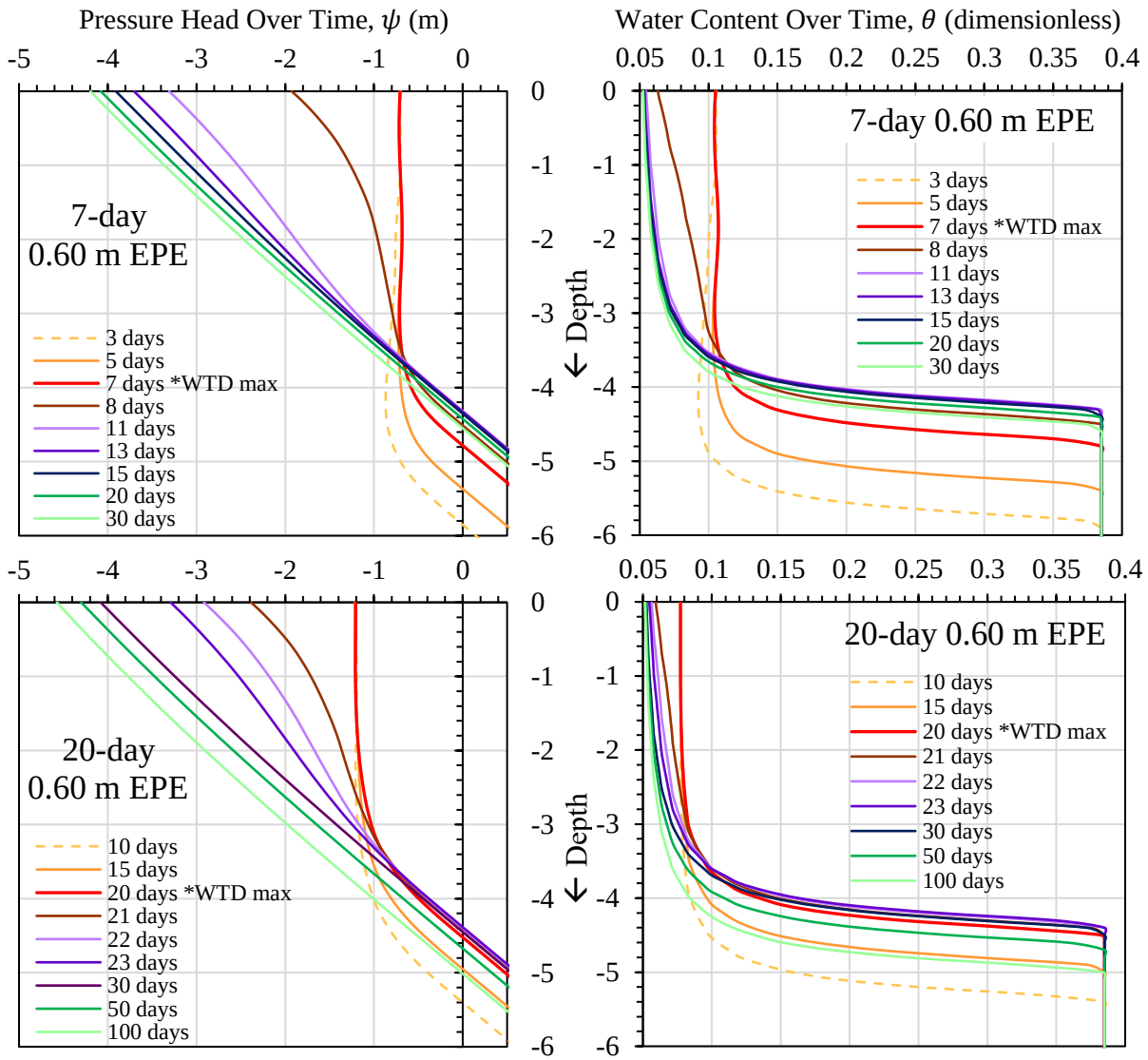

Figure 4.3. Pressure head and water content variations over time for a sandy soil over a 7-day (top row) and a 20-day (bottom row) duration.

4.3.3 Water-table recession time

Figure 4.4 depicts t_{rec} for the 12 soils. Generally, t_{rec} varies from 6.2 years (clay) to 2.4 years (sand) for all durations. The exception is clay, where t_{rec} ~ 8.0 years for the 20-day, 0.20 m EPE. An examination of the water balance error of the flow domain for this case showed a 0% error at the end of the simulation.

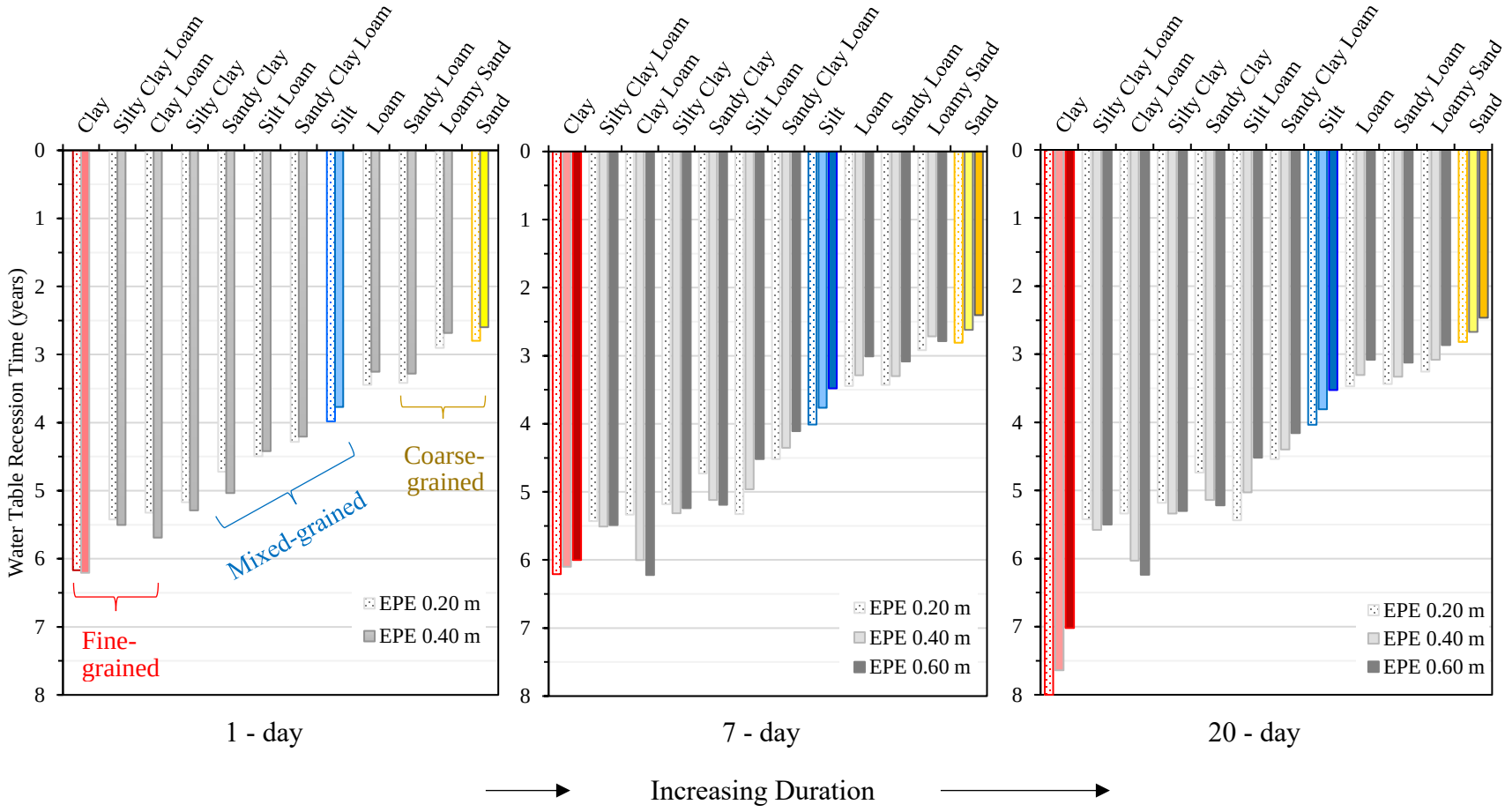

Figure 4.4. Water-table recession time (years), t_{rec}, for each of the 12 soils. The three bar plots are arranged by increasing duration of 1-day, 7-day, and 20-day. The colored bars highlight the three end-members of the USDA soil textural triangle: red is clay, blue is silt, and yellow is sand.

From a physical standpoint, clay soils have the lowest permeability, with pore spaces isolated, retarding flow of water. Here, the clay soil experiences a steady and long, low-intensity rainfall with no runoff. The clay soil has the smallest hydraulic conductivity, limiting the rate of downward flow. A small K_s, coupled with no other precipitation events to displace the water in the unsaturated zone, allows for the model to equilibrate slower than expected. In contrast to clay, the coarse- and mixed-grained soils showing similarities in t_{rec} across durations (Figure 4.4) highlight a possible limit to recession times regardless of EPE duration and amount. This limit could be due to runoff, infiltration removed by soil water storage, or increased recharge.

4.3.4 First-order recharge rates

Recharge is one of the most important components of the water budget, but recharge totals and rates vary greatly in time and space and are difficult to measure (Healy and Cook, 2002; Scanlon et al., 2002; Moeck et al., 2020). Studies considering EPEs in tropical monsoonal zones with predominantly sandy soils have demonstrated high recharge rates (Taylor et al., 2013; Jasechko and Taylor, 2015). In subtropical, mediterranean, alpine, and desert regions, all found globally, there is added uncertainty in predicting recharge due to climate change effects on precipitation patterns and the increase of EPEs (Meixner et al., 2016). This uncertainty is further complicated by variations in soil hydraulic properties, like the available porosity of a soil, which serves as an important control of water-table response to EPEs (Corona et al., 2023). Here we calculate total recharge for each soil, EPE amount and duration, while considering available porosity. Total recharge occurs at the water-table, following the processes of surface runoff, evapotranspiration, and soil water storage. We define recharge as follows:

$$R = (\theta_s - \theta_i) * \Delta_{WTD\,max} \quad (8)$$

where R is total recharge (m), θ_s (dimensionless) is the saturated water content, and θ_i (dimensionless) is the initial water content. Here, $\theta_s - \theta_i$ is the available porosity of the soil, and the $\Delta_{WTD\,max}$ (m) is the maximum water-table displacement. Total recharge (m), R, is calculated for each simulation (Table 4.4) and varies with EPE amount and duration. We convert total recharge (m) to percentages to make uniform comparisons across simulations. Comparing recharge percentages across soils, average recharge by EPE amount ranged from 68 - 73% (0.20 m EPEs), 61 - 72% (0.40 m EPEs), and 65 - 70% (0.60 m EPEs), with average recharge for all soils equaling ~70% of the EPE amount (Table 4.4).

For finer-grained soils (clay, silty clay, silty clay loam, clay loam), recharge ranged from 31% to 69% of the EPE amount across durations. For mixed-grained (sandy clay, silt loam, sandy clay loam, loam, silt) recharge ranged from 51 % to 77% of the EPE amount. For coarser-grained soils (sandy loam, loamy sand, and sand), recharge ranged from 73% to 96% of the EPE amount across durations. Coarser-grained soils have the greatest recharge and clay has the smaller recharge amount (Table 4.4). However, the overlap in recharge percentages between finer-grained (31-69%) and mixed-grained (51-77%) soils does not point to a conclusive trend between soil texture grain size and recharge. To examine this, we plot recharge (m) vs. EPE input (m) on net graphs (Figure 4.5).

Figure 4.5 is comprised of eight net graphs that show total recharge versus EPE input for the 12 soils. If 100% of the infiltration from the EPE input reached the water-table, then the total recharge net would overlap the EPE input net completely. If there were no recharge, the recharge net would not extend from zero. As an example, the 1-day, EPE of 0.20 m (top left) shows that the clay soil experiences a recharge total of 48%, the sandy soil, 96%, and mixed-grained soils (sandy clay, sandy clay loam, silt, and loam), experience ~75% recharge (Table 4.4).

Table 4.4. Total recharge (m) and percent equivalent per duration, per amount for the 12 soils.

Soil texture class	K_s (m/d)	Available Porosity $\theta_s - \theta_i$ (1)	1-day EPE		7-day EPE			20-day EPE			Range of Recharge (m) by Soil for all EPEs
			Precipitation Amount (m)								
			0.20	0.40	0.20	0.40	0.60	0.20	0.40	0.60	
Clay	0.05	0.205	0.10 48%	0.12 31%	0.10 49%	0.21 52%	0.26 43%	0.09 47%	0.19 49%	0.27 45%	0.10 – 0.27 31 - 52%
Silty Clay Loam	0.06	0.220	0.13 64%	0.17 41%	0.13 64%	0.27 67%	0.36 59%	0.12 60%	0.24 63%	0.37 62%	0.13 – 0.37 41 - 67%
Clay Loam	0.07	0.290	0.14 69%	0.19 47%	0.14 69%	0.26 66%	0.38 63%	0.13 66%	0.29 65%	0.38 63%	0.14 – 0.38 47 - 69%
Silty Clay	0.08	0.240	0.12 59%	0.16 40%	0.12 59%	0.23 58%	0.35 59%	0.11 56%	0.24 57%	0.34 57%	0.11 – 0.35 40 - 59%
Sandy Clay	0.10	0.285	0.15 75%	0.24 59%	0.15 68%	0.28 71%	0.40 67%	0.14 71%	0.28 69%	0.40 66%	0.14 – 0.40 59 - 75%
Silt Loam	0.11	0.210	0.14 68%	0.20 51%	0.13 65%	0.26 65%	0.43 72%	0.12 61%	0.26 64%	0.43 72%	0.13 – 0.43 51 - 72%
Sandy Clay Loam	0.12	0.210	0.15 74%	0.20 51%	0.14 68%	0.27 68%	0.41 68%	0.13 65%	0.27 67%	0.40 67%	0.13 – 0.41 51 - 74 %
Silt	0.20	0.215	0.15 73%	0.27 68%	0.14 68%	0.28 70%	0.43 71%	0.13 65%	0.28 69%	0.42 71%	0.13 – 0.42 65 - 73%
Loam	0.70	0.275	0.15 76%	0.31 77%	0.15 76%	0.30 76%	0.45 76%	0.15 73%	0.30 75%	0.45 75%	0.15 – 0.45 73 - 77%
Sandy Loam	1.10	0.320	0.17 84%	0.33 84%	0.17 84%	0.33 83%	0.49 81%	0.16 80%	0.32 81%	0.48 80%	0.16 - 0.48 80 - 84%
Loamy Sand	2.50	0.360	0.18 92%	0.35 88%	0.18 92%	0.35 89%	0.52 87%	0.17 86%	0.35 87%	0.51 85%	0.18 - 0.52 85 - 92%
Sand	5.00	0.340	0.19 96%	0.38 95%	0.19 96%	0.37 94%	0.55 92%	0.18 90%	0.36 91%	0.53 89%	0.18 – 0.53 89 - 96%
Average Recharge (m) by EPE Amount for all soils			0.15 73%	0.24 61%	0.14 72%	0.29 72%	0.42 70%	0.14 68%	0.28 70%	0.41 69%	Average Recharge 70%

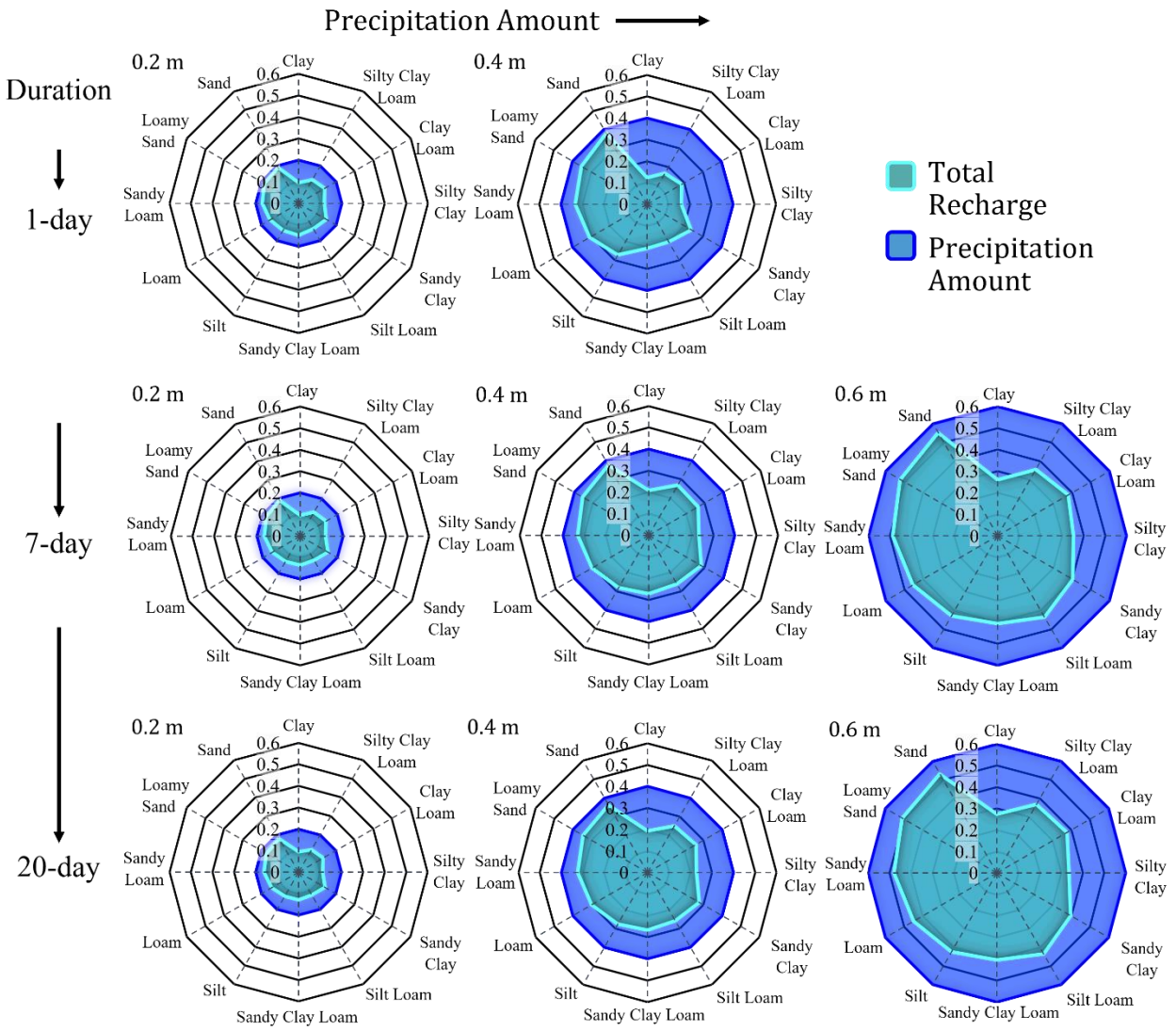

Figure 4.5. Net graphs comparing EPE amount (m) versus the total recharge (m) for the 12 soils, for each EPE duration and amount. Event duration increases from top to bottom (1-, 7-, 20-day) for EPE durations and precipitation amount (0.2, 0.4, 0.6) increases from left to right.

Comparing the net graphs highlights the influence of soil texture class on recharge. The coarser-grained soils (sandy loam, loamy sand, sand) consistently show the greatest recharge, whereas the soils with the highest clay percentages (clay, silty clay) show the least recharge (Figure 4.5). Finer-grained soils (clay, silty clay) show smaller recharge extents. In a one-dimensional model, processes that could prevent maximum recharge include runoff, evapotranspiration, and retention in the subsurface for soil water storage (Freeze, 1969). Runoff

is more likely to occur at the surface of soils with smaller K_s values like those of clay and silty clay (Table 4.1). Retention of water in pore spaces is more likely to occur in soils with higher clay percentages due to clay's ability to absorb and retain fluids for extended periods of time. This delays water flow to the water table for sandy clay, clay loam, and silty clay loam.

The clay soil has the least total recharge, followed by the silty clay soil (Figure 4.5), which is consistent with the recharge totals of Table 6. Silty clay has a low K_s and a low- to mid-range available porosity relative to the rest of the soils (Tables 4.1 and 4.4). Of the twelve soil texture classes (Soil Science Division Staff, 2017), silty clay has clay percentages of 40 – 60%, the second highest percentage after clay itself. The recharge response in the simulated silt clay is smaller than expected, raising the question of whether the silt clay soil hydraulic properties are more representative of a clay-rich, silt clay. A clay-rich soil will may retard flow and retain water for longer, which would explain the silty clay response.

In Figure 4.5 soils are organized in increasing K_s (clockwise) to examine whether K_s has an effect on recharge totals. Generally, there is a trend of greater recharge with increasing K_s for the coarser-grained soils like sand, loamy sand, and sandy loam. This trend is not as strong for the mixed-grained or fine-grained soils, again indicating that K_s is not the sole determining factor of recharge amount, and that other soil properties also influence recharge.

An examination of recharge totals (Table 4.4, Figure 4.5) does not show a pattern of increased or decreased recharge with longer EPE duration or amount. Instead, average recharge (m) for all soils varies between 61% and 73%. Average recharge for all simulations is 69% of the total. Instead, the stronger control of recharge is soil texture class, where finer-grained soils experience nearly half the recharge totals of the coarser-grained soils.

4.4 Conclusion

We used HYDRUS-1D to create models of twelve soil texture classes for eight EPE conditions, totaling 96 models. We simulated water-table response of varying soil textures to EPEs of 1-day, 7-day, and 20-day durations and amounts of 0.20 m, 0.40 m, and 0.60 m. We examined how EPE-infiltration affects: 1) water-table response time, 2) water-table displacement, 3) water-table recession time and 4) calculated first-order recharge totals and percentages. The following conclusions are drawn from this study:

- Response times are shorter with increasing precipitation amount and can vary from ~8 days to ~279 days, with water-table response occurring faster in coarser-grained soils and taking upwards of hundreds of days in finer-grained soils.
- Water-table displacements range from 0.5 m - 1.7 meters, and can be higher in mixed-grained soils than coarser-grained soils. Water-table displacement is positively correlated with increasing EPE amount, and poorly correlated with longer duration.
- Recession times range from 2.4 years to > 7 years for all EPE durations (1-, 7-, and 20-day) and EPE amounts (0.20 m, 0.40 m, 0.60 m), suggesting that soil properties exert the greater control of recession time.
- Average recharge totals ranged from 31% (clay) to 96% (sand), with the overall average equaling ~70% recharge-from-EPE. Total recharge is primarily a function of total EPE amount and soil properties.

4.4.1 Implications for water resources

As climate change continues to impact precipitation patterns, numerical models can be utilized with diverse types of data to study the effects of EPEs on groundwater resources. The implications of this work are as follows. First, artificially created spreading basins (Freeze and

Cherry, 1979) made up of coarse-grained soils will allow for faster water table response from permeable, unconfined aquifers. Depending on the soils of the spreading basins, maximum recharge may occur within days, with mixed-grain soil texture classes (silt, loam) potentially allowing the water-table to remain elevated for months after an EPE. A prolonged water-table rise could also benefit areas attempting to control seawater intrusion, as elevated water-tables are capable of keeping intruding sea water at bay (Freeze and Cherry, 1979). Second, water-table displacements are not solely a function of saturated hydraulic conductivity, meaning that areas with more mixed-grain soils and some fine-grained soils will also benefit from the infiltration from EPEs. Sites with naturally occurring mixed-grain soils include areas of ancient fluvial or lacustrine activity that could accept high infiltration such as paleo valleys (Gies, 2023) and wetlands (Van der Kamp and Hayashi, 1998). Third, the idea that infiltration from EPEs could result in elevated water content for up to 8 years post- EPE, could increase the likelihood of geologic hazards for areas with finer-grained layers, as the cascading effects of subsequent precipitation (after EPEs) could cause soils to reach saturation capacity sooner than expected in response to EPEs and result in geohazards such as flash flooding, mudslides, and landslides. Four, average recharge totals from the EPEs considered had an average recharge total of ~70% across EPE amounts, an ideal recharge percentage for areas in need of increasing their subsurface water storage.

BIBLIOGRAPHY

Alley, W.M., 2002. Flow and Storage in Groundwater Systems. Science 296, 1985–1990. https://doi.org/10.1126/science.1067123

Anderson, S.P., Anderson, R.S., Tucker, G.E., Dethier, D.P., 2013b. Critical zone evolution: Climate and exhumation in the Colorado Front Range, in: Classic Concepts and New Directions: Exploring 125 Years of GSA Discoveries in the Rocky Mountain Region. Geological Society of America. https://doi.org/10.1130/2013.0033(01)

Anderson, S.P., Ragar, D., 2022. Betasso - Well Water Levels - (BT_GW_1_Pducer) (2013-2018), Hydroshare, http://www.hydroshare.org/resource/6f8ee0a3ce5c45e4870976bb3d8d1bfc. Accessed: 07/25/2022.

Anderson, S.P., Rock, N., Ragar, D., 2022. BCCZO -- Meteorology, Air Temperature -- (BT_Met) -- Betasso -- (2009-2020). URL https://www.hydroshare.org/resource/6bf3e44b9de344749d8f665e139e7311/ (accessed 7.31.22).

BASIN, 2005. 1894 Flood of Boulder Creek [WWW Document]. Boulder Area Sustainability Information Network. URL http://bcn.boulder.co.us/basin/history/1894flood.html (accessed 5.13.20).

BcCZO, 2020. Gordon Gulch [WWW Document]. Boulder Creek Critical Zone Observatory. URL https://criticalzone.org/boulder/infrastructure/field-area/gordon-gulch/#data (accessed 4.23.20).

Befus, K.M., Sheehan, A.F., Leopold, M., Anderson, S.P., Anderson, R.S., 2011. Seismic Constraints on Critical Zone Architecture, Boulder Creek Watershed, Front Range, Colorado. Vadose Zone Journal 10, 915–927. https://doi.org/10.2136/vzj2010.0108

Boas, T., Mallants, D., 2022. Episodic extreme rainfall events drive groundwater recharge in arid zone environments of central Australia. Journal of Hydrology: Regional Studies 40, 101005. https://doi.org/10.1016/j.ejrh.2022.101005

Brooks, R.H., Corey, A.T., 1964. Hydraulic Properties of Porous Media. Hydrology Papers Colorado State University 3, 37.

Bruce, R.R., Klute, A., 1956. The measurement of soil moisture diffusivity. Soil Science Society of America Journal 20, 458–462. https://doi.org/10.2136/sssaj1956.03615995002000040004x

Carsel, R.F., Parrish, R.S., 1988. Developing joint probability distributions of soil water retention characteristics. Water Resources Research 24, 755–769. https://doi.org/10.1029/WR024i005p00755

Cary, J.W., Hayden, C.W., 1973. An index for soil pore size distribution. Geoderma 9, 249–256. https://doi.org/10.1016/0016-7061(73)90026-8

Chiorean, V.-F., 2017. Determination of Matric Suction and Saturation Degree for Unsaturated Soils, Comparative Study - Numerical Method versus Analytical Method. IOP Conf. Ser.: Mater. Sci. Eng. 245, 032074. https://doi.org/10.1088/1757-899X/245/3/032074

Coffman, K., 2013. Property losses from Colorado flood projected at about $2 billion [WWW Document]. REUTERS Environment. URL https://www.reuters.com/article/us-usa-colorado-flooding/property-losses-from-colorado-flood-projected-at-about-2-billion-idUSBRE98H1BA20130919 (accessed 4.22.20).

Corona, C.R., Ge, S., 2022. Examining subsurface response to an extreme precipitation event using HYDRUS-1D. Vadose Zone Journal 15. https://doi.org/10.1002/vzj2.20189

Corona, C.R., Ge, S., Anderson, S.P., 2023. Water-table response to extreme precipitation events. Journal of Hydrology 129140.

Corona, C.R., Gurdak, J.J., Dickinson, J.E., Ferré, T.P.A., Maurer, E.P., 2018. Climate variability and vadose zone controls on damping of transient recharge. Journal of Hydrology 561, 1094–1104. https://doi.org/10.1016/j.jhydrol.2017.08.028

Crosbie, R.S., 2003. Regional scaling of groundwater recharge (Doctoral Dissertation). University of Newcastle, Newcastle, Australia.

Dadgar, M.A., Nakhaei, M., Porhemmat, J., Eliasi, B., Biswas, A., 2020. Potential groundwater recharge from deep drainage of irrigation water. Science of The Total Environment 716, 137105. https://doi.org/10.1016/j.scitotenv.2020.137105

Diamond, J., Shanley, T., 1998. Infiltration Rate Assessment of Some Major Soils: End of Project Report, Proceedings Agricultural Research Forum. Johnston Castle Research Centre Wexford, Dublin, U.K.

Dieter, C.A., Maupin, M.A., Caldwell, R.R., Harris, M.A., Ivahnenko, T.I., Lovelace, J.K., Barber, N.L., Linsey, K.S., 2018. Estimated use of water in the United States in 2015 (U.S. Geological Survey Circular No. 1141), Water Availability and Use Science Program. U.S. Geological Survey, Reston, Virginia. https://doi.org/10.3133/cir1441.

Du, H., Donat, M.G., Zong, S., Alexander, L.V., Manzanas, R., Kruger, A., Choi, G., Salinger, J., He, H.S., Li, M.-H., 2022. Extreme precipitation on consecutive days occurs more often in a warming climate. Bulletin of the American Meteorological Society 103, E1130–E1145. https://doi.org/10.1175/BAMS-D-21-0140.1

Fiore, A.R., Ashland, F.X., Reilly, P.A., Mirus, B.B., 2021. Hydrologic, slope movement, and soil property data from the coastal bluffs of the Atlantic Highlands, New Jersey, 2016-2018. U.S. Geological Survey Data Release. https://doi.org/10.5066/P9A601HC

Freeze, R.A., 1969. The Mechanism of Natural Ground-Water Recharge and Discharge: 1. One-dimensional, Vertical, Unsteady, Unsaturated Flow above a Recharging or Discharging Ground-Water Flow System. Water Resources Research 5, 153–171. https://doi.org/10.1029/WR005i001p00153

Freeze, R.A., Cherry, J.A., 1979. Groundwater, 1st ed. Prentice-Hall, Inc., Englewood Cliffs, New Jersey, 07632, University of British Columbia, University of Waterloo.

Freeze, R.A., Witherspoon, P.A., 1967. Theoretical analysis of regional groundwater flow: 2. Effect of water-table configuration and subsurface permeability variation. Water Resour. Res. 3, 623–634. https://doi.org/10.1029/WR003i002p00623

French, R.H., Jacobson, R.L., Lyles, B.F., 1996. Threshold Precipitation Events and Potential Ground-Water Recharge. Journal of Hydraulic Engineering 122, 573–578. https://doi.org/10.1061/(ASCE)0733-9429(1996)122:10(573)

Gaines, T., 2023. Bay Area rainfall totals are in after atmospheric rivers flooded California [WWW Document]. KRON4 News. URL https://www.kron4.com/news/bay-area-rainfall-totals-are-in-after-atmospheric-rivers-flooded-california/ (accessed 2.25.23).

Garcia-Gaines, R., Frankenstein, S., 2015. USCS and the USDA Soil Classification System: Development of a Mapping Scheme. (No. ERDC/CRREL TR-15-4). U.S. Army Engineer Research and Development Center, Vicksburg, MS. https://erdc-library.erdc.dren.mil/jspui/bitstream/11681/5485/1/ERDC-CRREL-TR-15-4.pdf.

Geris, J., Comte, J.-C., Franchi, F., Petros, A.K., Tirivarombo, S., Selepeng, A.T., Villholth, K.G., 2022. Surface water-groundwater interactions and local land use control water quality impacts of extreme rainfall and flooding in a vulnerable semi-arid region of Sub-Saharan Africa. Journal of Hydrology 609, 127834. https://doi.org/10.1016/j.jhydrol.2022.127834

Gies, E., 2023. California Could Capture Its Destructive Floodwaters to Fight Drought. The New York Times.

Gochis, D., Schumacher, R., Friedrich, K., Doesken, N., Kelsch, M., Sun, J., Ikeda, K., Lindsey, D., Wood, A., Dolan, B., 2015. The great Colorado flood of September 2013. Bulletin of the American Meteorological Society 96, 1461–1487. https://doi.org/10.1175/BAMS-D-13-00241.1

Golian, M., Katibeh, H., Najafi, Z., Saadat, H., Saffarzadeh, A., Ahmadi, A., Khazaei, M., Sametzadeh, E., 2021. Large-scale replenishment of groundwater depletion by long-lived extreme rainstorms in arid regions: case study of the 2019 floods in Iran. Hydrogeology Journal. https://doi.org/10.1007/s10040-021-02370-8

Gray, D.M., Norum, D.I., 1967. The Effect of Soil Moisture on Infiltration as Related to Runoff and Recharge (No. 6), Proceedings of Hydrology Symposium. National Research Council of Canada.

Green, T.R., Taniguchi, M., Kooi, H., Gurdak, J.J., Allen, D.M., Hiscock, K.M., Treidel, H., Aureli, A., 2011. Beneath the surface of global change: Impacts of climate change on groundwater. Journal of Hydrology 405, 532–560. https://doi.org/10.1016/j.jhydrol.2011.05.002

Gurdak, J.J., Hanson, R.T., Green, T.R., 2009. Effects of Climate Variability and Change on Groundwater Resources of the United States (Fact Sheet No. 2009–3074). U.S. Geological Survey, Lakewood, Colorado.

Hale, K., 2018. Streamflow Sensitivity to Climate Warming and a Shift from Snowfall to Rainfall. Order No. 10980032 (Thesis). University of Colorado, Boulder, ProQuest Dissertations & Theses Global. (2178818422).

Healy, R.W., Cook, P.G., 2002. Using groundwater levels to estimate recharge. Hydrogeology Journal 10, 91–109. https://doi.org/10.1007/s10040-001-0178-0

Henning, S., 2016. Dynamic Response of Watershed Subsurface Systems to Extreme Precipitation Events. University of Colorado, Boulder.

Hopmans, J.W., Stricker, J.N.M., 1989. Stochastic Analysis of Soil Water Regime in a Watershed. Journal of Hydrology 105, 57–84. https://doi.org/10.1016/0022-1694(89)90096-6

Horton, R., Thompson, M.L., McBride, J.F., 1988. Determination of effective porosity of soil materials 148.

Horton, R.E., 1941. An Approach Toward a Physical Interpretation of Infiltration-Capacity. Soil Science Society of America Journal 5, 399–417. https://doi.org/10.2136/sssaj1941.036159950005000C0075x

Hosking, J.R.M., Wallis, J.R., 1997. Regional frequency analysis: An Approach Based on L-Moments. Cambridge University Press, New York, New York.

Hosking, J.R.M., Wallis, J.R., Wood, E.F., 1985. Estimation of the Generalized Extreme- Value Distribution by the Method of Probability-Weighted Moments. Technometrics 27, 251–261. https://doi.org/10.1080/00401706.1985.10488049

Hou, X., Li, T., Qi, S., Guo, S., Li, P., Xi, Y., Xing, X., 2021. Investigation of the cumulative influence of infiltration on the slope stability with a thick unsaturated zone. Bull Eng Geol Environ 80, 5467–5480. https://doi.org/10.1007/s10064-021-02287-2

Jasechko, S., Taylor, R.G., 2015. Intensive rainfall recharges tropical groundwaters. Environ. Res. Lett. 10, 124015. https://doi.org/10.1088/1748-9326/10/12/124015

Joachim, D.R., Gotkowitz, M.B., Potter, K.W., Bradbury, K.R., Vavrus, S.J., Loheide, S.P., 2011. Forecasting impacts of extreme precipitation events on Wisconsin's groundwater levels. Wisconsin Geological and Natural History Survey 22. https://wri.wisc.edu/wp-content/uploads/FinalWR09R005.pdf

Kløve, B., Ala-Aho, P., Bertrand, G., Gurdak, J.J., Kupfersberger, H., Kværner, J., Muotka, T., Mykrä, H., Preda, E., Rossi, P., Uvo, C.B., Velasco, E., Pulido-Velázquez, M., 2013. Climate Change Impacts on Groundwater and Dependent Ecosystems. Journal of Hydrology. https://doi.org/10.1016/j.jhydrol.2013.06.037

Kosugi, K., Hopmans, J.W., Dane, J.H., 2002. 3.3.4 Parametric Models. Methods of Soil Analysis: Part 4 Physical Methods 5, 739–757.

Langston, A.L., Tucker, G.E., Anderson, R.S., Anderson, S.P., 2015. Evidence for climatic and hillslope-aspect controls on vadose zone hydrology and implications for saprolite weathering: Climatic Control on Vadose Zone Moisture. Earth Surf. Process. Landforms 40, 1254–1269. https://doi.org/10.1002/esp.3718

Lehmann, J., Coumou, D., Frieler, K., 2015. Increased record-breaking precipitation events under global warming. Climatic Change 132, 501–515. https://doi.org/10.1007/s10584-015-1434-y

Leterme, B., Mallants, D., Jacques, D., 2012. Sensitivity of groundwater recharge using climatic analogues and HYDRUS-1D. Hydrol. Earth Syst. Sci. 16, 2485–2497. https://doi.org/10.5194/hess-16-2485-2012

Li, C., Zwiers, F., Zhang, X., Chen, G., Lu, J., Li, G., Norris, J., Tan, Y., Sun, Y., Liu, M., 2019. Larger Increases in More Extreme Local Precipitation Events as Climate Warms. Geophysical Research Letters 46, 6885–6891. https://doi.org/10.1029/2019GL082908

Maupin, M.A., 2018. Summary of estimated water use in the United States in 2015 (No. 2018–3035), Fact Sheet. US Geological Survey, Reston, VA. https://doi.org/10.3133/fs20183035.

Meixner, T., Manning, A.H., Stonestrom, D.A., Allen, D.M., Ajami, H., Blasch, K.W., Brookfield, A.E., Castro, C.L., Clark, J.F., Gochis, D.J., 2016. Implications of projected climate change for groundwater recharge in the western United States. Journal of Hydrology 534, 124–138. https://doi.org/10.1016/j.jhydrol.2015.12.027

Miguez-Macho, G., Fan, Y., Weaver, C.P., Walko, R., Robock, A., 2007. Incorporating water table dynamics in climate modeling: 2. Formulation, validation, and soil moisture simulation. Journal of Geophysical Research: Atmospheres 112. https://doi.org/10.1029/2006JD008112

Miller, J.F., Frederick, R.H., Tracey, R.J., 1973. NOAA Atlas 2, Precipitation Frequency Atlas of the Western U.S.: Volume IX, Washington. NOAA, Silver Spring, Maryland.

Mo'allim, A., Kamal, M., Muhammed, H., Yahaya, N., Zawawe, M., Man, H., Wayayok, A., 2018. An Assessment of the Vertical Movement of Water in a Flooded Paddy Rice Field Experiment Using Hydrus-1D. Water 10, 783. https://doi.org/10.3390/w10060783

Moeck, C., Grech-Cumbo, N., Podgorski, J., Bretzler, A., Gurdak, J.J., Berg, M., Schirmer, M., 2020. A global-scale dataset of direct natural groundwater recharge rates: A review of variables, processes, and relationships. Science of the total environment 717, 137042. https://doi.org/10.1016/j.scitotenv.2020.137042

Moriasi, D.N., Arnold, J.G., Van Liew, M.W., Bingner, R.L., Harmel, R.D., Veith, T.L., 2007. Model Evaluation Guidelines for Systematic Quantification of Accuracy in Watershed Simulations. Transactions of the ASABE 50, 885–900. https://doi.org/10.13031/2013.23153

Mualem, Y., 1976. A new model for predicting the hydraulic conductivity of unsaturated porous media. Water Resources Research 12, 513–522. https://doi.org/10.1029/WR012i003p00513

Myhre, G., Alterskjær, K., Stjern, C.W., Hodnebrog, Ø., Marelle, L., Samset, B.H., Sillmann, J., Schaller, N., Fischer, E., Schulz, M., Stohl, A., 2019. Frequency of extreme precipitation increases extensively with event rareness under global warming. Sci Rep 9, 16063. https://doi.org/10.1038/s41598-019-52277-4

NADP, 2020. National Atmospheric Deposition Program, NTN Site CO94 [WWW Document]. URL http://nadp.slh.wisc.edu/data/sites/siteDetails.aspx?net=NTN&id=CO94

Nemes, A., Schaap, M.G., Leij, F.J., Wösten, J.H.M., 2001. Description of the unsaturated soil hydraulic database UNSODA version 2.0. Journal of Hydrology 251, 151–162. https://doi.org/10.1016/S0022-1694(01)00465-6

Neto, D.C., Chang, H.K., van Genuchten, M.Th., 2016. A Mathematical View of Water Table Fluctuations in a Shallow Aquifer in Brazil: Ground Water. Groundwater 54, 82–91. https://doi.org/10.1111/gwat.12329

Nguyen, H.H., Peche, A., Venohr, M., 2021. Modelling of sewer exfiltration to groundwater in urban wastewater systems: A critical review. Journal of Hydrology 596, 126130. https://doi.org/10.1016/j.jhydrol.2021.126130

Nimmo, J.R., 2013. Porosity and Pore Size Distribution: Reference Module in Earth Systems and Environmental Sciences. Elsevier 3, 1–10. http://dx.doi.org/10.1016/B978-0-12-409548-9.05265-9

Nimmo, J.R., 2006. Unsaturated Zone Flow Processes, in: Anderson, M.G., McDonnell, J.J. (Eds.), Encyclopedia of Hydrological Sciences. John Wiley & Sons, Ltd, Chichester, UK.

Nimmo, J.R., Park, M., 2004. Porosity and Pore Size Distribution 3, 11.

NOAA, 2023a. Atmospheric Rivers Hit West Coast [WWW Document]. National Environmental Satellite Data and Information Service. URL https://www.nesdis.noaa.gov/news/atmospheric-rivers-hit-west-coast

NOAA, 2023b. Precipitation Frequency Data Server (PFDS) [WWW Document]. NOAA's National Weather Service, Hydrometeorological Design Studies Center, Precipitation Frequency Data server (PFDS). URL https://hdsc.nws.noaa.gov/hdsc/pfds/index.html (accessed 2.25.23).

NOAA, 2023c. January 2023 was nation's 6th warmest on record: Month marked by atmospheric rivers, numerous tornadoes [WWW Document]. NOAA News & Features. URL https://www.noaa.gov/news/january-2023-was-nations-6th-warmest-on-record#:~:text=Atmospheric%20rivers%20dropped%20record%20rain,the%20region%2C%20including%20power%20outages.

NOAA, 2017. National Oceanic and Atmospheric Association (NOAA) Atlas 14 Point Precipitation Frequency Estimates, https://hdsc.nws.noaa.gov/hdsc/pfds/pfds_map_cont.html. Accessed: 04/06/2022.

NRCS, 2022a. Official Soil Series Description by List. URL https://soilseries.sc.egov.usda.gov/ (accessed 7.31.22).

NRCS, 2022b. Official Soil Series Description by List: Webster Series. URL https://soilseries.sc.egov.usda.gov/OSD_Docs/w/webster.html (accessed 7.31.22).

NRCS, 2022c. Official Soil Series Description by List: Glendale Series. URL https://soilseries.sc.egov.usda.gov/OSD_Docs/g/glendale.html (accessed 7.31.22).

NRCS, 2022d. Official Soil Series Description by List: Konawa Series. URL https://soilseries.sc.egov.usda.gov/OSD_Docs/K/KONAWA.html (accessed 7.31.22).

NRCS, 2022e. Official Soil Series Description by List: Fullerton Series. URL https://soilseries.sc.egov.usda.gov/OSD_Docs/f/fullerton.html (accessed 7.31.22).

NRCS, 2022f. Official Soil Series Description by List: Plainfield Series. URL https://soilseries.sc.egov.usda.gov/OSD_Docs/p/plainfield.html (accessed 7.31.22).

Pendergrass, A.G., 2018. What precipitation is extreme? Science 360, 1072–1073. https://doi.org/10.1126/science.aat1871

Pendergrass, A.G., Knutti, R., 2018. The Uneven Nature of Daily Precipitation and Its Change. Geophysical Research Letters 45, 11,980-11,988. https://doi.org/10.1029/2018GL080298

Pepin, N., Bradley, R.S., Diaz, H.F., Baraër, M., Caceres, E.B, Forsythe, N., Fowler, H., Greenwood, G., Hashmi, M.Z., Liu, X.D., Miller, J.R., 2015. Elevation-dependent warming in mountain regions of the world. Nature Climate Change, Mountain Research Initiative EDW Working Group 5, 424–430. https://doi.org/10.1038/nclimate2563

Perica, S., Martin, D., Pavlovic, S., Roy, I., St. Laurent, M., Trypaluk, C., Unruh, D., Yekta, M., Bonnin, G., 2013. NOAA Atlas 14 Precipitation-Frequency Atlas of the United States Volume 9 Version 2.0: Southeastern States (Alabama, Arkansas, Florida, Georgia, Louisiana, Mississippi) (Volume No. 9). National Weather Service. https://www.weather.gov/media/owp/oh/hdsc/docs/Atlas14_Volume9.pdf.

Pfahl, S., O'Gorman, P.A., Fischer, E.M., 2017. Understanding the regional pattern of projected future changes in extreme precipitation. Nature Climate Change 7, 423–427. https://doi.org/10.1038/nclimate3287

Philip, J.R., 1956. The Theory of Infiltration: 5. The Influence of The Initial Moisture Content. Commonwealth Scientific and Industrial Research Organization 329–339.

Prein, A.F., Rasmussen, R.M., Ikeda, K., Liu, C., Clark, M.P., Holland, G.J., 2017. The future intensification of hourly precipitation extremes. Nature Climate Change 7, 48–52. https://doi.org/10.1038/nclimate3168

Reitz, M., Sanford, W.E., Senay, G.B., Sanford, W.E., 2017. Combining remote sensing and water-balance evapotranspiration estimates for the conterminous United States. Remote Sensing 9, 1181. https://doi.org/10.3390/rs9121181

Reusser, D.E., Blume, T., Schaefli, B., Zehe, E., 2009. Analysing the temporal dynamics of model performance for hydrological models. Hydrology Earth Systems Science. 20.

Richards, L., 1931. Capillary conduction of liquids in porous mediums. Physics 1, 318–333.

Salberg, L., 2021. Coupling Field Data and a Flow Model to Characterize the Role of Groundwater in a Montane, Semi-Arid, Headwater Catchment, Gordon Gulch, Colorado. (Order No. 28713822). University of Colorado, Boulder, ProQuest Dissertations & Theses Global. (2583029128).

Sanford, W.E., Selnick, D.L., 2013. Estimation of evapotranspiration across the conterminous United States using a regression with climate and land-cover data. Journal of the American Water Resources Association 49, 217–230. https://doi.org/10.1111/jawr.12010

Scanlon, B.R., Healy, R.W., Cook, P.G., 2002. Choosing appropriate techniques for quantifying groundwater recharge. Hydrogeology Journal 10, 18–39.

Scanlon, B.R., Zhang, Z., Save, H., Sun, A.Y., Schmied, H.M., van Beek, L.P., Wiese, D.N., Wada, Y., Long, D., Reedy, R.C., 2018. Global models underestimate large decadal declining and rising water storage trends relative to GRACE satellite data. Proceedings of the National Academy of Sciences 115, E1080–E1089.

Schaap, M.G., Leij, F.J., 2000. Improved Prediction of Unsaturated Hydraulic Conductivity with the Mualem-van Genuchten Model. Soil Sci. Soc. Am. J. 64, 843–851. https://doi.org/10.2136/sssaj2000.643843x

Shao, J., Si, B., Jin, J., 2018. Extreme Precipitation Years and Their Occurrence Frequency Regulate Long-Term Groundwater Recharge and Transit Time. Vadose Zone Journal 17, 0. https://doi.org/10.2136/vzj2018.04.0093

Shea, N., 2013. Spatial Patterns of Mobile Regolith Thickness and Meteoric 10Be in Gordon Gulch, Front Range, CO. Master's Theses 463, 81.

Šimůnek, J., Sejna, M., Saito, H., Sakai, M., van Genuchten, M.T., 2013. The HYDRUS-1D Software Package for Simulating the One-Dimensional Movement of Water, Hear, and Multiple Solutes in Variably-Saturated Media. Department of Environmental Sciences University of California Riverside.

Šimůnek, J., Van Genuchten, M.T., Sejna, M., 2005. The HYDRUS-1D software package for simulating the one-dimensional movement of water, heat, and multiple solutes in variably-saturated media. University of California-Riverside Research Reports 3, 1–240. https://www.pc-progress.com/Downloads/Pgm_hydrus1D/HYDRUS1D-4.08.pdf

Šimůnek, J., van Genuchten, M.Th., Šejna, M., 2008. Development and Applications of the HYDRUS and STANMOD Software Packages and Related Codes. Vadose Zone Journal 7, 587–600. https://doi.org/10.2136/vzj2007.0077

Singh, J., Knapp, H.V., Demissie, M., 2004. Hydrologic Modeling of the Iroquois River Watershed Using HSPF and SWAT. Illinois State Water Survey, Watershed Science Section 24.

Sistek, S., 2022. 6 rare "1,000-year" rain events within a month? Climate change may force NOAA to update criteria [WWW Document]. FOX Weather: Extreme Weather. URL https://www.foxweather.com/extreme-weather/5-rare-1000-year-rain-events-within-a-month-climate-change-may-force-noaa-to-update-criteria

Smith, J.B., Baum, R.L., Mirus, B.B., Michel, A.R., Stark, B., 2017. Results of Hydrologic Monitoring on Landslide-prone Coastal Bluffs near Mukilteo, Washington (USGS Numbered Series No. 2017–1095), Open-file report. U.S. Geological Survey, Reston, VA. https://doi.org/10.3133/ofr20171095.

Soil Science Division Staff, 2017. Soil Survey Manual (Agricultural Handbook No. 18). Soil Conservation Service, U.S. Department of Agriculture., Washington, D.C., U.S.

Sun, Q., Zhang, X., Zwiers, F., Westra, S., Alexander, L.V., 2021. A Global, Continental, and Regional Analysis of Changes in Extreme Precipitation. Journal of Climate 34, 243–258. https://doi.org/10.1175/JCLI-D-19-0892.1

Tashie, A.M., Mirus, B.B., Pavelsky, T.M., 2016. Identifying long-term empirical relationships between storm characteristics and episodic groundwater recharge. Water Resources Research 52, 21–35. https://doi.org/10.1002/2015WR017876

Taylor, R.G., Todd, M.C., Kongola, L., Maurice, L., Nahozya, E., Sanga, H., MacDonald, A.M., 2013. Evidence of the dependence of groundwater resources on extreme rainfall in East Africa. Nature Clim Change 3, 374–378. https://doi.org/10.1038/nclimate1731

Thomas, B., Behrangi, A., Famiglietti, J., 2016. Precipitation Intensity Effects on Groundwater Recharge in the Southwestern United States. Water 8, 90. https://doi.org/10.3390/w8030090

Trenberth, K.E., 2011. Changes in precipitation with climate change. Climate Research 47, 123–138. https://doi.org/10.3354/cr00953

Trenberth, K.E., Dai, A., Rasmussen, R.M., Parsons, D.B., 2003. The Changing Character of Precipitation. Bulletin of the American Meteorological Society 84, 1205–1218. https://doi.org/10.1175/BAMS-84-9-1205

Uccellini, L., 2014. The Record Front Range and Eastern Colorado Floods of September 11 - 17, 2013 (Service Assessment). National Weather Service, National Oceanic and Atmospheric Administration, Silver Spring, Maryland.

U.S. Geological Survey, 2003. Principal Aquifers of the 48 Conterminous United States, Hawaii, Puerto Rico, and the U.S. Virgin Islands. Water Mission Area NSDI Node. https://water.usgs.gov/GIS/metadata/usgswrd/XML/aquifers_us.xml. Accessed: 04/20/2022.

USDA, 1987. Soil Mechanics Level 1, Module 1. Unified Soil Classification System. Study Guide. National Employee Development Staff, Soil Conservation Service, U.S. Department of Agriculture., Washington, D.C., U.S.

Van der Kamp, G., Hayashi, M., 1998. The groundwater recharge function of small wetlands in the semi-arid northern prairies. Great Plains Research 39–56.

van Genuchten, M.Th., 1980. A Closed-form Equation for Predicting the Hydraulic Conductivity of Unsaturated Soils1. Soil Science Society of America Journal 44, 892. https://doi.org/10.2136/sssaj1980.03615995004400050002x

Vanapalli, S.K., Sillers, W.S., Fredlund, M.D., 1998. The Meaning and Relevance of Residual State to Unsaturated Soils. 51st Canadian Geotechnical Conference 8.

Vereecken, H., Huisman, J.A., Hendricks Franssen, H.J., Brüggemann, N., Bogena, H.R., Kollet, S., Javaux, M., van der Kruk, J., Vanderborght, J., 2015. Soil hydrology: Recent methodological advances, challenges, and perspectives. Water Resources Research 51, 2616–2633. https://doi.org/10.1002/2014WR016852

Vogel, T., Van Genuchten, M.Th., Cislerova, M., 2001. Effect of the shape of the soil hydraulic functions near saturation on variably-saturated flow predictions. Advances in Water Resources 12.

Wang, H., 2020. Groundwater Storage in Confined Aquifers. The Groundwater Project, Guelph, Ontario, Canada. https://gw-project.org/books/groundwater-storage-in-confined-aquifers/

Wang, H., Gao, J.E., Zhang, M., Li, X., Zhang, S., Jia, L., 2015. Effects of rainfall intensity on groundwater recharge based on simulated rainfall experiments and a groundwater flow model. Catena 127, 80–91. https://doi.org/10.1016/j.catena.2014.12.014

Wasko, C., Nathan, R., Stein, L., O'Shea, D., 2021. Evidence of shorter more extreme rainfalls and increased flood variability under climate change. Journal of Hydrology 603, 12. https://doi.org/10.1016/j.jhydrol.2021.126994

Wasko, C., Sharma, A., Westra, S., 2016. Reduced spatial extent of extreme storms at higher temperatures. Geophysical Research Letters 43, 4026–4032. https://doi.org/10.1002/2016GL068509

Westenbroek, S.M., Kelson, V.A., Dripps, W.R., Hunt, R.J., Bradbury, K.R., 2010. SWB--a modified Thornthwaite-Mather Soil-Water-Balance Code for estimating groundwater recharge. US Department of the Interior, US Geological Survey, Ground Resources Program.

Westra, S., Alexander, L.V., Zwiers, F.W., 2013. Global Increasing Trends in Annual Maximum Daily Precipitation. Journal of Climate 26, 3904–3918. https://doi.org/10.1175/JCLI-D-12-00502.1

Wilkinson, W.B., Cooper, D.M., 1993. The response of idealized aquifer/river systems to climate change. Hydrological Sciences Journal 38, 379–390. https://doi.org/10.1080/026266693099492688

Wittenberg, H., Aksoy, H., Miegel, K., 2019. Fast response of groundwater to heavy rainfall. Journal of Hydrology 571, 837–842. https://doi.org/10.1016/j.jhydrol.2019.02.037

Wu, W., Geller, M.A., Dickinson, R.E., 2002. The response of soil moisture to long-term variability of precipitation. Journal of Hydrometeorology 3, 604–613. https://doi.org/10.1175/1525-7541(2002)003<0604:TROSMT>2.0.CO;2

Youngs, E.G., 1988. Soil physics and hydrology. Journal of Hydrology 100, 411–431. https://doi.org/10.1016/0022-1694(88)90194-1

Zhang, C., Asce, A.M., Lu, N., Asce, F., 2019. Unitary Definition of Matric Suction. Journal of Geotechnical and Geoenvironmental Engineering 145, 1. https://doi.org/10.1061/(ASCE)GT.1943-5606.0002004

Zhang, J., Felzer, B.S., Troy, T.J., 2016. Extreme precipitation drives groundwater recharge: the Northern High Plains Aquifer, central United States, 1950-2010: Extreme Prep Drives GWR: The NHP Aquifer, Central US, 1950-2010. Hydrological Processes. 30, 2533–2545. https://doi.org/10.1002/hyp.10809

Zheng, W., Wang, S., Sprenger, M., Liu, B., Cao, J., 2019. Response of soil water movement and groundwater recharge to extreme precipitation in a headwater catchment in the North China Plain. Journal of Hydrology 576, 466–477. https://doi.org/10.1016/j.jhydrol.2019.06.071

Zhou, H., Zhao, W.Z., 2021. Evolution of soil-water states in the vadose zone of a desert soil after an extreme rainfall event and its impact on the ecosystem. Hydrogeology Journal. https://doi.org/10.1007/s10040-021-02372-6